

## CHAPTER 7

# Luminosity Performance Working Group Assessments

## 7.1 INTRODUCTION

### 7.1.1 Charge and Guidelines

Following the charge from ICFA which commissioned the second ILC-TRC report, the Steering Committee created two working groups to provide technical assessments of the current linear collider designs. This chapter provides the report of the second of these groups, the Luminosity Performance Group.

The charge to the Luminosity Performance Group is the following:

“This group will play a role similar to the former Beam Dynamics group, but will broaden its scope to analyze all those factors which affect the ultimate luminosity performance (both peak and integrated) of all four machines, including but not limited to, emittance dilution, beam jitter, tunability, and reliability. It will look at all phenomena which can reduce the luminosity at each machine subsystem, so as to predict the final emittances and luminosity reachable at the interaction point. Wherever possible, the members of this group (including a few detector representatives) should set common standards and use common computer codes to predict emittances, jitters, *etc.* Calculations should take into account mechanical and electrical tolerances, ground motions at various sites, *etc.* The standards and assumptions should be clearly spelled out.”

A group of 13 technically knowledgeable experts on linear colliders was formed to address this charge. The generic linear collider complex was divided into 4 subsystems. Four subgroups were formed, and each was charged with addressing the luminosity performance issues for its subsystem. A fifth subgroup was formed to address the impact of machine reliability on the integrated luminosity performance of the collider. The following general guidelines were established for the review of each subsystem:

## LUMINOSITY PERFORMANCE WORKING GROUP ASSESSMENTS

- Establish the key performance parameters which relate directly to the luminosity (peak and integrated) of the collider, or which relate to the performance of a downstream system. (The design values of these performance parameters are provided in the megatables.)
- Establish a common set of technical issues that are to be considered in evaluating the ability of a specific design to achieve the required performance.
- Establish a common method (a set of assumptions, analysis tools, codes, *etc.*) to be used to address each of the technical issues.
- For each of the four linear collider technical approaches, assess the ability of the proposed approach to realize the performance parameters. Identify the most difficult technical issues and indicate the scope of future R&D, if any, required to establish with confidence that the performance goal can be reached.

### 7.1.2 Subgroup Organization and Membership

The following is a tabulation of the subsystems, the members of the associated subgroups, and a description of the topics included in the analysis of each subsystem. Except where noted, each subsystem of TESLA, JLC-X/NLC, and CLIC was analyzed. No luminosity issues have been separately examined for JLC-C, since the designs of the damping rings and of the beam delivery system are identical to those of JLC-X, and no design was made available to the committee for the JLC-C main linac optics. For the same reason, compatibility issues arising in the upgrade of JLC-C through the addition of an X-band extension were also not considered by the group.

#### 1. Sources (Section 6.2)

Members: **W. Decking**, DESY (Subgroup leader); J. Gareyte, CERN; K. Kubo, KEK; P. Tenenbaum, SLAC

This group considered luminosity-related issues originating in the electron and positron sources. Because these issues are so intimately related to source technology, it was decided to merge this subgroup with the Injector technology subgroup of the Energy and Technology Performance Group (Chapter 6). The luminosity issues treated by this subgroup include electron source average current and polarization, and positron source yield and total emittance. Their conclusions are reported in Section 6.2.

#### 2. Damping Rings (Section 7.2)

Members: **J. Rogers**, Cornell (Subgroup leader); R. Assmann, CERN; W. Decking, DESY; J. Gareyte, CERN; K. Kubo, KEK; A. Wolski, LBNL

This group considered luminosity-related issues for the TESLA and JLC-X/NLC damping rings. The CLIC damping ring was not considered because a lattice

meeting all the requirements was not available to the group in time for the necessary evaluations to be made.

The luminosity parameters which were considered included extracted beam emittance and jitter, particle loss, and electron polarization. The beam dynamics issues which were studied included dynamic aperture in the presence of wiggler nonlinearities, emittance correction algorithms, beam jitter generated by ground motion and the extraction kickers, classical, ion-driven and electron-driven instabilities, intrabeam scattering, and depolarization effects.

### 3. Low Emittance Transport (Section 7.3)

Members: **D. Schulte**, CERN (Subgroup co-leader);  
**P. Tenenbaum**, SLAC (Subgroup co-leader); R. Assmann, CERN;  
 W. Decking, DESY; J. Gareyte, CERN; W. Kozanecki, CEA/Saclay;  
 K. Kubo, KEK; N. Phinney, SLAC; J. Rogers, Cornell; A. Seryi, SLAC;  
 N. Walker, DESY; A. Wolski, LBNL

This group considered luminosity issues in all the beamlines between the exit of the main damping rings and the interaction point. This includes the bunch compressor, the main linac, and the beam delivery system.

The luminosity parameters which were considered were emittance growth and beam jitter generated in the beamlines. The beam dynamics issues studied included single bunch and multibunch wakefields due to rf structures and collimators, chromatic emittance growth, beam jitter due to natural and cultural noise sources, synchrotron radiation, and beam-beam effects. Simulations were performed to study static-error tuning algorithms for each machine, using several different programs. The effect of dynamic misalignments on luminosity performance, including the effects of feedback systems, was evaluated.

### 4. Machine-Detector Interface (Section 7.4)

Members: **W. Kozanecki**, CEA/Saclay (Subgroup leader); N. Phinney, SLAC;  
 J. Rogers, Cornell; D. Schulte, CERN; A. Seryi, SLAC; R. Settles, MPI;  
 N. Walker, DESY

This group studied the issues related to the machine-detector interface. The systems that were examined include the interaction region, the spent-beam extraction lines, the background-suppression systems (post-linac collimation and synchrotron-radiation masking), and the beam-energy and beam-polarization diagnostics. The essential design choices (many of which are fundamentally linked to the crossing-angle issue) were examined from the viewpoints of beam-beam and single-beam backgrounds; detector coverage; stabilization, magnet technology and integration of final-doublet quadrupoles; technical feasibility and operability of the extraction line; and performance of the proposed collimation schemes in the presence of beam halo.

### 5. Reliability and Operability (Chapter 8)

Members from the Luminosity Performance Group:

**N. Phinney**, SLAC (Subgroup leader); R. Assmann, CERN;

W. Kozanecki, CEA/Saclay; D. Schulte, CERN; N. Walker, DESY

This group studied the impact of the design integrated luminosity performance on the required reliability of components and subsystems, and on the overall operability of the linear collider complex.

Because this topic is so intimately coupled to technology, this subgroup joined together with a similar subgroup from the Energy and Technology Performance Group. In addition to a consideration of the direct impact of component failure and replacement time on machine uptime, the group also considered requirements on the machine protection systems, and attempted to evaluate the tuning time required to re-establish the luminosity after a failure. The analysis and conclusions of this joint group are presented in Chapter 8.

### 7.1.3 Subgroup Report Structure

The reports of the subgroups presented in the three subsequent sections of this chapter have been organized in a parallel fashion. Each section begins with an overview, which sets the stage for the rest of the section. The major issues affecting the luminosity at the reference energy (500 GeV c.m.) are then presented. This constitutes the bulk of the work.

Luminosity issues at the upgrade energy are briefly considered in a dedicated subsection. Each section includes a ranked list of recommended R&D items, and closes with an assessment of the feasibility of the system, together with a prioritized list of concerns. Note that in Section 7.2 and Section 7.3, when the Damping Ring or LET working group concludes that the “feasibility” of a certain result is established, it means that the working group believes that this result, for example, luminosity performance, can realistically be approached or reached, but not necessarily without a considerable amount of work and time for machine tuning. This is in contrast to the criterion for “feasibility” of system designs in Chapter 6 where it is expected that specifications, for example, to reach a certain rf power or beam energy, must be met at the outset.

The R&D items are ranked according to the following criteria:

**Ranking 1:** R&D needed for feasibility demonstration of the machine

**Ranking 2:** R&D needed to finalize design choices and ensure reliability of the machine

**Ranking 3:** R&D needed before starting production of systems and components

**Ranking 4:** R&D desirable for technical or cost optimization

The R&D items associated with all three subsystems are collected in Chapter 9 in a comprehensive list, ranked and sorted by machine.

## 7.2 DAMPING RINGS

### 7.2.1 Introduction

#### 7.2.1.1 System Description

In this section we consider luminosity-related issues for the TESLA and JLC-X/NLC damping rings, from the injection kickers to the extraction kickers. Finally, as noted in Section 3.3, the beamline optics for the JLC-X and NLC designs differ slightly due to different optimizations. In this section, we only analyzed the NLC optics; however, the JLC-X optics is similar, and thus the designs are frequently referred to as the JLC-X/NLC design. A full solution for the CLIC damping ring lattice that satisfies the necessary requirements, including dynamic aperture, was not available to the committee at the time of the report and was therefore not evaluated in detail. TESLA uses one damping ring for electrons and one for positrons. To accommodate the large number of bunches, the TESLA damping rings each have a 17 km circumference and share the tunnel with the TESLA linac, leading to an unconventional “dog-bone” design. JLC-X/NLC and CLIC damp the positrons in a pre-damping ring (PPDR) with a large acceptance before transfer to a positron main damping ring (MDR). In these designs a single damping ring is used for electrons. The JLC-X/NLC and CLIC main damping ring designs are similar to the ATF damping ring, with which there is a great deal of operational experience.

#### 7.2.1.2 Luminosity Issues

We consider the extracted beam parameters which are relevant for emittance preservation in the subsequent parts of the machine and the luminosity. These are: the extracted vertical, horizontal, and longitudinal emittances; variation (train-to-train and along the train) of extracted  $\langle x \rangle$ ,  $\langle x' \rangle$ ,  $\langle y \rangle$ ,  $\langle y' \rangle$ ,  $\langle \Delta t \rangle$ , and  $\langle \Delta p/p \rangle$ ; extracted electron polarization; and particle loss.

Critical issues for emittance preservation and luminosity are:

- Correction of vertical emittance in the misaligned damping rings.
- Control of impedance to avoid the longitudinal microwave instability.
- Ion-related tune shift and instability in the electron damping rings.
- Electron-cloud-related tune shift and head-tail and coupled bunch instabilities in the positron damping rings.
- Dynamic aperture in the presence of wiggler nonlinearities.

### 7.2.2 Experience at Operating Machines

#### 7.2.2.1 Introduction

The linear collider damping ring designs should be evaluated in the context of operational experience with similar machines: the SLC damping rings, third generation light sources,

and the ATF damping ring. The linear collider damping ring designs, the ATF damping ring, and the third generation light sources have the common goal of maintaining a very low vertical emittance and low beam jitter. The ATF damping ring is the only ring which has achieved a vertical emittance close to that required for the planned linear collider damping rings. Third generation light sources, which need to maintain a long Touschek lifetime, do not attempt to achieve a vertical emittance as low as needed for the planned damping rings. The ATF was able to reach its target emittance (roughly a factor of 2 larger than the design emittance of the planned damping rings) even in the presence of substantial ambient temperature fluctuations, which would be much smaller in the case of the underground enclosures planned for the linear collider designs. The ATF uses combined function magnets, which complicate tuning and beam-based alignment (because the quadrupole magnets cannot be varied independently of the dipoles). The ATF serves as a good testbed for tuning and alignment techniques, especially for the JLC-X/NLC MDR and CLIC MDR, which also use combined-function magnets. The ATF is sensitive to intrabeam scattering due to its low emittance and low (1.3 GeV) energy, and has been used extensively to investigate intrabeam scattering. All of the planned damping rings use wigglers to provide most of the damping. The ATF usually operates with its damping wigglers off, so experiments in other machines may be necessary to gain experience with wiggler-related effects.

The SLC experience emphasized the importance of low particle losses and the suppression of collective instabilities. Based on the SLC experience, particle losses and extracted beam stability are likely to be more important for integrated luminosity than extracted emittance. Excessive loss leads to radiation damage and downtime for the replacement or repair of damaged components. Beam instability and jitter can lead to severe instantaneous luminosity reduction, and can cause fluctuating backgrounds which make the machine inoperable. In contrast, because of the expected emittance growth in the linac, the dependence of the luminosity on the extracted emittance is weak (less than linear).

### 7.2.2.2 Experience at the SLC Damping Rings

**7.2.2.2.1 Particle Loss** The linear collider damping rings differ from the third generation light sources in that there is a very large average beam power entering the rings. In the SLC, the average beam power was approximately 2 kW in the  $e^-$  ring and 1.2 kW in the  $e^+$  ring. The capture efficiency was 90 to 95% for  $e^-$  and 70 to 80% for  $e^+$  (due to the larger incoming emittance for  $e^+$ ), so there were losses of 100 to 200 W at 1.19 GeV in both rings. This particle loss caused the failure of kicker magnets, resulted in the replacement of all of the permanent magnet sextupoles, damaged coils in the dipole and quadrupole magnets, and damaged sputter ion pump cables. Some of these component failures could have been avoided with a different, radiation-resistant design. However, the average beam power entering the linear collider damping rings is one to two orders of magnitude larger than that entering the SLC damping rings. The capture efficiency for all damping ring designs must be close to 100%.

**7.2.2.2.2 Beam Stability and Jitter** The SLC damping rings suffered from several operationally significant collective instabilities. A longitudinal coupled bunch  $\pi$ -mode instability was cured with a passive cavity. Subsequently, a longitudinal microwave

instability was diagnosed, which had a relaxation-oscillator behavior, and created a sawtooth in the bunch length and phase [1]. The phase jitter caused the occasional loss of beam on collimators in the linac, or in the IR, tripping off the detector.

For a month following a vacuum accident in the  $e^-$  ring, the vertical emittance was degraded by a factor of 4–20. Ions were trapped in the beam immediately after injection when the beam was large. As the beam shrank a coherent ion instability occurred.

Fast temperature changes due to the beam being turned on and off, and slow ones due to access to the machine and to seasonal variation, caused significant changes of the extracted orbit and the ring circumference, respectively.

**7.2.2.2.3 Damping Times** The measured transverse damping times were somewhat longer than the calculated values and varied with time. These damping times remain unexplained.

### 7.2.2.3 Experience at Third Generation Light Sources

**7.2.2.3.1 Vertical Emittance** The vertical geometric emittances specified for the linear colliders are smaller than the emittances that have been achieved in the third generation light sources. The TESLA damping ring specifies an equilibrium vertical emittance below 1.4 pm·rad (0.014  $\mu\text{m}\cdot\text{rad}$  normalized), while the JLC-X/NLC damping ring vertical emittance must be below 3.4 pm·rad (0.013  $\mu\text{m}\cdot\text{rad}$  normalized). The lowest vertical emittances that have been claimed to date in the ATF and third generation light sources are in the range 10–15 pm·rad [2, 3]. The corresponding beam sizes are on the order of 10  $\mu\text{m}$ . Some direct measurements have been made of emittances in this range, but the data often depend on studies of Touschek lifetime. The equilibrium emittance ratio  $\epsilon_y/\epsilon_x$  must be less than 0.18% in the TESLA damping rings and less than 0.59% in the JLC-X/NLC main damping rings. The NSLS X-ray ring, SPring-8, and Swiss Light Source (SLS) have reported emittance ratios of 0.1% or less, and several other storage rings have reported ratios of 0.5% or less.

**7.2.2.3.2 Beam Jitter** Transverse beam jitter is due to correlated motion of the quadrupole magnets (from certain types of ground motion) or uncorrelated motion (due to other types of ground motion, or vibration from local sources). The measured quadrupole magnet vibration in the APS (after the addition of viscoelastic pads and welding of cooling water headers to the tunnel ceiling) was 90 nm rms in a 4 to 50 Hz band [4]. Roughly half of the vibration was due to the flow of cooling water.

The beam in a linear collider damping ring can be stabilized by a local orbit feedback at the extraction point. The SLS reports that a global orbit feedback operating at correction rates of up to 1 Hz stabilizes the beam position and angle at the insertion devices to  $\sim 0.6 \mu\text{m}$  rms and  $\sim 0.3 \mu\text{rad}$  rms [5]. This level of stabilization is better than what is needed for the extraction point of the TESLA or JLC-X/NLC damping rings.

### 7.2.2.4 Experience at the ATF Damping Ring

**7.2.2.4.1 Emittance Correction Algorithm** The tuning method to minimize the vertical emittance of the ATF damping ring is a series of three corrections based on orbit measurements: (i) COD (closed orbit distortion) correction; (ii) vertical COD and dispersion correction; and (iii) Coupling correction. These corrections minimize, respectively, the following quantities:

$$\sum_{\text{BPM}} x_{\text{meas}}^2 \quad \text{and} \quad \sum_{\text{BPM}} y_{\text{meas}}^2 \quad (\text{i})$$

$$\sum_{\text{BPM}} y_{\text{meas}}^2 + r^2 \sum_{\text{BPM}} \eta_{y,\text{meas}}^2 \quad (\text{ii})$$

$$C_{xy} \equiv \sum_{\text{steer BPM}} \left[ \sum (\Delta y)^2 / \sum (\Delta x)^2 \right] \quad (\text{iii})$$

Here  $x_{\text{meas}}$ ,  $y_{\text{meas}}$  and  $\eta_{y,\text{meas}}$  are the horizontal position, vertical position and vertical dispersion at each BPM. The factor  $r$  is the relative weight of the dispersion and COD, and it was chosen to be 0.05 based on the results of a simulation study. The horizontal and vertical position responses to each horizontal steering magnet are  $\Delta x$  and  $\Delta y$ . Usually two horizontal steering magnets, separated in betatron phase by  $\approx 3\pi/2$  horizontally and  $\pi/2$  vertically, are chosen for this correction. In the COD correction and the vertical COD + dispersion correction, steering magnets (48 horizontal and 51 vertical) are used. For the coupling correction, trim coils of all 68 sextupole magnets, wired to produce skew quadrupole fields, are used.

**7.2.2.4.2 Simulations** To study this tuning method, simulations were performed with realistic magnet misalignments and random BPM errors [6]. The measured transverse offsets of all the magnets were used, with random offsets added to account for survey errors. Random rotation errors were also included. Each BPM was assumed to have random offset and rotation errors. These assumed errors are listed in Table 7.1.

TABLE 7.1  
Assumed errors in simulation

Magnet offset	measured + random 30 $\mu\text{m}$
Magnet rotation	random 0.3 mrad
BPM offset	random 0.3 mm
BPM rotation	random 20 mrad

The simulation suggests that the target vertical emittance of  $1.1 \times 10^{-11}$  m-rad, which corresponds to a normalized emittance of  $2.8 \times 10^{-8}$  m-rad, is likely to be achieved. The average simulated emittance and the fraction of seeds which gave an emittance less than  $1.1 \times 10^{-11}$  m-rad are listed in Table 7.2. Note that this should be regarded as the emittance in the zero intensity limit. Further simulation showed that the expected emittance strongly

TABLE 7.2  
Simulated vertical emittance after corrections

Correction	Average vertical emittance [ $\times 10^{-11}$ m·rad]	Fraction of seeds yielding emittance [ $< 1.1 \times 10^{-11}$ m·rad]
COD	2.3	20%
+ Dispersion	1.7	51%
+ Coupling	0.58	91%

depends on the BPM offset error. If the BPM offset error is assumed to be 0.1 mm rather than 0.3 mm, then the average simulated vertical emittance after corrections is reduced to  $0.27 \times 10^{-11}$  m·rad.

**7.2.2.4.3 Experiments** In the experiments the typical measured rms COD, rms vertical dispersion and  $C_{xy}$  are consistent with the simulated COD (including the effects of BPM offset and rotation error), vertical dispersion and  $C_{xy}$  after corrections. The consistency suggests that the error assumptions of the simulation are valid.

The beam size in the damping ring (DR) is measured using two kinds of monitors. One is a two-slit optical interferometer which measures the interference pattern created by the synchrotron radiation (SR monitor). The other is a laser-wire monitor using a thin horizontal “wire” of light created in an optical cavity. As the laser wire is scanned vertically the photons Compton-scattered by the beam are detected.

In the extraction line, the beam size is measured using tungsten wire scanners. There are five wire scanners in the dispersion-free region of the beam line. The emittance is determined using the measured beam sizes and beam optics between the wire scanners.

Figure 7.1 shows the emittance as a function of the bunch intensity. The left figure shows the horizontal emittance measured in the extraction line. The right figure summarizes measurements of the vertical emittance using the laser wire monitor and the wire scanners on different days with different conditions, but all after low emittance tuning. The curves in these figures are from calculations, including intrabeam scattering, using the SAD program [7] assuming emittance ratios (ratio of vertical to horizontal emittance) of 0.002, 0.004, and 0.008.

The measured horizontal emittance agrees well with the calculation. There was a large variation in the measured vertical emittance on different days, suggesting different conditions in the damping ring or in the extraction line. The diagnostics used for the vertical emittance measurements were at their resolution limit, and work on these measurements is continuing. It was concluded that the vertical emittance, extrapolated to zero current, was smaller than  $1.1 \times 10^{-11}$  m·rad, corresponding to a normalized emittance of  $2.8 \times 10^{-8}$  m·rad at 1.3 GeV.

**7.2.2.4.4 Intrabeam Scattering** Due to the high electron density and relatively low beam energy (1.3 GeV), strong intrabeam scattering (IBS) was observed in the ATF DR. Intrabeam scattering is expected to have a much smaller effect at the TESLA and

# LUMINOSITY PERFORMANCE WORKING GROUP ASSESSMENTS

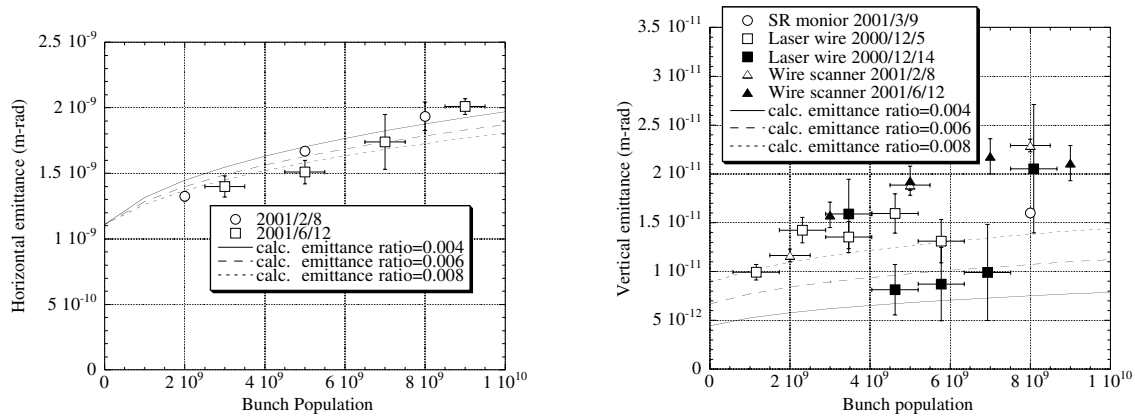


FIGURE 7.1. Left: Horizontal emittance measured in the extraction line versus bunch intensity. Right: Vertical emittance measured in the damping ring and in the extraction line versus bunch intensity. The curves are from calculations assuming emittance ratios of 0.004, 0.006, and 0.008.

JLC-X/NLC damping rings. The increase of the horizontal emittance with intensity is shown in Figure 7.1. The effect is more clearly observed in the energy spread. In order to evaluate the energy spread of the extracted beam, the horizontal beam size was measured using a screen monitor at a high dispersion region in the extraction line.

The left side of figure of Figure 7.2 shows the energy spread measured in the extraction line as a function of the bunch intensity. The intensity dependence of the horizontal emittance and the energy spread agree with the intrabeam scattering calculation, assuming a zero current emittance ratio between 0.004 and 0.008.

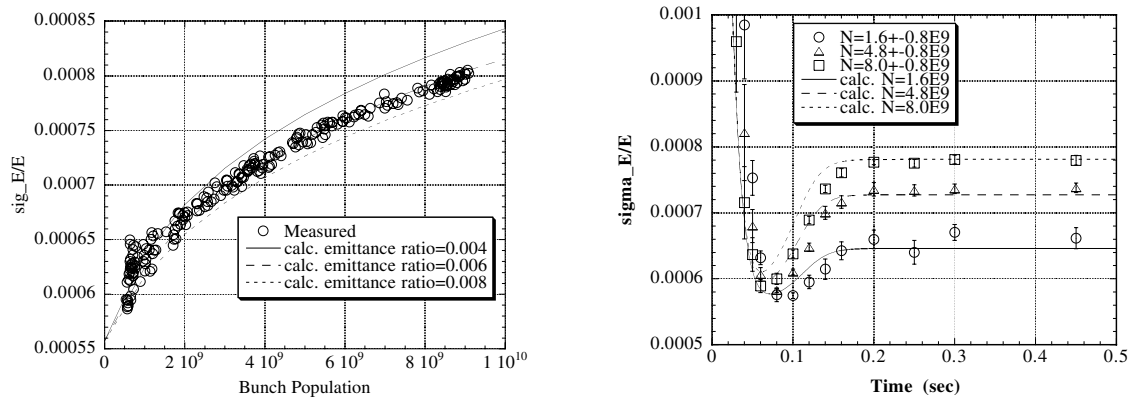


FIGURE 7.2. Left: Energy spread measured in the extraction line versus bunch intensity. The curves are from calculations assuming emittance ratios of 0.004, 0.006, and 0.008. Right: Energy spread versus store time for three different bunch intensities. The curves are from calculations assuming an emittance ratio of 0.006.

The right side of Figure 7.2 shows the energy spread as a function of store time in the damping ring at different intensities. The horizontal emittance was also measured in the extraction line as a function of the store time. The results show that the beam energy spread and the horizontal emittance exhibit a minimum at a store time of 70 ms, before reaching stable equilibrium values. This behavior is explained by the fact that the vertical damping time (calculated to be 27 ms) is longer than the longitudinal (20 ms) and horizontal (17 ms) damping times. At first, while the vertical emittance is still large, the longitudinal and horizontal emittances are damped. Later, the vertical emittance becomes smaller, so intrabeam scattering increases the longitudinal and horizontal emittances. The curves are from simulations based on SAD, assuming an emittance ratio of 0.006.

The calculation of intrabeam scattering has uncertainties, particularly in the value of the Coulomb log factor [7]. For the design of future damping rings it is necessary to understand the reliability of the calculation. The measured data are consistent with the SAD calculation assuming an emittance ratio of 0.006. However, the accuracy of the theory cannot be evaluated because of the uncertainties in the measurement of the vertical emittance. A report comparing different theoretical models with data from the ATF shows consistency between the experiments and theory, if a zero current emittance ratio between 0.004 and 0.008 is assumed, and the Coulomb logarithm is allowed to vary [8]. Better measurements of the vertical emittance are needed to fully validate the theory.

## 7.2.3 Extracted Emittances

### 7.2.3.1 Introduction

The extracted emittances from the damping rings have a direct influence on the emittance at the interaction point and the luminosity of the collider. The emittances of the beams extracted from the damping rings depend on the equilibrium emittances, the damping rates and store times. The equilibrium emittances are dependent on the tuning and alignment of the lattice, collective effects such as intrabeam scattering, and impedance-driven emittance growth. The vertical divergence of the radiation introduces a fundamental lower limit on the vertical geometrical emittance of 0.11 pm·rad and 0.24 pm·rad, for the TESLA DR and JLC-X/NLC MDR, respectively. Mismatch of the linear or nonlinear injection phase space can increase the effective injected beam size, and this can increase the extracted emittance.

The principal alignment issues are those which increase the vertical emittance, either through the generation of vertical dispersion or from betatron coupling. Coupling correction systems are specified and designed to minimize the vertical emittance generated by these effects. We first consider the alignment tolerances in the JLC-X/NLC and TESLA damping rings, and describe the respective coupling correction schemes, before evaluating the effectiveness of these schemes. We then discuss various collective effects, and complete the discussion by considering emittance dilution from the extraction systems. Our calculations include: a correction model; misalignment and ATL ground motion models; a lattice with sextupoles and wigglers; rf parameters; intrabeam scattering; an extraction kicker model; impedance, electron cloud, and ion effects.

### 7.2.3.2 Alignment Tolerances

The low target values for the emittance in the damping rings are demanding, and will require the effective use of a combination of techniques for correcting both the dispersion and coupling. Vertical emittance generation and correction have been studied in the TESLA and JLC-X/NLC damping rings using analytical estimates and simulations. The simulation codes, MAD and MERLIN, have each been applied to both rings. Only a restricted subset of the errors and limitations that are to be expected in practice have so far been considered in any detail. These are:

- Quadrupole vertical alignment errors
- Quadrupole rotations about the beam axis
- Sextupole vertical alignment errors
- Limited BPM resolution
- BPM vertical alignment errors

The BPM resolution limits the precision with which the dispersion may be measured. Since dispersion correction to better than 1 mm is generally required, if the energy variation is limited to the order of 0.1% the BPM resolution must be 1  $\mu\text{m}$  or better.

Demonstration of effective emittance correction in simulations at the present level is a necessary but not sufficient condition for the ability of the designs to achieve the specifications. The simulations may also give some indication of the likely difficulty of achieving the specified emittances given a more complete set of machine errors, although this involves some subjective judgment.

Other considerations that will likely be important, and should be included in further simulations, are:

- Dipole vertical alignment<sup>1</sup> and rotation errors
- Horizontal orbit and dispersion errors
- Optics errors arising from focusing variations
- BPM rotations
- Effects of nonlinear wiggler fields
- Limitations from malfunctioning BPMs and correctors
- Tuning of the skew quadrupoles used to implement beam coupling in the TESLA damping ring

---

<sup>1</sup>This is potentially more important for combined-function dipoles as in the JLC-X/NLC main damping rings

Both TESLA and JLC-X/NLC tuning algorithms depend on application of response matrices, which need to be accurately determined and, in the simulations, are calculated for the ideal machine. The effectiveness of the correction can be sensitive to the response matrices. Verification of storage ring optics by analysis of the measured response matrices has been applied at a number of machines and has proven a valuable technique.

**7.2.3.2.1 Sensitivity Indicators and Estimates** To understand the performance requirements on the damping rings, it is useful to estimate the sensitivity of the ring to random misalignments. In a storage ring, the equilibrium vertical emittance is determined by the residual vertical dispersion and betatron coupling in the bending magnets (including the wigglers) where the beam emits synchrotron radiation. Usually the betatron coupling and vertical dispersion are generated by errors distributed around the ring. There are three main driving terms: closed orbit offsets, quadrupole rotations, and vertical sextupole misalignments. It is straightforward to estimate the contributions to the vertical equilibrium emittance from random quadrupole rotations and sextupole misalignments. The effect of the closed orbit offsets is more difficult to calculate because it depends on detailed correlations from point to point; however, the sensitivity also tends to be much weaker than for either of the other effects.

Table 7.3 compares the energy, circumference, and typical operating emittances of the Advanced Light Source (ALS), the Advanced Photon Source (APS), the ATF at KEK, and the Swiss Light Source (SLS), with the NLC and TESLA damping rings. Although the synchrotron radiation facilities have operated with small  $\varepsilon_y/\varepsilon_x$  emittance ratios, only the ATF approaches the emittance values that are required in the linear collider damping rings.

TABLE 7.3

Comparison of calculated sensitivities in operating rings with the NLC and TESLA damping rings.  $Y_{\text{align}}$ : sextupole vertical misalignment; Roll align: quadrupole roll alignment;  $Y_{\text{jitter}}$ : quadrupole vertical jitter;  $\Delta k/k$ : fractional quadrupole strength error. [9]

Parameter	ALS	APS	ATF	SLS	NLC MDR	TESLA DR
Energy [GeV]	1.9	7	1.3	2.4	2	5
Circumference [m]	200	1000	140	288	300	17,000
$\gamma\varepsilon_x$ [ $\mu\text{m}\cdot\text{rad}$ ]	24	34	2.8	23	2.2	8
$\gamma\varepsilon_y$ [nm·rad]	500	140	28	70	13	14
$Y_{\text{align}}$ [ $\mu\text{m}$ ]	135	74	87	71	31	11
Roll align [ $\mu\text{rad}$ ]	860	240	1475	374	322	38
$Y_{\text{jitter}}$ [nm]	850	280	320	230	75	76
$\Delta k/k$ [0.01%]	1.5	1.4	2.1	1.5	1.8	1.1

Table 7.3 presents, in its lower half, two sets of numbers that describe the sensitivities of the rings to random errors due to vertical misalignments of the sextupoles or rolls of the quadrupoles. These numbers assume purely uncorrelated errors and are equal to the values that would generate the equilibrium vertical emittance. Following these are the values of

the random vertical quadrupole motion that would cause beam motion equal to the beam size and quadrupole strength fluctuations that would lead to an  $x$  or  $y$  tune shift of 0.001. It should be noted that none of these values are alignment tolerances. The real misalignments of the components will not be purely random and the actual tolerances must include the effectiveness of the emittance correction procedures, which are discussed in the following section. However, the values in Table 7.3 are useful to compare the *relative* difficulty of operating the rings to the linear collider damping rings. One can see that the vertical alignment sensitivities are typically  $\sim 100 \mu\text{m}$  in the operating facilities while they are about 40 and  $15 \mu\text{m}$  in the NLC and TESLA rings, respectively. The operating rings typically have a roll sensitivity that is a few hundred  $\mu\text{rad}$ , which is similar to the NLC ring, but the TESLA ring is roughly an order-of-magnitude tighter. The jitter sensitivities, in the operating rings, are a few hundred nanometers while those in the NLC and TESLA damping rings are a factor of 3 tighter. Finally, the sensitivities to the quadrupole strength errors are typically 0.01% and are not significantly tighter in the damping rings.

The alignment and jitter sensitivities indicate that the operation and emittance tuning of the linear collider damping rings should not be vastly different than in the operating synchrotron radiation facilities and, in this sense, the damping ring operation should be possible. However, while not vastly different, the damping rings will require more effort to control and stabilize the beam than has been typically achieved. Since the radiation facilities already devote significant effort to achieving excellent beam stability, the required improvement over those results could be significant. Although vertical emittance is an important parameter for a light source (a lower emittance gives a higher brightness photon beam) the radiation facilities generally do not attempt the lowest possible emittances in standard operation, since this has a detrimental effect on the beam lifetime. Thus, although some light sources have achieved vertical emittances close to those required in the damping rings, there is limited experience in tuning operating storage rings for such conditions.

### 7.2.3.3 Vertical Emittance Correction

The ATF has achieved a vertical dispersion of 3 mm rms, using BPMs with an intrinsic resolution of 20 to  $40 \mu\text{m}$ , and averaging. Assuming that the TESLA and JLC-X/NLC damping ring BPMs achieve an intrinsic resolution of  $1 \mu\text{m}$ , dispersion correction to levels well below 1 mm rms in TESLA and JLC-X/NLC should be straightforward. Achieving the unprecedented vertical emittance in the TESLA or JLC-X/NLC damping rings will be challenging, but there are no indications that the damping ring emittance goals are unrealistic.

**7.2.3.3.1 Evaluation of TESLA DR Emittance Correction Algorithm** The TESLA correction system uses a BPM and steering magnet located at every quadrupole. Initial correction uses a combined orbit and dispersion response matrix to set the steering magnet strengths. This generally brings the vertical emittance to less than a few times the target, with further dispersion correction usually being effective in reaching the target.

The correction algorithm acts only in the vertical plane and is appropriate for an uncoupled machine. When the coupling bump is turned off, a global correction is achieved for 85% of random seeds. With the coupling bump, the success rate is 70%. The TESLA damping ring correction algorithm should be improved to accommodate the coupling bump.

**7.2.3.3.2 Evaluation of JLC-X/NLC MDR Emittance Correction Algorithm** The JLC-X/NLC MDR correction system consists of BPMs placed at each quadrupole, with the quadrupoles and sextupoles positioned on movers. An orbit correction is first performed using the response matrix between the BPMs and the quadrupole movers, and a dispersion correction is then applied in an analogous fashion, using a response matrix between the vertical dispersion at the BPMs and the sextupole movers.

In practice, this simple correction strategy is effective since it minimizes local errors. For a given set of misalignments, the correction system is capable of meeting the specification for the vertical emittance in about 90% of cases.

**7.2.3.3.3 Summary** Table 7.4 summarizes the evaluation of the vertical emittance correction. We find that:

- In a simulation model including the most important misalignments and limited BPM resolution, the emittance (disregarding collective effects) is corrected to below the design level for most, but not all, random seeds. The margin is adequate for both TESLA and JLC-X/NLC. Experiments in the ATF give confidence that the simulation models work well, and additional correction strategies will tend to widen the margin.
- When the coupling bump is turned on in the TESLA damping ring, the vertical-only correction is not as effective. It is expected that when horizontal correction is added, the correction algorithm will be effective for TESLA with the coupling bump.

TABLE 7.4

Summary of vertical emittance correction evaluation. All simulated misalignments and rolls have a Gaussian distribution truncated at  $3\sigma$ .

	TESLA DR	NLC MDR
Quadrupole vertical misalignment [ $\mu\text{m}$ rms]	100	100
Quadrupole roll [ $\mu\text{rad}$ rms]	100	100
Sextupole vertical misalignment [ $\mu\text{m}$ rms]	100	100
BPM resolution [ $\mu\text{m}$ ]	1	0.5
BPM vertical misalignment <sup>a</sup> [ $\mu\text{m}$ rms]	10	5
Energy variation [%] for dispersion measurement	$\pm 0.2$	$\pm 0.1$
Fraction of random seeds for which the vertical emittance is corrected to less than the design value [%]	85 (no coupling bump) 70 (with coupling bump)	90

<sup>a</sup> Relative to the design orbit.

### 7.2.3.4 Fast and Slow Ground Motion

The amplitude of fast magnet motion following from the standard ground motion models [10] is too small to have an effect on emittance. Slow magnet motion may be described by the ATL model, which gives temporal and spatial correlations in reasonable agreement with observations. We have used a 2-dimensional implementation of the model in MERLIN to estimate the timescale over which orbit and dispersion correction need to be applied.

**7.2.3.4.1 Evaluation** Figure 7.3 and Figure 7.4 show the normalized vertical emittance in the TESLA damping rings and the JLC-X/NLC main damping rings resulting from diffusive (ATL) ground motion, for noisy ( $A=10^{-17}$  m<sup>2</sup>/m/s) and intermediate ( $A=5\times 10^{-19}$  m<sup>2</sup>/m/s) sites. Starting from lattices with the only misalignments being 100  $\mu$ rad rms rotations of the quadrupoles about the beam axes, 50 hours of ATL motion were applied, and the orbit and dispersion were corrected by using the procedure described above. The BPMs were fixed to girders, and thus moved with the ground motion, but not with the correction of the quadrupole positions using the magnet movers. ATL motion was then applied at hourly intervals up to 24 hours, either with no correction or with orbit correction only. No vertical dispersion correction was applied. Averages over 20 seeds are shown. An hourly orbit correction to 5  $\mu$ m rms is sufficient to maintain the vertical emittance well within tolerances for the TESLA DR and JLC-X/NLC MDR for both noisy and intermediate sites over a 24 hour period. Because the model includes only the most important effects, we expect that the correction will be somewhat less effective in the actual damping rings.

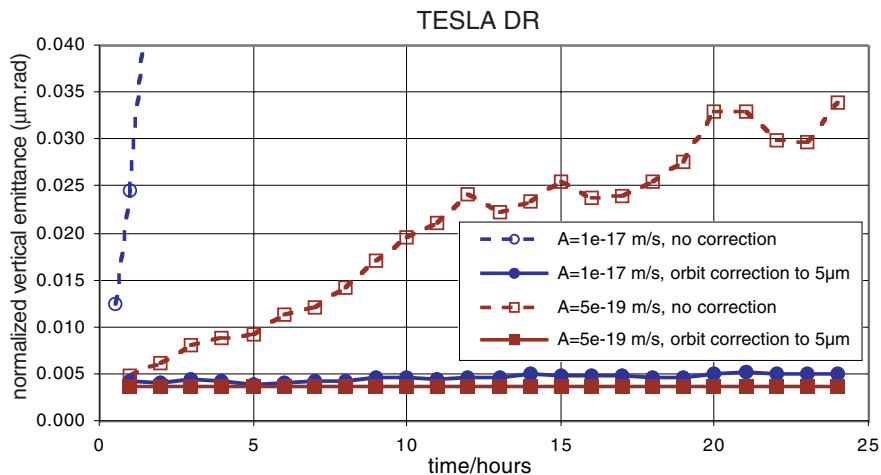


FIGURE 7.3. Vertical emittance in the TESLA damping rings resulting from diffusive (ATL) ground motion.

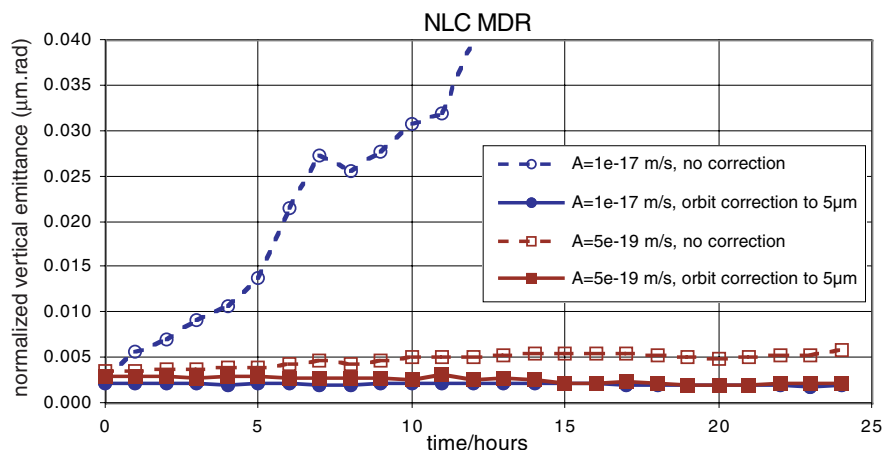


FIGURE 7.4. Vertical emittance in the NLC main damping rings resulting from diffusive (ATL) ground motion.

#### 7.2.3.4.2 Summary

- The effect of ground motion on the emittance can be continuously corrected in the TESLA damping rings and the JLC-X/NLC main damping rings using only hourly orbit corrections. As Figure 7.3 and Figure 7.4 show, dispersion correction, which is incompatible with luminosity production, is needed less than once per day.

#### 7.2.3.5 Classical Collective Instabilities

The high bunch density, together with the small value of the momentum compaction factor, make the damping rings prone to single bunch effects like the longitudinal microwave instability. The instability can only be avoided by making the beam enclosure sufficiently smooth. A very comprehensive calculation of the residual high frequency broad-band coupling impedance of the NLC damping rings has been done. Summing the calculated wakefields of the major components of the vacuum chamber gives a value of  $Z/n=25 \text{ m}\Omega$ , mostly resistive [11]. TESLA calculates  $Z/n=25 \text{ m}\Omega$  for the resistive part (mainly from kickers) and  $28 \text{ m}\Omega$  for the inductive part (mainly from bellows and BPMs). Using the Keil-Schnell-Boussard criterion for a rough estimate one finds a microwave instability impedance threshold of  $70 \text{ m}\Omega$  for the NLC MDR and  $59 \text{ m}\Omega$  for the TESLA electron DR at the design bunch intensities. Thus the impedance threshold is two to three times higher than the estimated impedance for both machines. Bunch lengthening is only about 5%. This looks comfortable, but experience has shown that impedances measured with beam in real machines are usually larger than anticipated. For instance measurements of bunch lengthening in the KEK ATF indicate a value of  $Z/n$  three times larger than calculated. Measurements of bunch lengthening in KEKB give values of  $Z/n$  ( $76 \text{ m}\Omega$  in the HER and  $72 \text{ m}\Omega$  in the LER) which are five times larger than the design values. We conclude that the vacuum chamber of the damping rings must be designed with extreme care in order to minimize its impedance.

Coupled bunch instabilities are also important in damping rings, owing to the large number of bunches stored. At low frequencies the resistive wall instability dominates and must be suppressed by feedback (up to about 10 MHz). Considerable experience has been gained in recent years on damping of higher rf cavity modes and on high frequency feedback. Residual effects can be suppressed by a bunch-by-bunch feedback as foreseen for JLC-X/NLC and TESLA.

### 7.2.3.5.1 Summary

- Experience with other modern machines indicates that extreme care will be needed to attain the low impedances required to avoid the single bunch longitudinal microwave instability in the TESLA damping rings and the JLC-X/NLC main damping rings.
- Coupled bunch instabilities can be suppressed using standard bunch by bunch feedback techniques.

### 7.2.3.6 Space Charge

Space charge should have negligible effects in damping rings except for TESLA where the space-charge induced tune spread would reach 0.26 in the vertical plane. Such a value is known to produce emittance increase through resonance crossing, though the effects in this case have not been quantified. A sixfold increase in the vertical emittance would reduce the tune spread to 0.1, a value thought to be tolerable, but with a sizeable luminosity penalty. Since most of the tune spread arises in the long straight sections, it is proposed to increase the beam dimensions there by fully coupling the transverse oscillations. This reduces the vertical tune spread to 0.06, which is expected to be tolerable. A difference in the vertical and horizontal tunes of 0.02 arising within the coupling bump region gives rise to a 10% vertical emittance increase outside the coupling bump. Much smaller tune differences can readily be achieved.<sup>2</sup> A variation of beam intensity or size of 10 to 20% is also of no practical importance for the bump closure.

### 7.2.3.6.1 Summary

- The coupling bump appears to be a satisfactory solution to the space charge tune spread in the TESLA damping rings.

### 7.2.3.7 Ion Effects in the Electron Damping Rings

The ion effects have been estimated based on a design vacuum pressure of  $10^{-9}$  Torr for both the JLC-X/NLC and TESLA damping rings.

---

<sup>2</sup>Phase measurements with a random error of less than  $0.2^\circ$ , which produces a tune change of 0.0006, are routinely made in CESR.

**7.2.3.7.1 Ion Trapping** Without an ion-clearing gap, all ions are trapped in the TESLA  $e^-$  DR. A gap of roughly 600 ns in the TESLA bunch train is needed to clear  $\text{CO}^+$  and lighter ions. Such a gap would create, through beam loading, a phase variation across the train of  $1.2^\circ$ . This small phase variation would not have significant consequences. The injection/extraction gaps in the JLC-X/NLC  $e^-$  MDR are sufficient for ion clearing.

**7.2.3.7.2 Tune Shift** In the JLC-X/NLC  $e^-$  MDR,  $\text{CO}^+$  and heavier ions accumulate during the passage of the bunch train. In the straight sections of the TESLA  $e^-$  DR, all ions accumulate, producing an unacceptable tune shift of 0.28 at the end of the bunch train. It may be necessary to design the TESLA  $e^-$  DR for a vacuum of  $10^{-10}$  Torr, especially in the straight sections.

**7.2.3.7.3 Fast Ion Instability** At the design vacuum pressure of  $10^{-9}$  Torr, the calculated growth time of the fast ion instability is of the order of 100  $\mu\text{s}$  in the TESLA  $e^-$  DR and the JLC-X/NLC  $e^-$  MDR. Although the very complex dynamics of this two-stream instability makes it difficult to predict the behavior of the beam from such a simple calculation, this is cause for concern. More precise evaluations using computer simulations are needed before the present designs can be validated.

#### 7.2.3.7.4 Summary

- The TESLA damping ring requires an ion-clearing gap of 600 ns.
- The TESLA damping ring should be designed for an average pressure of the order of  $10^{-10}$  Torr to avoid an unacceptably large tune spread.
- The fast ion instability may have a growth rate too fast to control with feedback in both the TESLA damping rings and the JLC-X/NLC damping rings. There are very large uncertainties in the estimate of the growth rate. If simulations or experiments show that the growth time is less than a few hundreds of  $\mu\text{s}$ , then a redesign of the vacuum system for substantially lower pressure may be required.

#### 7.2.3.8 Electron Effects in the Positron Damping Rings

Electrons present in the vacuum chamber are accelerated toward the walls by the passage of the positron bunches. Upon impact secondary electrons are emitted, thus increasing the electron density. If the secondary electron yield (SEY) is sufficiently large, then the total number of electrons increases until global neutralization is reached. The initial electrons can be produced in large numbers by synchrotron radiation photons impinging on the vacuum chamber walls. In the JLC-X/NLC damping rings this source is largely suppressed since most of the photons escape into the antechamber. However, the small fraction which remains may constitute a sufficient seed. In any case there are always the electrons produced by beam ionization of the residual gas. All calculations and simulations suggest that neutralization is reached well before the end of the bunch train, even when starting from ionization electrons. Figure 7.5 shows the average electron density in the TESLA DR and JLC-X/NLC MDR chambers as a function of the SEY of the chamber material,

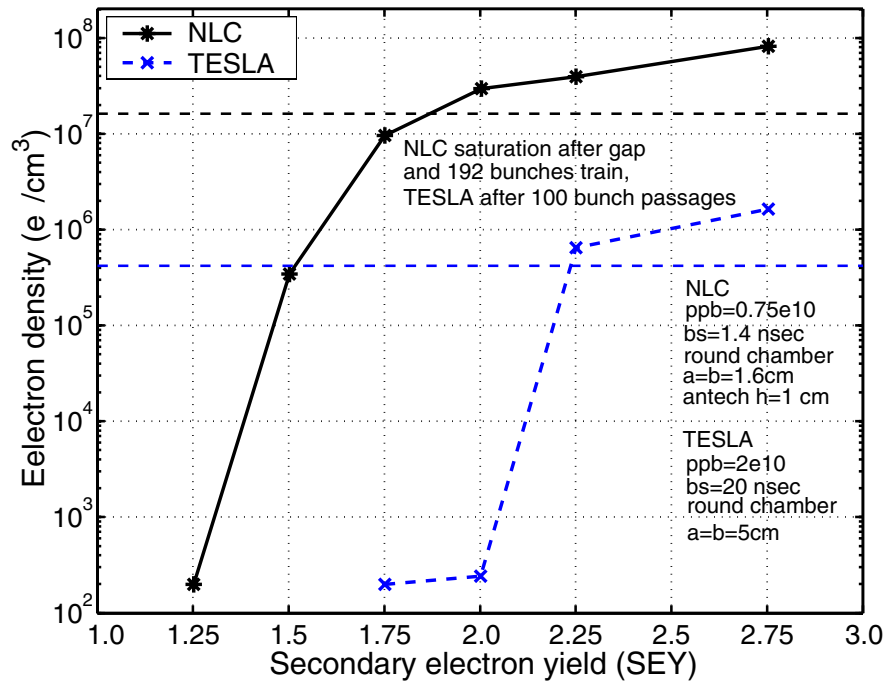


FIGURE 7.5. Average electron density versus secondary electron yield for the TESLA DR and the NLC MDR. The simulation uses only the round chamber geometry of the TESLA DR field-free straight sections, and only the chamber geometry (which includes an antechamber) of the field-free regions in the NLC MDR. The neutralization densities for NLC and TESLA are represented by the upper and lower horizontal dotted lines, respectively.

predicted by simulation. The simulation uses the round chamber geometry of the TESLA DR straight sections, and the chamber geometry (which includes an antechamber) of the field-free regions in the NLC MDR. Above a critical value for the SEY, the neutralization density is reached for both rings. The peak SEY at normal incidence is typically 1.0 to 1.5 for TiN coated copper, 1.4 to 1.7 for copper, and 2.2 for aluminum, depending on the preparation of the surface and scrubbing by the beam. Stainless steel, which has an SEY similar to copper, is likely to be unacceptable as a chamber material due to its high resistivity, which exacerbates the resistive wall instability.

When the neutralization density is reached, fast coupled bunch instabilities with growth times as small as 15 to 30  $\mu\text{sec}$  as well as single bunch instabilities are predicted. At this time the simulation results should be regarded as estimates, which must be refined, taking advantage of the constant progress of the knowledge in this field, both from experience and theory. Analytical estimates can be made of the incoherent tune shift, head-tail instability threshold, and coupled bunch instability growth time, by assuming global neutralization and a uniform electron density across the chamber [12]. These estimates are given in Table 7.5, and should be regarded as order-of-magnitude estimates only. The assumption of uniform electron density across the chamber is optimistic, because some simulation results indicate an enhancement of the electron density within the positron bunch of one to two orders of magnitude. We note that the fastest transverse feedback systems built to date

TABLE 7.5  
Analytical estimates of electron cloud effects in the damping rings.

	TESLA DR	JLC-X/NLC MDR	JLC-X/NLC PDR
Incoherent tune shift	0.06	0.019	0.003
Head-tail threshold charge/nominal charge	2.6	0.8	10
Coupled bunch growth time [ $\mu\text{s}$ ]	170	20	370

have a damping time for coupled bunch instabilities of a few hundreds of  $\mu\text{s}$ . Experience with  $e^+e^-$  colliders suggests that the maximum tolerable incoherent tune shift is of the order of 0.1. If the neutralization electron density is reached, then the estimated incoherent tune shift and coupled-bunch growth time in the TESLA damping ring are barely tolerable, and the JLC-X/NLC MDR is likely to suffer from both head-tail and coupled bunch instabilities. It is imperative for the success of these machines to suppress the electron cloud to well below the neutralization density. Possible cures are coating the chamber walls to reduce the secondary emission and superimposition of a magnetic field in otherwise field free regions. Gaps in the trains may also help suppress the electron cloud, but may be impractical due to the loss of luminosity and the increase of beam loading effects.

### 7.2.3.8.1 Summary

- Without intervention to reduce the electron cloud density well below the neutralization density, the damping rings are likely to suffer from an unacceptable incoherent tune shift, head-tail instability, or coupled bunch instability. The TESLA damping rings may be particularly susceptible to a large incoherent tune shift. The JLC-X/NLC main damping rings may be particularly susceptible to head-tail and coupled bunch instabilities.

### 7.2.3.9 Intrabeam Scattering

Intrabeam scattering limits the six-dimensional phase space density and therefore can be important in damping rings. Several computer programs exist to accurately calculate the effect of IBS. They are being checked by comparison with measurements done in the KEK ATF, described in Section 7.2.2.4. Calculated extracted emittances in the presence of IBS are listed in Table 7.6. We have used the Piwinski formalism. IBS has very little influence on the TESLA damping ring due to its relatively large energy. It has a small but significant influence on the horizontal and vertical emittances of the JLC-X/NLC main damping ring. There is significant theoretical uncertainty in the calculation of IBS growth rates, as described in Section 7.2.2.4. If it is found that IBS prevents the design emittances from being reached, then a lattice redesign or energy increase may be necessary. Such a change, if needed, is expected to be successful. IBS is a major problem for the design of the CLIC main damping ring, which must deliver extremely small emittances, and is an important driver in the optimization of the lattice.

TABLE 7.6  
Intrabeam scattering calculation results.

	TESLA DR		JLC-X/NLC MDR	
	$e^+$	$e^-$	$e^+$	$e^-$
Equil. $\gamma\epsilon_x / \gamma\epsilon_y$ (no IBS) [ $\mu\text{m}\cdot\text{rad}$ ]	8.0 / 0.014	8.0 / 0.014	2.2 / 0.013	2.2 / 0.013
Calculated extr. $\gamma\epsilon_x / \gamma\epsilon_y$ (with IBS) <sup>a</sup> [ $\mu\text{m}\cdot\text{rad}$ ]	8.1 / 0.014	8.1 / 0.014	2.5 / 0.018	2.5 / 0.017
Specified extr. $\gamma\epsilon_x / \gamma\epsilon_y$ [ $\mu\text{m}\cdot\text{rad}$ ]	8.0 / 0.020	8.0 / 0.020	3.0 / 0.020	3.0 / 0.020

<sup>a</sup> The values for TESLA assume that there is no coupling bump.

### 7.2.3.10 Extraction Kickers

An extraction kicker that does not turn off fully when the next stored bunch passes will deflect the stored bunch, ultimately increasing its emittance through filamentation. Preliminary simulations indicate that the residual kick must be held within the limits shown in Table 7.7 to avoid appreciable emittance growth through filamentation.

TABLE 7.7  
Acceptable residual extraction kicker deflection.

	TESLA DR	JLC-X/NLC MDR
Nominal deflection [mrad]	0.6	2.5
Maximum acceptable residual deflection [ $\mu\text{rad}$ ]	2–3	20–30
Maximum acceptable residual deflection/nominal deflection [%]	0.3–0.5	0.8–1.2

## 7.2.4 Extracted Beam Jitter

### 7.2.4.1 Introduction

Jitter in the quantities  $\langle x \rangle$ ,  $\langle x' \rangle$ ,  $\langle y \rangle$ ,  $\langle y' \rangle$ ,  $\langle \Delta t \rangle$ , and  $\langle \Delta p/p \rangle$  in the extracted beam can cause emittance growth downstream through wakefield and filamentation effects. We evaluate jitter from several significant sources. Our calculations include: a ground motion model; an extraction kicker model; and an rf system model.

### 7.2.4.2 Vertical Beam Jitter from Ground Motion and Vibration

Vertical motion of the quadrupole magnets will result in vertical orbit jitter and a jitter of the first moments  $\langle y \rangle$  and  $\langle y' \rangle$  of the extracted beam. Some types of ground motion result in a correlated motion of the quadrupole magnets. Other types of ground motion,

and vibration from local noise sources (*e.g.*, the flow of cooling water), result in uncorrelated motion. In this section we calculate the orbit jitter due to correlated and uncorrelated motion.

**7.2.4.2.1 Correlated Motion** We use the “quiet” (A), “intermediate” (B), and “noisy” (C) ground motion models of [10] (see also Section 7.3.4.1) with parameters of [13] to calculate the orbit jitter due to ground motion. These models contain both diffusive (ATL) motion and a set of elastic ground wave peaks. It is found that the ATL part of the ground motion spectrum has a negligible effect. Table 7.8 summarizes the predicted jitter of a bunch train from elastic ground waves in models A, B, and C. The jitter is negligible in models A and B, and still within tolerable limits in model C. In all cases the jitter within a single bunch train is negligible.

TABLE 7.8  
Predicted beam jitter from correlated ground motion.

Model	$\langle y \rangle_{rms} / \sigma_y$	
	TESLA DR	JLC-X/NLC MDR
A	0.0012	0.00054
B	0.016	0.0071
C	0.217	0.099

**7.2.4.2.2 Uncorrelated Motion** For both the TESLA DR and the JLC-X/NLC MDR, an uncorrelated vertical motion of the quadrupole magnets of approximately 80 nm rms would result in an orbit jitter equal to the vertical beam size. The measured quadrupole magnet vibration in the APS was reduced, with great effort, to 90 nm rms in a 4 to 50 Hz band [4], indicating that with considerable care it should be possible to keep the vibration in this range.

This degree of uncorrelated vibration is considerably larger than that due to ground motion, even with model C. It may be difficult to reach the pure ground motion level in damping rings, due to the high density of local noise sources, and the low resonant frequency of heavy magnet support systems. It should be noted, however, that local orbit feedback at the extraction point, such as has been demonstrated at the SLS ( $\sim 0.6 \mu\text{m}$  rms in position and  $\sim 0.3 \mu\text{rad}$  rms in angle [5]; see Section 7.2.2.3), should be capable of stabilizing the extracted beam position and angle jitter at the  $0.1 \sigma$  level.

### 7.2.4.3 Horizontal Beam Jitter from Extraction Kicker Errors

Bunch-to-bunch variation in the kick delivered by the extraction kicker leads to jitter in the horizontal motion of the extracted beam. A roll of the extraction kicker about the beam axis leads to a vertical kick to the extracted beam. This vertical kick is systematic and can be corrected by steering in the extraction line. Variations in the vertical kick due to jitter in

the kick strength are negligibly small. These parameters and errors are summarized in Table 7.9.

TABLE 7.9  
Nominal parameters and jitter in the damping ring extraction kickers.

	TESLA DR	JLC-X/NLC MDR
Horizontal deflection $\theta_x$ [mrad]	0.6	2.5
Specified bunch-to-bunch variation $\Delta\theta_x$ [ $\mu$ rad]	$\pm 0.42$ ( $\pm 0.07\%$ )	$\pm 1.25$ ( $\pm 0.05\%$ )
Specified roll angle [ $\mu$ rad]	$< 35$	$< 35^a$
Vertical deflection $\theta_y$ [mrad]	$< 21$	$< 88$
Normalized horizontal kick stability $\Delta\theta_x/\sigma_{x'}$	$\pm 0.11$	$\pm 0.052$
Normalized systematic vertical deflection $\theta_y/\sigma_{y'}$	$< 0.11$	$< 0.063$

<sup>a</sup> Assumed value for JLC-X/NLC MDR.

JLC-X/NLC plan to use a system in which two kickers are driven by a common source. The second kicker, a half-integer number of betatron wavelengths down the extraction line from the first kicker, cancels the jitter caused by the first kicker. The degree of cancellation that is possible is unknown. A single-bunch experiment [14] with a double-kicker system at the ATF showed a reduction of the net jitter by a factor of 3.3. The values in Table 7.9 do not include any horizontal jitter cancellation or effect of a second kicker on vertical deflection. Pulse-to-pulse variation in existing kicker systems is of the order of 0.1% [15].

#### 7.2.4.3.1 Summary

- A single well-designed extraction kicker may just suffice for the TESLA and JLC-X/NLC damping rings, but it is more likely that a double-kicker system (as planned for JLC-X/NLC) may be needed.

#### 7.2.4.4 Circumference Variations

The circumference of a ring may vary due to ground motion, earth tides, temperature variations, and magnet vibration. Only the diffusive (ATL) component of ground motion, earth tides, and temperature variations have significant effects on circumference, and each of these acts on long time scales of the order of a day or longer. These circumference changes will result in a variation of the beam energy. We consider changes on the time scale of one day, assuming that energy correction can be done daily. We assume a “noisy” ( $A=10^{-17}$  m<sup>2</sup>/m/s) ground motion model and a tidal strain of  $4\times 10^{-8}$  [16]. Table 7.10 summarizes the estimates of circumference and energy variation. Because of its large circumference, the TESLA damping ring is influenced by tides more than by ATL; the reverse is true for the JLC-X/NLC main damping ring. In all cases the energy variation is

TABLE 7.10

Estimates of circumference and energy variation due to ATL ground motion and earth tides.

	TESLA DR	JLC-X/NLC MDR
Circumference $C$ [m]	17,000	231
Circumference variation $\Delta C_{rms}$ (ATL) [ $\mu\text{m}$ ]	170	20
Circumference variation $\Delta C$ (tidal) [ $\mu\text{m}$ ]	680	9.2
Energy variation $\Delta E_{rms}/E$ (ATL)	$8.4 \times 10^{-5}$	$2.9 \times 10^{-4}$
Energy variation $\Delta E/E$ (tidal)	$3.3 \times 10^{-4}$	$1.4 \times 10^{-4}$

less than the energy spread of the beam. The effect of temperature is more difficult to estimate. Experience with other machines suggests that the small temperature variations expected for the damping rings will not have a significant effect on beam energy (see Section 7.2.2.2).

### 7.2.4.5 Longitudinal Phase Transients from Beam Loading

Random variations in bunch charge, gaps in the fill pattern, and transients in the beam current due to injection and extraction can cause variations in beam loading, which, in turn, affect the energy and rf phase of the extracted bunches. These beam loading variations were simulated using a macroparticle model for the bunches. Table 7.11 shows the parameters included in the simulations. The bunch population variation is an uncorrelated Gaussian random variable.

TABLE 7.11

RF system and lattice parameters for longitudinal jitter simulations.

	TESLA $e^+$ DR	TESLA $e^-$ DR	JLC-X/NLC MDR
Harmonic number $h$	28200	28200	714
Number of bunches	2820	2820	3 trains of 192
Slip factor $\eta$	$0.12 \times 10^{-3}$	$0.12 \times 10^{-3}$	$0.295 \times 10^{-3}$
Energy loss per turn $U_0$ [MeV]	21	12	0.792
RF voltage [MV]	54	36	1.07
Number of cavities	12	8	3
$R/Q$ per cavity [ $\Omega$ ]	45	45	118
$Q_L$	$1.1 \times 10^6$	$1.1 \times 10^6$	2273
Bunch population variation $\Delta N/N$	0.05 (peak-peak)	0.05 (peak-peak)	0.02 (rms)

For each of the rings the energy jitter at extraction is negligible compared with the energy spread of the beam. For the TESLA rings the size of the gap due to extraction is one missing bunch (assuming no ion clearing gap) and the phase jitter at extraction is dominated by beam loading due to the random bunch population variation. The phase jitter in the TESLA  $e^+$  DR ( $0.035^\circ$  rms at 500 MHz) and  $e^-$  DR ( $0.029^\circ$  rms) is roughly

0.05 mm or 1% of the bunch length. In Section 7.2.3.7, it was noted that an ion clearing gap of up to 600 ns will be needed for the TESLA  $e^-$  DR. This introduces, through beam loading, an additional systematic phase variation with a full width of  $1.2^\circ$ , which is roughly 2.0 mm, or 33% of the rms bunch length. For the JLC-X/NLC MDR the phase variation is dominated by the gap between trains. This phase slewing is systematic from train to train, with a full width of  $5.4^\circ$  at 714 MHz, which is 6.3 mm or 1.7 times the rms bunch length.

## 7.2.5 Particle Loss

### 7.2.5.1 Introduction

Particle loss in the damping rings must be minimal to reduce radiation damage, to prevent lost particles from intercepting beam diagnostics, and to avoid loss of bunch charge (and luminosity). We consider particle loss due to injection into the nonlinear lattice, and Touschek scattering. Our calculations include: a lattice with sextupoles and wiggler nonlinearities; physical apertures; and rf parameters.

### 7.2.5.2 Injection Efficiency

The injection efficiency of a damping ring depends on the 6-dimensional phase space distribution of the injected beam, including jitter, and is limited by the physical and dynamic apertures in the ring. Collective effects that can influence the dynamics should also be taken into account.

In damping rings, the wigglers give much larger energy losses than is common in conventional storage rings, and systematic nonlinearities in the wiggler fields can destabilize the dynamics to a significant extent. To estimate the severity of the effect, a description of the calculated field as a kick map may be constructed. A symplectic integrator using the kick map is then used in a tracking code to determine the dynamic aperture. This procedure, applied to the JLC-X/NLC main damping ring wiggler, is described in [17]. An attempt was made to apply the same procedure to the TESLA damping ring wiggler, but a good match of the kick map to the calculated field was not obtained. A linear hard-edged dipole model was used for the JLC-X/NLC positron pre-damping ring wiggler.

Preliminary results including sextupole magnets and nonlinear wiggler fields derived from field maps indicate that the dynamic aperture is limited by the wiggler nonlinearities in the TESLA damping rings and the JLC-X/NLC main damping rings<sup>3</sup>. The simulations indicate some particle loss at injection in the TESLA positron damping ring, for which the injected emittance is large. Optimization of the wiggler and/or lattice to improve dynamic aperture is needed. The dynamic aperture is more than adequate in the TESLA electron damping ring and the JLC-X/NLC main damping rings because of the much smaller injected emittance. Simulations of the JLC-X/NLC positron pre-damping ring with a linear hard-edged dipole wiggler model indicate adequate dynamic aperture. The simulations do not include systematic and random multipole errors or random wiggler errors, which may further reduce the dynamic aperture.

---

<sup>3</sup>When the tracking simulations use a linear hard-edged dipole wiggler model, the calculated dynamic aperture is much larger than when the nonlinear wiggler kick map is used.

Necessary work is in progress to: improve the calculation of wiggler fields, including end fields; to develop a more robust field fitting procedure; and to develop a dynamic model that will avoid many of the approximations required for the kick map approach. Future R&D should include wiggler prototyping and benchmarking the tracking calculations against experience in operating machines.

### 7.2.5.2.1 Summary

- Simulations of injection efficiency including sextupole magnets and nonlinear wiggler fields derived from field maps show that the dynamic aperture is limited by the wiggler nonlinearities in the TESLA damping ring and the JLC-X/NLC main damping rings. The simulations do not include systematic and random multipole errors or random wiggler errors, which may further reduce the dynamic aperture.
- The simulations indicate some particle loss at injection for the TESLA positron damping ring, because the injected emittance is large and the dynamic aperture is similar to the size of the injected beam. This indicates that an optimization of the wiggler and/or lattice to improve dynamic aperture is needed. The dynamic aperture is more than adequate in the JLC-X/NLC main damping rings because of the much smaller injected emittance.

### 7.2.5.3 Touschek Lifetime

The Touschek lifetime in low-energy, low emittance damping rings is short. For both the TESLA damping ring and the JLC-X/NLC main damping rings the Touschek lifetime is several orders of magnitude larger than the store time (see Table 7.12), so Touschek loss will not significantly decrease the bunch population. The short Touschek lifetime in the JLC-X/NLC MDR prohibits commissioning and tuning of the damping ring with long stores at nominal parameters. This is not expected to be a severe shortcoming.

The values of the Touschek lifetime listed in Table 7.12 assume a constant energy aperture of 1.0% for both TESLA and JLC-X/NLC. Careful studies of momentum aperture need to be made to better quantify the injection efficiency and the Touschek lifetime.

TABLE 7.12

Touschek lifetime at equilibrium emittance for a momentum aperture of 1.0%.

	TESLA DR	JLC-X/NLC MDR
Touschek lifetime [s]	1300	56
Store time [s]	0.2	0.025

### 7.2.5.4 Space Charge

The effect of space charge on particle loss has not been analyzed. We note, however, that the space charge tune shift is large only when the beams are small and most particles are

well within the dynamic aperture. For this reason space charge is not likely to be a significant source of particle loss. Nonetheless, we recommend that particle tracking simulations including space charge should be run to rule out the possibility that space charge tune shifts could result in particle loss.

## 7.2.6 Extracted Polarization

### 7.2.6.1 Introduction

All linear collider projects foresee producing an electron beam with 80% polarization at the source. This polarization should be preserved during the subsequent transport to the IP. A first estimate of the depolarization time was obtained from first order perturbation theory, as implemented in the code SLIM [18, 19]. The calculations include: a linear lattice with a hard-edged dipole linear wiggler model, and orbit errors. The treatment of spin motion is valid under the assumptions that for the low energies considered (1.98 GeV for JLC-X/NLC, 5 GeV for TESLA) the spin precession is dominated by the effect of vertical closed orbit distortions leading to the coupling of spin to the horizontal dispersion [19]. This assumption may not be valid for large transverse particle amplitudes. Further work should thus include spin-tracking studies.

### 7.2.6.2 SLIM calculations

The calculations were performed for the JLC-X/NLC main damping ring and the TESLA positron ring with a vertical orbit error of 1 mm rms simulated through randomly distributed vertical kicks.

Figure 7.6 shows the depolarization time as a function of the energy for the JLC-X/NLC damping ring.

Figure 7.7 shows the depolarization time for the TESLA damping ring with the vertical bends and the coupling bump in the straight sections.

### 7.2.6.3 Summary

First order perturbation analysis shows that both damping rings have a safety margin of several orders of magnitude for the depolarization time. Even directly on a resonance, the depolarization time is on the order of 100 times the storage time for the TESLA damping ring. The NLC damping ring shows only the first order synchrotron resonances. This huge margin suggests that depolarization is not an issue in the damping rings. Spin tracking should be used to understand the behavior of particles with large betatron amplitudes at injection.

## 7.2.7 Upgrade to Higher Energy

**7.2.7.0.1 TESLA Upgrade** For an upgrade of TESLA from 500 GeV to 800 GeV c.m. energy (see Table 4.1), the bunch spacing within a train is halved from 20 ns to 11.5 ns, the bunch population is reduced from  $2.0 \times 10^{10}$  to  $1.4 \times 10^{10}$  and the extracted transverse

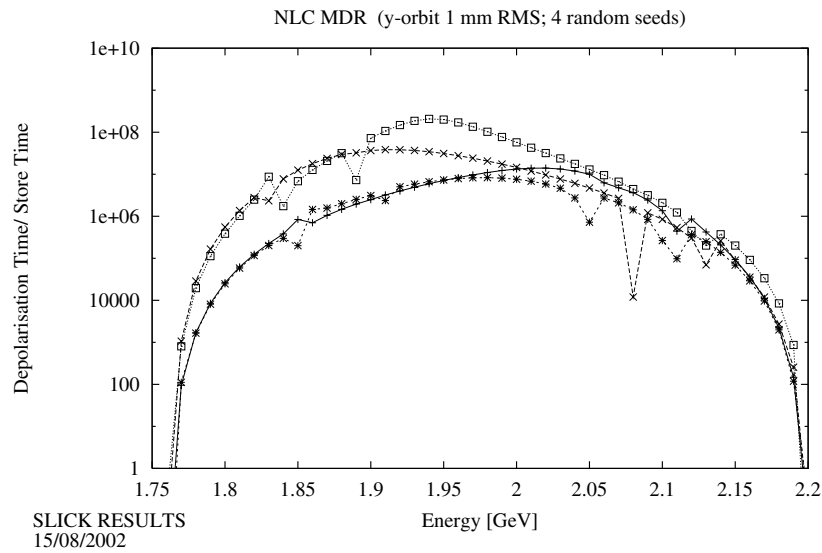


FIGURE 7.6. Depolarization time of the NLC main damping ring (normalized to standard store time 0.025 sec) versus energy.

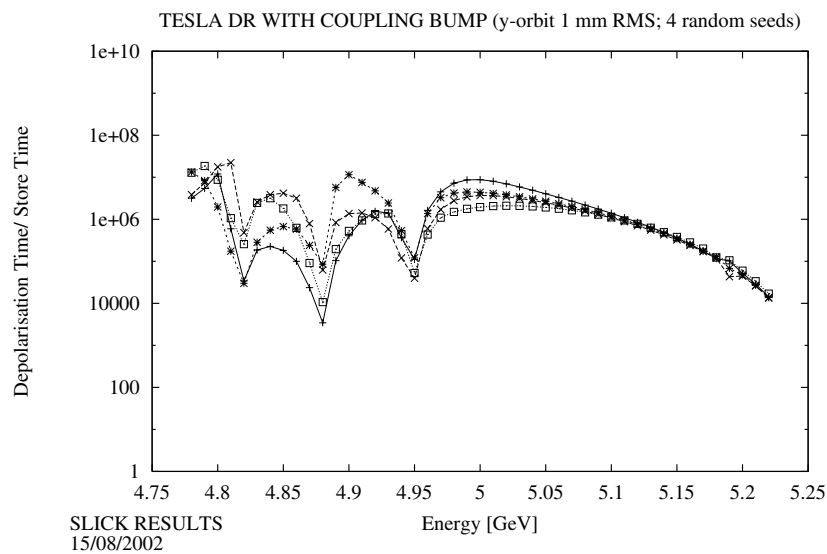


FIGURE 7.7. Depolarization time of the TESLA damping ring with vertical bends and coupling bump (normalized to standard store time 0.2 sec) versus energy.

emittances are reduced from  $\gamma\epsilon_x / \gamma\epsilon_y=8.0 / 0.020 \mu\text{m}\cdot\text{rad}$  to  $6.0 / 0.010 \mu\text{m}\cdot\text{rad}$ . This requires the development of injection and extraction kickers which are twice as fast as those for 500 GeV, and requires better correction of dispersion and coupling. As for the 500 GeV case, these kickers are technologically challenging, and simulations of the correction algorithms are needed to verify that the required emittance can be maintained. The electron cloud instability and ion effects are expected to be more severe, although we have not evaluated these at 800 GeV. An alternative energy upgrade, albeit with lower luminosity, is possible (see Table 4.2). This upgrade does not require improved damping ring performance.

**7.2.7.0.2 JLC-X/NLC Upgrade** An upgrade of JLC-X/NLC from 500 GeV to 1 TeV has no consequences for the damping ring complex.

**7.2.7.0.3 CLIC Upgrade** An upgrade of CLIC from 500 GeV to 3 TeV requires a reduction of the extracted beam emittances from  $\gamma\epsilon_x / \gamma\epsilon_y=1.6 / 0.005 \mu\text{m}\cdot\text{rad}$  to  $0.45 / 0.003 \mu\text{m}\cdot\text{rad}$ . As in the 500 GeV case, simulations of dispersion and coupling correction and IBS and other collective effects are needed to evaluate the damping ring design for 3 TeV.

## 7.2.8 Conclusions

Overall, the TESLA and JLC-X/NLC damping ring designs are well advanced. The required performance is not far from the performance achieved by the ATF. (We note that the JLC design for 150 Hz must be completed).

This committee examined many potential problems. Many of these were found to have satisfactory solutions or negligible impact: correction of the emittance increase due to ground motion; coupled bunch instabilities due to wakefields; space charge; intrabeam scattering; beam jitter due to ground motion and vibration, and beam loading; circumference variations; Touschek lifetime; and polarization preservation. However, we have identified several other issues that are critical for successfully producing the design luminosities. These issues are listed in Section 7.2.8.1 in order of greatest to least concern.

### 7.2.8.1 Concerns (TESLA and JLC-X/NLC)

- Without intervention to reduce the electron cloud density well below the neutralization density the  $e^+$  damping rings are likely to suffer from an unacceptable incoherent tune shift, head-tail instability, and/or coupled bunch instability. The TESLA damping rings may be particularly susceptible to a large incoherent tune shift. The JLC-X/NLC main damping rings may be particularly susceptible to head-tail and coupled bunch instabilities. We note that PEP-II and KEKB have used multiple techniques to suppress the electron cloud, but do not operate with their design bunch pattern due, at least in part, to the electron cloud instability. This issue poses a serious technical risk. A solution to this problem must be aggressively pursued (TESLA, JLC-X/NLC).
- The fast ion instability may have a growth rate too fast to be controlled with feedback in both the TESLA damping rings and the JLC-X/NLC damping rings. There are

very large uncertainties in the estimate of the growth rate. If simulations or experiments show that the growth time is less than a few hundreds of  $\mu\text{s}$ , then a redesign of the vacuum system for substantially lower pressure (as low as  $10^{-10}$  Torr) may be required (TESLA, JLC-X/NLC).

- Simulations indicate some particle loss for the TESLA  $e^+$  damping ring, because the injected emittance is large and the dynamic aperture is similar to the size of the injected beam. The limited dynamic aperture, caused by nonlinearities from the wiggler field, may result in unacceptable radiation in the tunnel. This issue requires an aggressive effort to optimize the TESLA DR wiggler and/or lattice design. Such an effort is expected to produce a satisfactory solution (TESLA).
- The broadband impedance budgeted for the TESLA damping rings and JLC-X/NLC main damping rings is roughly one third of the measured value in recently constructed machines in which pains were taken to minimize the impedance. While the estimated impedance threshold for the longitudinal microwave instability is a factor of 2–3 larger than the design impedance for the TESLA DR and JLC-X/NLC MDR, it is expected to be difficult to achieve that margin. This issue places stringent demands on the calculations for, and design and implementation of, the vacuum chamber (TESLA, JLC-X/NLC).
- In a simulation model including several significant classes of misalignments and design BPM resolution, the emittance (disregarding collective effects) is corrected to below the design level for most, but not all, random seeds in both the TESLA DR and the JLC-X/NLC MDR. The dependence of luminosity on DR equilibrium emittance is soft, and the experience at the ATF shows that such simulations can successfully predict the effectiveness of the correction algorithm. However, not all effects have been included in the simulation, and the margin is not large. Additional correction strategies should be considered to widen this margin. This issue also places stringent demands on BPM resolution and stability (TESLA, JLC-X/NLC).
- To avoid an unacceptably large tune spread due to ions, the TESLA  $e^-$  damping ring should be designed for an average pressure of the order of  $10^{-10}$  Torr and must use an ion-clearing gap. (TESLA).
- While calculations indicate that the dynamic aperture for the JLC-X/NLC  $e^-$  and  $e^+$  MDR and the TESLA  $e^-$  DR is adequate, it decreases rapidly for off-momentum particles. Efforts should be made to increase the dynamic aperture for off-momentum particles (TESLA, JLC-X/NLC).
- We have not calculated the effect of collective instabilities on the closure of the coupling bump in the TESLA damping rings. Such a calculation should be made to determine whether a problem exists (TESLA).

### 7.2.8.2 Comments on CLIC

We note that most of these issues are critical for the CLIC damping rings as well. Initial design studies suggest that emittance growth from intrabeam scattering and electron cloud instabilities will present serious challenges for CLIC. IBS is an important driver in the optimization of the CLIC main damping ring lattice.

## 7.2.9 Items for Further R&D

We present here the suggested R&D items for the Damping Ring designs. The items have been ranked in their importance according to the ranking scheme described in Section 7.1.3. No specific R&D items appear for CLIC, for the reason noted in Section 7.2.1.1.

### 7.2.9.1 Ranking 2

Items Common to All Machines:

- Further simulation studies are needed to understand the magnitude of the electron cloud effects and to explore possible means of suppression of these effects. Experiments in existing rings are needed to test the electron cloud simulations. Possible cures for the electron cloud (including chamber coatings, superimposed magnetic fields, and gaps in the bunch pattern) need to be experimentally investigated.
- Further simulations of the fast ion instability are necessary. Experiments in the ATF and other suitable rings are needed to test the predictions of the simulations.
- Extraction kicker stability, required at the level of  $< 10^{-3}$ , is an important issue. Further studies including experiments with the ATF double kicker system are needed.
- Additional simulations of emittance correction are needed, including the effects listed in Section 7.2.3.2. Additional experiments in the ATF and other operating rings are needed to test emittance correction algorithms.

Items Specific to TESLA:

- Inclusion of systematic and random multipole errors and random wiggler errors are needed in the particle loss simulations. Further dynamic aperture optimization is needed.
- The energy and luminosity upgrade to 800 GeV will put tighter requirements on alignment and on suppression of electron and ion instabilities. Further studies of these effects are required.

### 7.2.9.2 Ranking 3

Items Common to All Machines:

- Detailed reviews of the impedance budgets are needed.
- Development of BPMs with  $\leq 0.5$  to  $1 \mu\text{m}$  resolution and excellent stability ( $\sim 10 \mu\text{m}$  over 1 day) is necessary. The development of fast, high resolution beam size diagnostics must be continued.

Items Specific to TESLA:

- A calculation of the effect of collective instabilities on the closure of the coupling bump in the damping rings should be made to determine whether a problem exists.

Items Specific to JLC-X/NLC:

- Inclusion of systematic and random multipole errors and random wiggler errors are needed in the particle loss simulations. Further dynamic aperture optimization is needed.
- Further experiments at the ATF and other low-emittance rings are necessary to determine the validity of the theoretical models of IBS.

### 7.2.9.3 Ranking 4

Items Common to All Machines:

- Additional experiments in the ATF and other operating rings are needed to verify that beam-based alignment can be used to align BPMs with respect to their associated quadrupole and sextupole magnets within a few  $\mu\text{m}$  and to study drifts and systematic errors in the BPMs.

Items Specific to TESLA:

- A correction algorithm including both vertical and horizontal planes is needed.

## 7.3 LOW EMITTANCE TRANSPORT (LET)

### 7.3.1 Introduction

The Low-Emittance Transport (LET) region of a linear collider includes all of the beamlines between the exit of the main damping ring and the interaction point. Generically, the LET includes the bunch compressor, main linac, and beam delivery sections of the linear collider.

The principal luminosity requirements of the LET are: preservation of the small emittances generated by the main damping rings, in order to achieve a small beam spot at the interaction point; and minimization of relative beam motion at the IP, to permit the beams to collide. Generically, the obstacles to achieving the requirements are as follows:

- The normalized emittances of the linear colliders are all significantly smaller than those achieved at even the brightest of the synchrotron light sources; hence, the tolerances on traditional sources of emittance dilution (synchrotron radiation, magnet misalignment, *etc.*) are correspondingly tighter than in any existing facility.

## LUMINOSITY PERFORMANCE WORKING GROUP ASSESSMENTS

- The small betatron functions and strong focusing required to achieve the desired spot size impose stringent optical requirements on the beam delivery (magnet strength tolerances, matching of sextupole strengths for aberration cancellation, *etc.*)
- The RMS vertical beam size at the IP is in all cases measured in nanometers, and the beams must collide with an offset significantly less than the beam size in order to achieve acceptable luminosity. Extremely small motions of the LET magnets can drive the beams out of collision.

The bunch compressor and beam delivery regions of the various LET designs must satisfy fairly similar requirements, and are to some extent interchangeable. The differences in the designs, their parameters, and their overall performance are driven primarily by the different choices in main linac accelerating technology, and the ways in which the main linac technology interacts with the beam dynamics:

- The superconducting, low-frequency (1.3 GHz) TESLA cavities generate much weaker short-range wakefields than the higher-frequency JLC-X/NLC (11.424 GHz) or CLIC (30 GHz) accelerator structures; this in turn implies that the transverse alignment tolerances for the latter designs will be tighter than for TESLA.
- The JLC-X/NLC and CLIC designs have compensated their relatively strong wakefields through use of stronger focusing in the main linac, a correlated energy spread for the suppression of the most severe wakefield-driven instability (see Section 7.3.2.1), improved diagnostics (primarily higher-resolution BPMs, BPMs integrated into rf accelerator structures, and additional profile monitors), and improved correction systems (remote-controlled translation stages for quadrupoles and rf structure girders). These features permit the “warm,” high-frequency LET designs to meet their tighter alignment tolerances and achieve luminosity performance comparable to TESLA’s, at the expense of introducing more stringent requirements on the instrumentation and correction devices.
- TESLA accelerates a long (950  $\mu$ sec) train of bunches in a single rf pulse, which in principle permits significant optimization of certain parameters within a train (for example, the relative offset and angle of the beams at the collision point). The JLC-X/NLC and CLIC designs use shorter trains (100 to 300 nanoseconds), which limit the effectiveness of any intra-train feedback or optimization.
- The high-frequency LET designs accelerate a large number of bunch trains per second (100 to 200 for JLC-X/NLC and CLIC, compared to 5 for TESLA), which allows them to implement highly effective train-by-train feedback systems, including feedbacks which maintain the collision of the very small spots at the IP. The effectiveness of these train-by-train feedbacks compensates for the relatively limited effectiveness of intra-train feedbacks for the “warm” designs.

In addition, the LETs all operate in a regime in which the intense interaction of the colliding beams must be taken into account. TESLA’s IP parameters result in a larger enhancement of the luminosity from the beam-beam pinch effect than the parameters chosen for JLC-X/NLC or CLIC (the enhancement factor is 2.1 for TESLA, 1.5 for

JLC-X/NLC, and 1.4 for CLIC); but as a consequence, TESLA is more sensitive to beam-beam offsets at the IP and to correlated distortions of the bunch shape.

In this section we enumerate the beam dynamics effects in the LET which can lead to degraded luminosity, and summarize their expected impact on each of the linear collider designs. For this purpose the effects have been divided into four categories: effects present in a beamline with no misalignments or other errors of any kind (Section 7.3.2); effects which are static or quasi-static (Section 7.3.3); dynamic misalignments from ground motion or cultural noise sources (Section 7.3.4); and other dynamic effects in the accelerator (Section 7.3.5). Although there are several areas of concern which have been identified by this review, and a number of research and development topics which must be addressed, it is the consensus of the reviewers that, from the point of view of luminosity performance, the feasibility (as defined in Section 7.1.3) of each LET design has been established.

**A Note on LET Subdivisions** As mentioned previously, the LET is typically divided into three regions. The bunch compressor, as the name suggests, contains elements for reducing the length of the bunch extracted from the damping ring to something acceptable to the main linac and IP; it also contains a spin manipulation beamline, which allows the beam polarization vector at the IP to be adjusted to match the experimental requirements. The bunch compressor is followed by the main linac, which accelerates the beam to the desired energy. The main linac is followed by the beam delivery system, which consists of a post-linac collimation system for removal of particles which would generate unacceptable detector backgrounds, followed by a final focus system, which performs the chromatically corrected demagnification of the beam to a small enough RMS transverse size to generate luminosity. JLC-X/NLC and CLIC each include a two-stage bunch compressor system, with a low-frequency “pre-linac” sandwiched between the two bunch compressor stages. JLC-X/NLC also includes a coasting transport line between the last accelerating element of the main linac and the start of the post-linac collimation system. TESLA’s bunch compressor region includes a set of horizontal and vertical doglegs immediately upstream of its spin manipulation system.

In addition, each linear collider design includes a collimation system immediately downstream of the main damping ring for removal of particles with large betatron amplitudes; these so-called “pre-collimation” systems have not yet been designed, and thus are not reviewed here. Also, the CLIC bunch compressor design did not become available until fairly late in the review process; as a result, its design and properties are generally not considered here. It is not expected that these omissions will have any significant impact on the conclusions of this review. Finally, as noted in Section 3.3, the beamline optics for the JLC-X and NLC designs differ slightly due to different optimizations. In this section, we only analyzed the NLC optics; however, the JLC-X optics is similar, and thus the designs are frequently referred to as the JLC-X/NLC design.

### 7.3.2 Performance Limitations Present by Design in Error-Free Machine

Even in the absence of misalignments or other errors, each LET design will experience a number of effects which limit the final performance of the system. Inherent design limitations are often the most difficult to address *post facto*, hence it is essential that they be understood and limited well in advance.

At present, the majority of all present-by-design limitations are well under control in all three LET designs. Outstanding issues include the wakefield effects due to collimators in the vertical plane, and electron or ion effects on multibunch emittance. In addition, the luminosity bandwidth of the CLIC beam delivery system is somewhat smaller than desired, although this is considered a problem in optimization rather than a fundamental limitation.

#### 7.3.2.1 Single Bunch Beam Breakup (BBU)

A beam which undergoes a betatron oscillation in a linear accelerator can experience a resonant type of head-tail instability known as beam breakup (BBU). BBU can be suppressed by limiting the bunch charge, or through introduction of a longitudinally correlated energy spread; the latter process is usually referred to as “BNS Damping,” after its inventors [20]. Figure 7.8 shows: (a) the “BNS” energy spread introduced to eliminate single-bunch BBU, and (b) the total RMS energy spread in the main linac of each design, including the incoming energy spread. Table 7.13 shows the single-bunch emittance growth in the linac for a  $1\sigma_y$  initial oscillation under 3 conditions: without the initial energy spread and without the “BNS” energy spread; without initial energy spread but with “BNS” energy spread; with both initial and “BNS” energy spread. Table 7.13 shows that the present TESLA parameters are far from the BBU regime, but that JLC-X/NLC and CLIC require “BNS” damping. Nonetheless, it is clear that single-bunch BBU in the main linac is not a serious limitation for any of the designs.

TABLE 7.13

Emittance growth due to a  $1\sigma_y$  initial oscillation in the main linac. Cases without and with correlated energy spread, but without initial energy spread, are shown; also shown is the case with both initial and correlated energy spread.

	TESLA			NLC			CLIC		
Initial energy spread	No	No	Yes	No	No	Yes	No	No	Yes
BNS energy spread	No	Yes	Yes	No	Yes	Yes	No	Yes	Yes
$\gamma\epsilon_y$ initial [nm·rad]	20	20	20	20	20	20	5	5	5
$\Delta\gamma\epsilon_y$ [nm·rad]	0.162	0.107	4.3	235	3.04	7.7	28.8	0.26	2.1
$\Delta\gamma\epsilon_y/\gamma\epsilon_y$ [%]	0.81	0.54	22	1180	15.2	39	574	5.2	42

Although the bunch compressors and pre-linacs of the LET designs also contain accelerator structures, the parameters of these systems are such that beam breakup is not a concern for any of them. This is amply demonstrated in Section 7.3.2.3, in which a  $1\sigma$  initial betatron

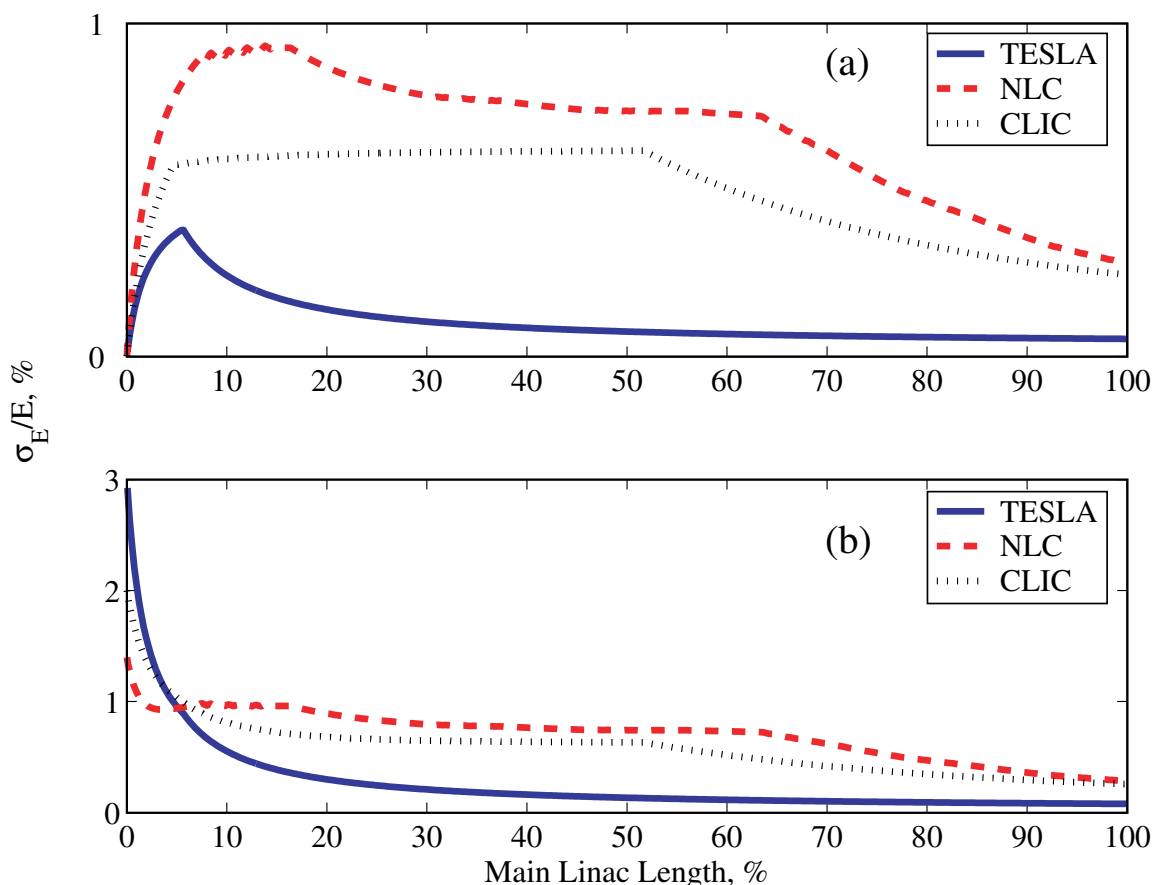


FIGURE 7.8. Energy spread in the main linac of each linear collider design: (a) correlated (“BNS”) energy spread for BBU control; (b) total energy spread, including incoming energy spread and BBU-control energy spread.

oscillation leads to relatively little BBU-induced emittance growth upstream of the main linac in all cases.

### 7.3.2.2 Multibunch Beam Breakup

Multibunch beam breakup is a phenomenon similar to the short-range instability of the same name; in this case, the transverse wakefields from leading bunches in a train can resonantly deflect the trailing bunches in the same train.

The main approach to managing multibunch BBU is reduction of the long-range wakefield. The techniques used by each project for this purpose are discussed in Section 6.5.1.3 and Section 6.5.2.3. Using the design long-range wakefields, all projects have evaluated the vertical emittance growth due to a  $1 \sigma_y$  initial offset for all bunches. Table 7.14 summarizes the simulation results for multibunch beam breakup and the design multibunch wakefields. Note that single-bunch wakefields and BNS damping are present in the multibunch simulations. Injected energy spread is not. The multibunch emittance growth is negligible

in the case of TESLA, which is a consequence of the weak long-range wakefields in the low frequency, superconducting cavities. The emittance growth is larger for the normal-conducting machines, and is larger than the emittance growth from single-bunch BBU shown in Table 7.13. The multibunch emittance growth remains within the realm of acceptability, however, especially when the effect of the uncorrelated energy spread at main linac injection is included [21]. The uncorrelated energy spread will lead to a faster de-coherence of the oscillation and the multibunch growth will be suppressed to below the values in Table 7.14.

TABLE 7.14

Growth in normalized vertical emittance due to a  $1\sigma_y$  offset of all bunches at the start of the linac. The simulation included single bunch wakefields and BNS damping, but no initial uncorrelated energy spread. NLC result from T. Raubenheimer, private communication. TESLA result based on DESY TESLA-00-28, 2000. CLIC result from D. Schulte, private communication.

Machine design	$\Delta\gamma\epsilon_y$ [nm·rad]	
	Single-Bunch	Total (SB+MB)
JLC-X/NLC	3.0	6.8
TESLA	0.11	0.11
CLIC	0.3	1.6

The simulation of long-range BBU is straightforward and high confidence can be placed on the simulation results, provided that two prerequisites are satisfied in the real-world implementation of the LET. The first prerequisite is that the design process for the structures be mature: the process used to calculate the long-range wake given the structure geometry parameters as input must be accurate. The second is that the construction process for the structures be mature: the geometry parameters that yield the desired long range wakefield must be achieved in the actual structure. The former pre-requisite has been achieved, and excellent agreement is found between calculated and measured higher-order modes. In the implementation phase, all designs have encountered abnormalities which have driven the measured wakefield away from the design wakefield, but these abnormalities are in general understood, and it can be reasonably expected in all designs that the accelerator structures will meet the design requirements for HOM's. The simulations described previously have shown that, for structures which possess the design wakefield, multibunch BBU will not be a problem for any LET. Although the pre-linacs and bunch compressors have not been explicitly evaluated here, no source of multibunch BBU is expected in these areas.

### 7.3.2.3 Optical Sources of Emittance Growth

Optical sources of emittance growth in a perfect beamline include uncorrected chromaticity, uncorrected high-order dispersion functions, and aberrations related to the presence of high-order multipole magnets (sextupoles and higher). Typically these sources contribute to beams which pass on-axis through perfect accelerators, and in general some of the sources

contribute even more strongly to beams which undergo betatron oscillations through the accelerator.

The optical emittance growth for on-axis beams is summarized in Table 7.15; all growths are acceptably small. Table 7.16 shows the simulated emittance growth for beams with  $1\sigma$  initial offsets in either horizontal or vertical. In Table 7.15 and Table 7.16, the values reported are *effective* emittances, in which the beam sizes and angular divergences have been corrected to suppress the contribution of non-linear tails; also, the contribution of the design value of  $\eta_x^*$  to the angular divergence has been removed in the case of the JLC-X/NLC and CLIC final focus systems.

For a filamenting oscillation, the expected fractional emittance growth for a  $1\sigma$  oscillation is  $\sqrt{2} - 1$ , or 41%; this value is shown in the “Ideal” row of Table 7.16. Most of the emittance growths in Table 7.16 are somewhat larger, typically 50% and in some cases 90%, which indicates that there are other nonlinear effects which are important. No significant dependence on the phase of the initial oscillation was seen. In all three cases, the expected jitter on the beam at the entrance to the LET is on the order of  $0.1\sigma$ ; since the emittance effect scales quadratically with the jitter amplitude, this source of emittance growth is expected to be acceptable in all cases.

The TESLA design anticipates the use of vertical dipole magnets to permit the main linac to follow the curvature of the earth; this causes a periodic vertical dispersion which, in principle, can cause some emittance dilution through unclosed high-order dispersion functions. Because the vertical dispersion function is small—typical values of  $\eta_y$  would be  $150\ \mu\text{m}$ —and the residual dispersion from misalignment and steering is expected to be several times as large (see Section 7.3.3), we do not expect this source to contribute to the TESLA emittance budget.

### 7.3.2.4 Bandwidth

The bandwidth of a beamline refers to its general capacity for transporting beams with off-nominal centroid energies without introducing unacceptable emittance dilution. Bandwidth is a key consideration for any beamline which can be expected to experience significant jitter in the energy of the incoming beam, or any beamline which relies upon delicate cancellations of optical aberrations: specifically, the spin manipulation beamlines of TESLA and the NLC, the  $180^\circ$  arc at the 8 GeV point in the NLC, and the beam delivery systems of each LET fall into this category.

In the case of the spin manipulation beamlines the incoming energy centroid jitter is simply the jitter in damping ring extraction energy, which is expected to be negligible compared to the RMS energy spread of the beam in all cases (see Section 7.2.4.4). Previous studies of the NLC spin manipulation system have shown that the emittance dilution due to chromatic effects is minuscule [22]; the TESLA system is nearly identical to the NLC design, and the TESLA damping ring energy spread is comparable to the NLC damping ring energy spread, so the TESLA system should be similarly well-behaved.

The beam dynamics of the NLC’s  $180^\circ$  arc was the subject of a detailed study [23]; the study indicated that the vertical emittance growth reached  $3\ \text{nm}\cdot\text{rad}$  for 2% energy error, and was dominated by high-order chromaticity and dispersion. The design specification for

TABLE 7.15: Emittance growth in Linear Collider LETs for on-axis beams. Initial emittances are damping ring extraction for TESLA and NLC, main linac injection for CLIC.

	TESLA		NLC		CLIC	
	$\Delta\gamma\epsilon_x$ [ $\mu\text{m}\cdot\text{rad}$ ]	$\Delta\gamma\epsilon_y$ [ $\text{nm}\cdot\text{rad}$ ]	$\Delta\gamma\epsilon_x$ [ $\mu\text{m}\cdot\text{rad}$ ]	$\Delta\gamma\epsilon_y$ [ $\text{nm}\cdot\text{rad}$ ]	$\Delta\gamma\epsilon_x$ [ $\mu\text{m}\cdot\text{rad}$ ]	$\Delta\gamma\epsilon_y$ [ $\text{nm}\cdot\text{rad}$ ]
Initial values	8	20	3	20	1.8	5.0
Budget	2	10	0.6	20	0.2	5
On-axis	0.12	1.5	0.06	0.8	0.02	0.44

TABLE 7.16: Emittance growth in Linear Collider LETs from  $1\sigma$  oscillations in horizontal or vertical planes. These values are growth in addition to the on-axis growth, and include short-range wakefields. Initial emittances are damping ring extraction for TESLA and NLC, main linac injection for CLIC. "Ideal" refers to the expected effect for a fully filamented oscillation,  $\Delta\gamma\epsilon = (\sqrt{2} - 1)\gamma\epsilon$ . Note that emittance growths due to initial oscillation scale quadratically with the amplitude of the oscillation.

Location	TESLA				NLC				CLIC				
	$1\sigma_x$	$\Delta\gamma\epsilon_x$ [ $\mu\text{m}\cdot\text{rad}$ ]	$y/\sigma_y$	$1\sigma_y$	$1\sigma_x$	$\Delta\gamma\epsilon_x$ [ $\mu\text{m}\cdot\text{rad}$ ]	$y/\sigma_y$	$1\sigma_y$	$1\sigma_x$	$\Delta\gamma\epsilon_x$ [ $\mu\text{m}\cdot\text{rad}$ ]	$y/\sigma_y$	$1\sigma_y$	$\Delta\gamma\epsilon_y$ [ $\text{nm}\cdot\text{rad}$ ]
Start	1	0	1	0	1	0	1	0	1	0	1	0	0
End BC	0.67	2.9	0.65	7.2	0.99	0.8	0.79	5.2	N/A	N/A	N/A	N/A	N/A
End ML	0.28	4.5	0.19	13.1	0.39	1.8	0.29	12	0.44	0.70	0.45	1.8	1.8
IP	0.26	4.6	0.20	15.7	0.31	1.8	0.33	12	0.21	0.70	0.45	2.0	2.0
Ideal	0	3.3	0	8.3	0	1.2	0	8.3	0	0.75	0	2.1	2.1

the pre-linac calls for an energy jitter of 1% full width [24]; for such an energy jitter the emittance growth in the arc should be negligible.

In the case of the beam delivery system, the only appropriate metric for bandwidth is the luminosity performance. This is because both the size of the two beams and their relative offsets are crucial in determining the delivered luminosity, and because the beam-beam effect can amplify or mitigate the impact of offsets, skewness, or kurtosis in the colliding beams. For present purposes, the chosen metric is the luminosity obtained when a beam of varying centroid energy is transported through the beam delivery system to collide with a beam of nominal (250 GeV) centroid energy. The energy variation is accomplished by systematically varying the on-crest energy gain of all linac structures. The resulting luminosity bandwidth of TESLA, NLC, and CLIC is shown in Figure 7.9. Note that the principal source of luminosity dilution in all 3 cases is the beam delivery system and not the main linacs. Figure 7.9 implies that, from the point of view of luminosity, NLC will likely be more tolerant of klystron phase and amplitude jitter or loss of rf power units than TESLA or CLIC will be.

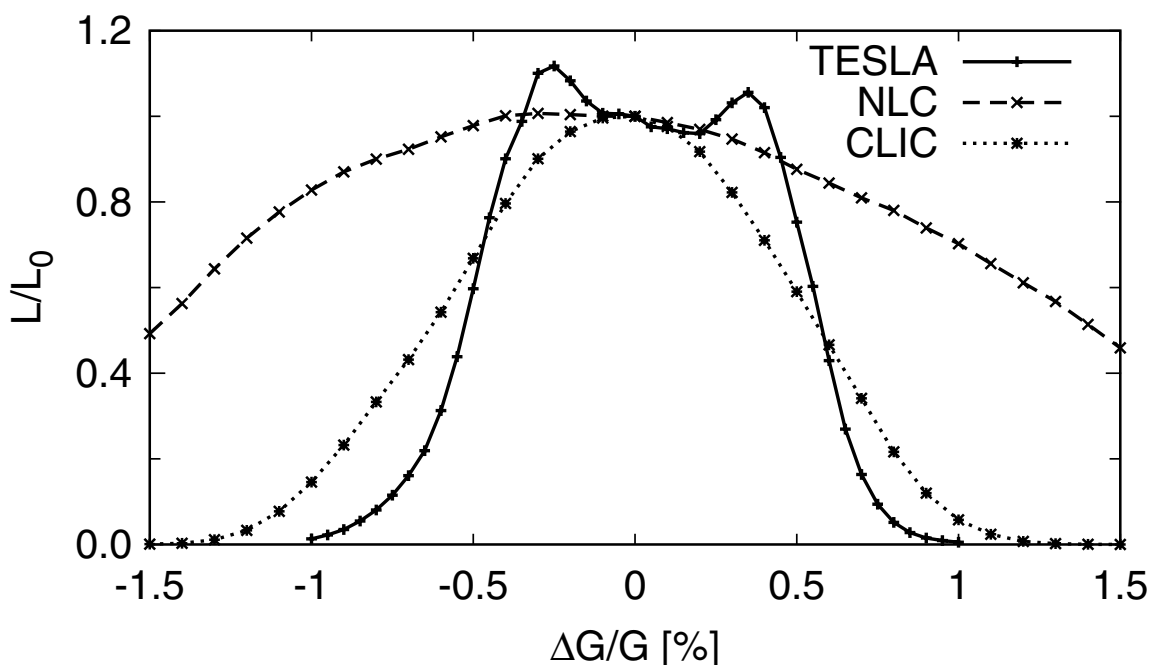


FIGURE 7.9. Relative luminosity as a function of beam energy. In this case, the energy of one beam at the IP is held constant, while the IP energy of the other beam is varied by uniformly scaling the accelerating gradient of its linac.

### 7.3.2.5 Synchrotron Radiation

Despite the implications of the name “LINEAR collider,” the LETs contain bending in their spin manipulation, bunch compression, and beam delivery areas; the JLC-X/NLC also

contains several diagnostic chicanes in the main linac and horizontal extraction and injection lines to transport the beam to and from the main linac bypass line. These bend magnets can all introduce emittance growth through incoherent emission of synchrotron radiation photons in bend magnets. The bend magnets are all in the horizontal plane, and thus the emittance growth is confined to this plane. The expected emittance growths in the cases of TESLA, JLC-X/NLC, and CLIC, are  $0.037 \mu\text{m}\cdot\text{rad}$ ,  $0.216 \mu\text{m}\cdot\text{rad}$ , and  $0.005 \mu\text{m}\cdot\text{rad}$ , respectively. In addition, the vertical bends used to transport the TESLA beam from the damping ring elevation to the main linac elevation contribute  $0.245 \text{ nm}\cdot\text{rad}$  vertical emittance growth. Although the TESLA main linac is curved to follow the curvature of the Earth, the radius of curvature is large and the resulting emittance growth is orders of magnitude smaller than the design emittance.

In the case of high-energy linear colliders, an additional source of emittance dilution arises from the stochastic energy loss in the final bends and final doublet; these synchrotron emissions cause a breakdown in the chromatic correction of the final focus and can lead to vertical beam size growth [25]. For beams with the nominal IP parameters listed in Table 2.6, this effect results in vertical RMS beam size increase of 1.2% for TESLA, 1.8% for JLC-X/NLC, and 2.2% for CLIC. Particles far from the beam core, which do not contribute much luminosity, will be more strongly influenced by this effect than the luminosity-producing particles in the core, and therefore the RMS beam size increase overestimates the luminosity effect; a luminosity-weighted beam size calculation shows a spot size increase of 0.8% for TESLA, 1.3% for JLC-X/NLC, and 1.4% for CLIC.

In addition to the incoherent synchrotron radiation effects described, linear collider bunch compressors are potentially subject to emittance dilution from coherent synchrotron radiation (CSR). The horizontal emittance growth from CSR is  $0.08 \mu\text{m}\cdot\text{rad}$  for both the TESLA and JLC-X/NLC bunch compressors. Emittance growth from CSR is a strong function of bunch length; thus, this effect will be important to evaluate in the case of the CLIC bunch compressor system.

### 7.3.2.6 Collimator Wakefields

The collimator jaws in the post-linac collimation region and the final focus of the LETs introduce single-bunch transverse wakefields. The principal effect of these wakefields is to amplify any incoming jitter; the kick given by a collimator is proportional to the beam transverse position in the collimator, hence the collimators add an angle jitter which is proportional to position jitter. From this it follows that the collimators at the betatron phase of the final doublet are the most critical, since these collimators add to the position jitter of the beam at the IP. In addition, any collimator at a location of nonzero dispersion will couple the incoming energy jitter into betatron motion. Finally, the collimator wakefields will also introduce some single-bunch emittance dilution, since the tail of each bunch will be deflected but the head will not be. This emittance dilution has a longitudinal correlation—a “banana”—which can be quite damaging to the luminosity performance (see Section 7.3.2.9).

In order to afford some protection against collimator damage from individual errant pulses or bunch trains, each LET post-linac collimation system uses a set of thin collimators (“spoilors”), which enlarge the beam angular divergence through multiple Coulomb scattering; these are followed at some distance by thick collimators (“absorbers”), which

stop the beam halo and, if necessary, the core of an errant beam. The geometric wakefield was calculated using the expressions in [26], while the resistive wakefield was calculated using the expressions in [27]; the overall procedure describing the algorithm used here is summarized in [28]. Table 7.17 shows the jitter amplification figure of merit for each subcomponent of the post-linac collimation systems of each LET design, based on the collimation system descriptions [29]. For betatron collimators the figure of merit ( $\mathcal{A}_{x,y}$ ) represents sigmas of outgoing angle jitter for  $1\sigma$  of incoming position jitter; in the case of the energy collimators the parameter  $\mathcal{A}_\delta$  has units of sigmas of angle jitter per percent energy centroid jitter. Table 7.17 shows the collimator-wakefield contribution to beam jitter at the IP, which is the most relevant to luminosity performance. There is also a collimator wakefield contribution to beam jitter at the final doublet magnets, but the luminosity impact of this jitter is small and is not tabulated here.

TABLE 7.17

Jitter-amplification figures of merit for collimators in the final doublet betatron phase. “N/A” indicates that the collimator classes in question (FF spoilers, *etc.*) are not present in the design and thus contribute no wakefields.

Parameter	TESLA			NLC			CLIC		
	$\mathcal{A}_x$	$\mathcal{A}_y$	$\mathcal{A}_\delta$	$\mathcal{A}_x$	$\mathcal{A}_y$	$\mathcal{A}_\delta$	$\mathcal{A}_x$	$\mathcal{A}_y$	$\mathcal{A}_\delta$
$\delta$ spoilers	0.035	0.054	0.27	0.0010	0.045	0.053	0.0017	0.16	0.049
$\delta$ absorbers	0.0063	0.034	0.058	0.0053	0.016	0.019	0.0035	0.37	0.10
$\beta$ spoilers	0.066	0.55	0	0.081	0.59	0	0.099	1.67	0
$\beta$ absorbers	0.032	0.51	0	0.0032	0.014	0	0.12	0.33	0
FF spoilers	0.080	0.73	0.019	N/A	N/A	N/A	0.034	0.32	0.13
FF absorbers	0.024	0.38	0.029	0.062	0.53	0.0019	N/A	N/A	N/A
Total	0.24	2.26	0.34	0.15	1.20	0.074	0.26	2.84	0.027

The values in Table 7.17 indicate that, in the horizontal plane, 24%, 15%, and 26% of the doublet-phase jitter will be coupled into the IP phase; since this jitter adds in quadrature with the collimator-free jitter, the resulting growth in the absolute jitter amplitude will be at the few percent level in all cases, which should be acceptable. Similarly, an energy jitter of 1% will contribute  $0.34\sigma_x^*$ ,  $0.074\sigma_x^*$ , and  $0.026\sigma_x^*$  at the IP for the three designs; assuming that the energy jitter is comparable to  $\sigma_E/E$  in each case, this should also be negligible.

The situation is somewhat less favorable in the vertical plane. In this case, the IP jitter for each LET design will be dominated by FD-phase jitter which is coupled to the IP phase by the collimator wakefields. This is probably unacceptable for any LET design. Several strategies for mitigation of jitter amplification due to collimator wakefields are presented in [28], including: relaxing the collimation depth requirements by increasing the aperture of the vertex detector; reducing the taper angle of the collimators, although this may prove difficult from an engineering point of view; and elimination of collimators that have little influence on the collimation efficiency, including potentially eliminating some of the spoilers in the betatron collimation section if possible. It is also worthwhile to note that in the case of CLIC, the spoilers have been assumed to be copper-coated beryllium, 0.5 radiation lengths thick; this requires that each spoiler include a 71 cm long region with a 215  $\mu\text{m}$  half-gap, which causes a huge resistive wakefield. Use of copper or titanium would nearly eliminate this part of the wakefield, which is the dominant contribution to the CLIC spoiler

wakes. Finally, the collimator apertures can be relaxed without any change to the vertex detector if non-linear focusing is used to “fold” the final-doublet phase of the beam halo into a smaller area [30]. The NLC LET design includes octupoles for this purpose, but the study of collimator wakefields assumed that the octupoles are switched off and that the collimators must be set tightly in order to obtain a conservative performance estimate. It is expected that the octupole solution can be adapted to any of the LETs.

The emittance dilution from wakefields near the center of a collimator can be estimated as follows [31]:

$$\frac{\Delta\epsilon}{\epsilon} = (0.4n\mathcal{A})^2$$

where  $n$  is the number of sigmas of beam jitter. The values in Table 7.17 indicate that beam jitter at the level of  $10\sigma_x$  or  $1\sigma_y$  will lead to significant emittance dilution from this source.

It is important to remember that the theory used to perform the calculations is rather complicated and makes a number of simplifications relative to a realistic, engineered system of collimators with adjustable gaps. In all cases, the LETs were designed using a simpler theory applicable only to round collimators, which indicated that the small gaps needed for background control would be acceptable from a wakefield point of view; the results are new, and are a product of the ILC-TRC process. Also, the experimental measurements of collimator wakefields have in some cases yielded deflections which are smaller than those predicted by the theory, and no measurements have yet been performed in the regime which is relevant for the LET designs. This constitutes an excellent candidate for further R&D, especially given the existence of a dedicated collimator wakefield test facility [32].

### 7.3.2.7 Damping Ring Extraction Phase Variation

In Section 7.2.4.4, it was determined that the centroid energy jitter at damping ring extraction would be extremely small for both TESLA and NLC. For TESLA, the phase jitter at extraction (see Section 7.2.4.5) is 2 mm full width, which corresponds to 33% of the rms bunch length of 6 mm. For NLC, the phase jitter would be 6.3 mm full width. NLC’s extraction phase variation is longer than the RMS bunch length of 3.6 mm given in Table 2.3; it is therefore important to ensure that the extraction phase variation does not cause unacceptable changes in the longitudinal phase space of the beam at the IP.

Figure 7.10 shows the longitudinal phase-space parameters— $\Delta E/\sigma_E$ ,  $\Delta\sigma_E/\sigma_E$ ,  $\Delta z/\sigma_z$ ,  $\Delta\sigma_z/\sigma_z$ —as a function of extraction phase for NLC. The variations in centroid energy and energy spread are both small compared to the nominal energy spread; similarly, the variations in arrival phase and bunch length are both small compared to the nominal bunch length. Thus, all of the parameters are tolerably insensitive to the injection phase. With its smaller phase jitter, TESLA’s longitudinal phase space properties are also acceptable.

### 7.3.2.8 Multibunch Collective Effects—Ions and Electrons

Linear collider LET designs are unique amongst single-pass accelerators in that their combination of small emittances and long bunch trains imply a potential sensitivity to electron-cloud and ion effects. Preliminary estimates indicate that neither of these effects will have significant impact in the bunch compressor or main linac of any LET, but more study is required of how these phenomena influence the beam in the beam delivery system.

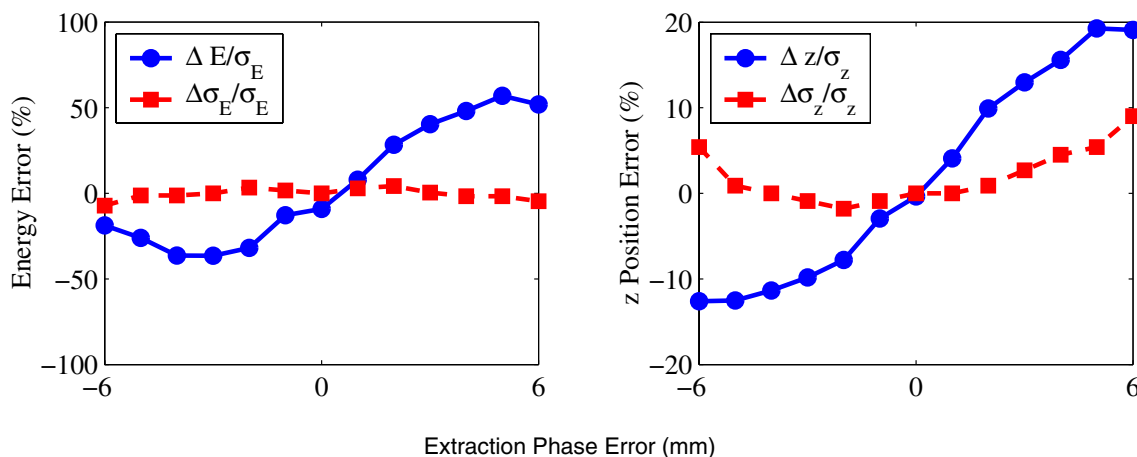


FIGURE 7.10. Variation in NLC IP parameters as the phase of LET injection is varied from  $-6$  mm to  $6$  mm: (left) centroid energy and energy spread, normalized to design RMS energy spread; (right) centroid longitudinal position and bunch length, normalized to design RMS bunch length. Note that vertical axis is in percent in both cases.

### 7.3.2.9 Beam-Beam Effects

At the interaction point, the beam has to be focused to very small transverse dimensions so that high luminosity can be achieved. As a result, each bunch gives rise to a very strong electromagnetic field which focuses the oncoming beam. The strength of this focusing is described by the disruption parameter  $D = \sigma_z/f$ , which is the ratio of the bunch length to the focal length. In the horizontal plane of all designs one has  $D_x \ll 1$ ; in this case one beam focuses the other like a thin lens. In the vertical plane all designs have  $D_y \gg 1$ ; the beams act as thick lenses. The beam fields strongly modify the particle trajectories during the collision, which results in an increase of the luminosity by a factor of 1.5–2, see Table 2.6, but also to the emission of beamstrahlung which degrades the luminosity spectrum; for a more detailed discussion, see Section 7.4.2.1. At  $E_{cm}=500$  GeV all designs have chosen beam parameters that lead to a dilution of the luminosity spectrum that is comparable to initial state radiation. A better spectrum can be achieved in all of them at the cost of a reduced luminosity.

If the beams do not collide exactly head-on but with small offsets, which are induced by dynamic effects, then the luminosity is reduced. The dependence of the luminosity on the offset is strongly modified by the beam-beam effect compared to the expectation for rigid beams which do not focus one another. Figure 7.11 shows the dependence of the luminosity on the vertical offset for all designs. It is evident that a small offset leads to a larger relative luminosity loss in TESLA than in JLC-X/NLC or CLIC, while at larger offsets the loss in CLIC is larger than in TESLA; the effect is due to the larger vertical disruption  $D_y$  in TESLA.

In addition, each bunch can include a longitudinally correlated emittance dilution—a correlation of transverse and longitudinal positions of particles within the bunch—which is induced by wakefields and dispersive effects. It has been shown that this correlation must be

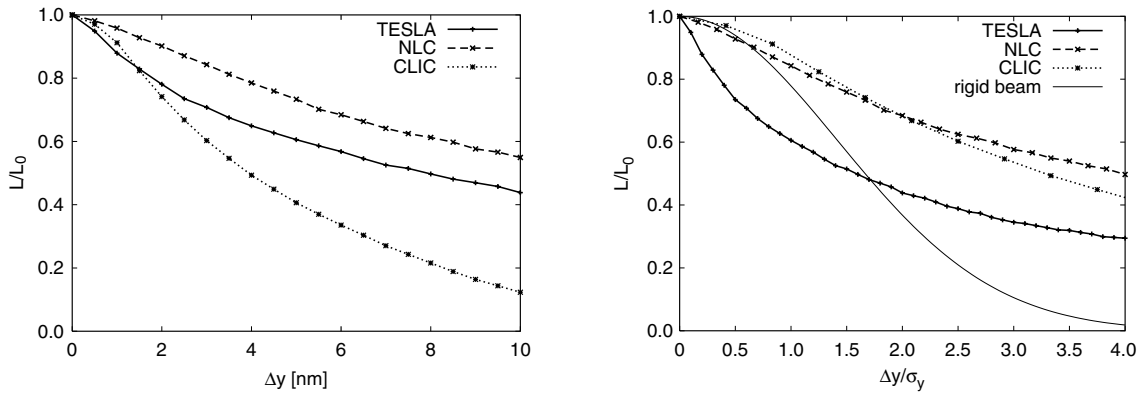


FIGURE 7.11. Luminosity as a function of the vertical offsets of the two beams in absence of correlated emittance growth. Left: offset in absolute values. Right: offset in units of beam size  $\sigma_y$ ; an approximation for the luminosity of rigid beams which do not focus one another is shown for comparison.

taken into account in the presence of strong beam-beam interaction (the so-called banana effect); this is again particularly important in the case of TESLA because of the large  $D_y$ . It has been shown for TESLA that already a very small growth of the emittance may lead to a large loss in luminosity [33], even if the mean angle and position are corrected to zero.

For this review, simulations of the luminosity in presence of static emittance growth have been performed for all designs [34]. A simplified model for the initial static misalignments was used to achieve the budgeted vertical emittance growth. The beam offsets and angles were not set to zero but rather optimized to obtain maximum luminosity, assuming that no dynamic effects are present. In Figure 7.12, the luminosity in TESLA is shown as a function of the emittance growth in the linac. Three cases are compared: correction of the mean offset and angle to zero; optimizing the mean offset to maximize luminosity while zeroing the mean angle; optimizing the mean offset and mean angle to maximize luminosity. The differences are very significant: in the case of angle and offset optimization, the luminosity impact of a correlated emittance dilution is almost identical to that of an uncorrelated emittance dilution, which is also shown in Figure 7.12 for reference. For the other machines the differences still exist but are less important. With full optimization all designs came close to their target luminosity. If one compares the luminosity found to the target value  $\mathcal{L}_0$  before subtracting the allowance for tuning, then one finds  $\mathcal{L}/\mathcal{L}_0 = 0.96$ ,  $\mathcal{L}/\mathcal{L}_0 = 1.05$ , and  $\mathcal{L}/\mathcal{L}_0 = 1.13$ , for TESLA, JLC-X/NLC, and CLIC. So the effect of the correlation is not severe in case it is static.

The correlation can however be important in the case for which one cannot optimize the luminosity but is limited to the use of BPM based corrections; this is the case for many feedbacks in the presence of dynamic errors. While TESLA will be more sensitive to the correlated emittance growth than the other machines, it has the advantage of the very long bunch train. This makes it possible to perform a more complete optimization of the collision parameters: the vertical crossing angle and offset can be adjusted bunch to bunch within a train, until maximum luminosity is achieved. This reduces the sensitivity to the banana effect. The dynamic issues will be discussed in more detail in Section 7.3.4.

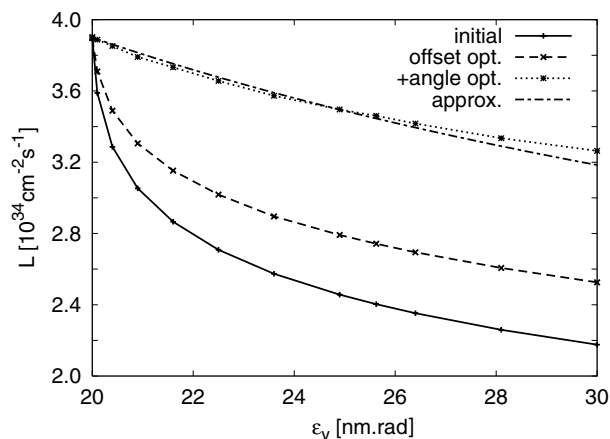


FIGURE 7.12. The luminosity in TESLA as a function of the vertical emittance growth using different levels of optimizations: zeroing the offset and vertical crossing angles of the beams (crosses), varying the offset to maximize luminosity (x's), and varying both the offset and the vertical crossing angle to maximize luminosity (stars). For comparison the approximate scaling with  $\mathcal{L} \propto 1/\sqrt{\epsilon_y}$  is also shown; this is the luminosity scaling for an uncorrelated emittance growth.

### 7.3.2.10 Multibunch Beam-Beam Effects

In the normal conducting designs, the multibunch kink instability is a potential source of luminosity loss. If bunches collide with a small vertical offset at the interaction point, then they receive a strong vertical deflection. After the collision these bunches will have parasitic crossings with the next ones of the incoming beams and, because of their now large vertical offset, will kick them vertically. In the likely case that all bunches in each train have the same offset  $\Delta y_0$  with respect to the oncoming train, this effect will increase the effective offset at the interaction point  $\Delta y$ . In the limit of an infinitely long train and for small offsets one can express  $\Delta y$  as a function of the crossing angle  $\theta_c$  in a similar fashion as in [35]:

$$\Delta y = \frac{\Delta y_0}{1 - n_c \frac{4Nr_e}{\gamma\theta_c^2} \frac{\partial y'}{\partial \Delta y}}, \quad n_c \frac{4Nr_e}{\gamma\theta_c^2} \frac{\partial y'}{\partial \Delta y} < 1$$

Here,  $n_c$  is the number of parasitic crossings before the beams are separated,  $r_e$  is the classical electron radius and  $\partial y'/\partial \Delta y$  is given by the beam-beam deflection at the collision point and is derived from simulation. For NLC and CLIC one has  $n_c = 14$  and  $n_c = 15$  and finds  $\Delta y = 1.16\Delta y_0$  and  $\Delta y = 1.14\Delta y_0$ , respectively. Consequently, the luminosity loss due to beam jitter is increased by at most 30% compared to the single bunch case. In JLC-X ( $n_c=9$ ) the crossing angle is smaller than in NLC (7 mrad compared to 20 mrad) so this formula cannot be applied. In this case, the offset continues to increase from bunch to bunch, and numerical evaluation is necessary. In Figure 7.13 the tolerable offset is shown as a function of the acceptable luminosity loss. In case of NLC and CLIC the multibunch effect is small, as expected, while it tightens the JLC-X tolerances by a significant factor. In JLC-X, to achieve  $\Delta y = 1.2\Delta y_0$ , which would be roughly comparable to the effect in the NLC, either the crossing angle has to be increased or it would be necessary to have a

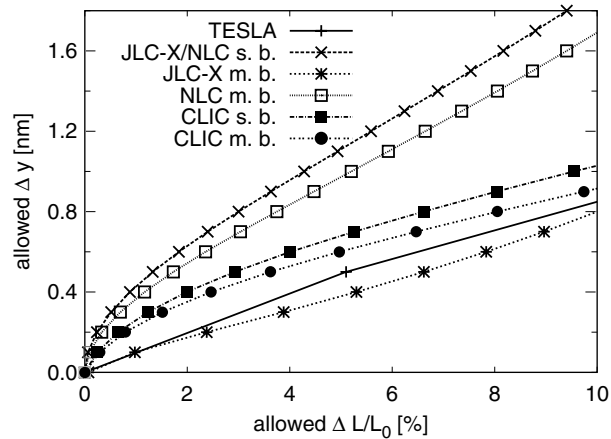


FIGURE 7.13. The allowed offset as a function of the allowed luminosity loss. In the case of NLC and CLIC the multibunch case (m.b.) does not require much better stability than the single bunch case (s.b.). In the case of JLC-X the tolerance is tightened significantly by the multibunch kink instability. In TESLA no multibunch effects exist.

conductive shield between the incoming and the outgoing beamline starting at about 60 cm from the IP, leading to  $n_c=2$ . The resulting wakefield effects and the impact that the shield has on the background conditions in the detector need careful study. In the case of TESLA, the very large bunch spacing implies that even if a crossing angle were adopted there would be no parasitic crossing, hence no luminosity loss from the multibunch kink instability.

### 7.3.2.11 Bunch-Charge and Train-Charge Variation

The luminosity impact of bunch-by-bunch and train-by-train variation in charge extracted from the damping ring has not been reviewed. The impact of variation in charge is expected to be small for all LET designs.

### 7.3.2.12 Emittance Growth in Error-Free LET—Summary

It is now possible to summarize the sources of emittance growth which are anticipated in the error-free LET:

- Initial emittances (see Table 2.3)
- On-axis optical growth, from Table 7.15
- Single-bunch jitter, from Table 7.16, and assuming that the initial beam jitter is  $0.1 \sigma$  in each plane and betatron phase
- Multibunch wakefield effects, from Table 7.14, and assuming the same  $0.1 \sigma$  jitter
- Incoherent and coherent synchrotron radiation, including the final doublet, from Section 7.3.2.5

- Assuming that the initial jitter is  $0.1 \sigma$ , and that the jitter has filamented as shown in Table 7.16, the effect of collimator wakefields can be neglected for the error-free LET, although these wakefields are likely to become more important when beam jitter induced by quadrupole vibration is included
- The beam-beam offset at the IP due to incoming jitter will be under  $0.1 \sigma$  in all cases, and the luminosity loss indicated by Figure 7.11 can be neglected
- The luminosity loss from the “banana” and from the beam delivery system bandwidth are neglected

Table 7.18 summarizes the resulting growth in emittance, and compares the result to the IP emittances from Table 2.6. In most cases the emittance growth which is inherent to the designs is small compared to the growth budget, which implies that there is considerable “margin” available to errors and tuning limitations. The exception is the horizontal plane emittance growth in NLC, which exceeds 50% of the growth budget.

TABLE 7.18

Emittance growth for each LET design due to effects present in an error-free LET lattice. “N/A” indicates a value that was not yet available at the time of writing. Initial emittances for TESLA and JLC-X/NLC are damping ring extraction values, while for CLIC, main linac injection values are used.

Item	TESLA		JLC-X/NLC		CLIC	
	$\gamma\epsilon_x$ [ $\mu\text{m}\cdot\text{rad}$ ]	$\gamma\epsilon_y$ [nm·rad]	$\gamma\epsilon_x$ [ $\mu\text{m}\cdot\text{rad}$ ]	$\gamma\epsilon_y$ [nm·rad]	$\gamma\epsilon_x$ [ $\mu\text{m}\cdot\text{rad}$ ]	$\gamma\epsilon_y$ [nm·rad]
Initial	8.0	20	3.0	20	1.8	5
On-axis optical	0.12	1.5	0.06	0.8	0.02	0.44
Jitter	0.05	0.16	0.02	0.12	0.007	0.02
MB BBU	0	0	0.006	0.04	0.005	0.013
Incoherent SR	0.037	0.57	0.22	0.52	0.005	0.14
Coherent SR	0.080	0	0.08	0	N/A	0
Total	8.29	22.2	3.39	21.5	1.84	5.61
Nominal at IP	10	30	3.6	40	2	10

### 7.3.3 Quasi-Static Errors

The luminosity performance of a linear collider is influenced by a large class of errors that are approximately constant in time. This class of quasi-static errors is typically related to manufacturing or installation tolerances of the beamline elements. With few exceptions, quasi-static errors are amenable to tuning via the use of beam-derived signals (BPM or beam size measurements, luminosity, *etc.*). Thus, in most cases the problem of quasi-static errors reduces to ensuring that the specifications on the diagnostics and control points of the LET are adequate, and that the algorithms that fall between the diagnostics and the control points are properly designed and capable of functioning in the real-world accelerator environment.

The most pressing issues in the LET's quasi-static regime are the alignment of the beamline elements, especially those in the main linacs, and the tuning of the beam delivery system. This is where the vast majority of the effort has been invested in LET studies in the last several years. Ironically, it is just this aspect of the LET that has proven impossible to review adequately due to the sheer volume of the task. Fortunately, all other quasi-static error issues in the LETs appear to be in good condition, and even the tuning and alignment issues are close enough to convergence to give confidence that in the near future a review of the latter will be completed and that it will, indeed, find that the LET can be tuned to yield the desired luminosity performance.

**A Note on Emittance Budgets** All three of the LET designs considered has a “budget” of the amount of emittance dilution that can be accepted, and a tentative distribution of the amount of dilution from each source (quadrupole misalignments, rf misalignments, *etc.*). These budgets are briefly described in Chapter 3. Although we conclude that the total budgeted emittance dilution is reasonable in each case, we were not able to validate the expected distributions; in particular, emittance dilutions from the misalignments of the main linacs tended to be larger than what is anticipated in the designs. A completely validated emittance budget, backed by an expected distribution of sources which is supported by analytic and/or simulation studies, is an important R&D project which must be pursued.

### 7.3.3.1 Beamline Magnets: Field Quality, Strength Errors, and Stray Fields

Comprehensive studies on the effect of magnet field quality and absolute setting accuracy have not been performed for any of the candidate LET beamlines. Nonetheless, there is good reason to believe that the tolerances on these parameters will be extremely loose for nearly all magnets in all the LET designs.

A small number of magnets will have relatively tight tolerances on their strength and/or field quality: the final doublet quadrupoles and a few other quads at the high-beta points in the beam delivery areas, the quadrupoles in the spin manipulation beamlines, and the quadrupoles in the high-beta points of the NLC's pre-linac energy collimation may fall into this category. These devices constitute a small fraction of all the magnets in the LET, and thus can be constructed and tested to tighter tolerances than the “rank and file” magnets. If necessary, tuning multipole magnets can be used to compensate multipole errors in some of the magnets. Finally, beam-derived signals can be used to tune the strengths of the magnets in many cases.

The effects of stray fields, from the magnetic field of the Earth to “cultural stray fields” introduced by the accelerator and its support systems, have not been considered in any systematic fashion. Their impact on the accelerator in general and in particular on the tuning algorithms should be studied carefully.

### 7.3.3.2 RF System Errors

Fixed errors in the phase or amplitude of the accelerating field can arise from calibration errors in the rf sources, or from installation or construction errors in the accelerator structures. The luminosity performance is most dependent upon the accurate control of the

bunch compressor rf systems. The sensitivity of several parameters to the bunch compressor rf phase and amplitude jitter is studied in Section 7.3.5.3; the sensitivity to static errors is comparable to the sensitivity to jitter. In the likely event that these tolerances cannot be met *ab initio*, it will be necessary to tune the bunch compressor rf systems with beam-derived signals (see Section 7.3.3.4).

The principal luminosity impact of small errors in the other rf systems is an energy mismatch between the beam and the final focus; in Section 7.3.2.4 it was shown that the bandwidth over which the final focus will deliver luminosity was about 1% at best for all three designs. All three LET designs can accommodate errors in the IP beam energy by adjusting the linac energy gain or by adjusting the strengths of magnets in the beam delivery system. A secondary impact of small rf errors is that the beam energy is not known precisely at all points in the LET, and hence the knowledge of the optics is limited. Limited knowledge of the optics can influence the effectiveness of beam-based tuning, as discussed in Section 7.3.3.4.

### 7.3.3.3 Misalignment of Elements at Time of Installation, and Beam-Based Alignment

The alignment tolerances of elements in the LET which are required for luminosity performance are extremely tight. Table 7.19 shows RMS vertical misalignments of the main linac components which would result in a 1 nm vertical emittance growth, and the expected *ab initio* accuracy of equipment installation. Inspection of Table 7.19 shows that none of the LET designs will meet the required performance if the beam is simply steered to minimize the RMS BPM readings, and therefore a more aggressive beam-based alignment procedure is required. In addition, both JLC-X/NLC and CLIC have tight beam-to-rf-structure tolerances that can only be met by using certain beam signals to align the rf elements; TESLA currently foresees no need for such a correction.

Each of the LET designs has received significant attention in the area of main linac alignment and tuning; tuning and alignment of the bunch compressors and beam delivery systems is much less mature. The key features of each design as regards beam-based alignment are summarized here.

**TESLA:** The TESLA main linac quadrupole magnets are superconducting; each quad is installed at the longitudinal center of a cryomodule which also contains a beam position monitor near the quad position, a vertical steering dipole, a horizontal steering dipole (in the case of horizontally focusing quads) and 12 accelerating cavities. Not all cryomodules contain quads: in the first half of the linac, 50% of all cryomodules are so equipped, while in the second half only 33% of all cryomodules contain quads.

During cryomodule assembly, the contents of each module are aligned with respect to its external fiducials to the tolerances shown in Table 7.19. The assembled module is then installed in the tunnel and aligned to a precision of 0.2 mm with respect to the survey line. The survey line itself is constructed with an absolute accuracy of approximately 20  $\mu\text{m}$  over several hundred meters.

The procedure for beam-based alignment of the linac calls for minimization of the BPM RMS values, followed by dispersion-free steering [36] (DFS) to minimize the

TABLE 7.19

Upper table: RMS misalignments required to achieve a 1 nm growth in vertical emittance in the main linac of each LET. Emittance growth estimates assume that the beam is steered to zero BPM readings (TESLA), or that the beam is steered via quad movers and that rf girders are then aligned to the beam trajectory (JLC-X/NLC and CLIC). Lower table: Expected *ab initio* component installation accuracy.

	TESLA	JLC-X/NLC	CLIC
<b>Luminosity tolerances</b>			
BPM offsets [ $\mu\text{m}$ ]	11	1.3	0.9
RF structure-to-girder offsets [ $\mu\text{m}$ ]	300	200	115
RF structure-to-beam offsets [ $\mu\text{m}$ ]	300	5.0	4.0
RF structure tilts [ $\mu\text{rad}$ ]	240	135	225
<b>Installation accuracy</b>			
Quadrupoles [ $\mu\text{m}$ ]	300	50	50
with respect to	Cryomodule	Survey line	Stretched wire
Structure offsets [ $\mu\text{m}$ ]	300	25	20
with respect to	Cryomodule	Girder	Girder
Structure tilts [ $\mu\text{rad}$ ]	300	33	20
with respect to	Cryomodule	Girder	Girder
BPMs [ $\mu\text{m}$ ]	200	100	10
with respect to	Cryomodule	Quadrupole	Stretched wire
Module/girder offsets [ $\mu\text{m}$ ]	200	50	7
with respect to	Survey line	Survey line	Stretched wire
Module/girder tilts [ $\mu\text{rad}$ ]	20	15	7
with respect to	Survey line	Survey line	Stretched wire
BPM resolution [ $\mu\text{m}$ ]	10	0.3	0.1
Structure BPM resolution [ $\mu\text{m}$ ]	N/A	5	10

emittance. Depending on how well the DFS converges, local orbit oscillations designed to globally cancel either dispersion or wakefield emittance growth can be applied.

**JLC-X/NLC:** The JLC-X/NLC quadrupoles are at room-temperature: the baseline design calls for maximal use of hybrid iron-dominated/permanent magnets, with iron-dominated electromagnets in a small number of locations where the hybrids are not acceptable. Quadrupoles are installed on dedicated supports (*i.e.*, they do not share a girder with any rf devices), and each quad is mounted on a remote-controlled magnet mover based on the FFTB design [37]. Each quad also has a BPM attached to it, so that the magnet mover moves both the quad and the BPM. Six rf structures, each 0.9 m long, are installed on a single 6 m girder. Each rf girder has a mover which allows horizontal, vertical, pitch, and yaw motions.

Quadrupole-BPM packages and rf girders are assembled and aligned to the tolerances specified in Table 7.19. The girder is then installed in the tunnel and aligned to the survey line with accuracy of 50  $\mu\text{m}$  and 15  $\mu\text{rad}$  in the vertical.

The beam-based alignment procedure calls for the initial use of quadrupole variation to measure the approximate BPM-to-quad offset. The beam is then steered to minimize the RMS of the BPM readings via the quadrupole movers. It is foreseen that some form of DFS may be required for the NLC main linac quads, as well as orbit bumps for minimization of dispersion. The alignment of the rf girders relies upon measurement of the beam-to-structure offsets via measurement of the phase and amplitude of higher order modes in the structures [38]. This technique permits the offset of the beam with respect to the structure to be measured with an approximate accuracy of 5  $\mu\text{m}$ . The girder is then moved to reduce the average offset and the average slope of the structure readouts to zero. Because the betatron phase advance per structure is not large, this allows the wakefield deflections of the 6 structures on a girder to be nearly cancelled.

**CLIC:** The CLIC main linac quadrupoles are electromagnets with dedicated supports. Each quad is mounted on a magnet mover, and also contains dipole steering magnets. There is a beam position monitor immediately upstream of each quad; the BPMs do not move with the quadrupoles. Four rf structures, each 0.5 m long, are mounted on a common girder 2.23 m long. Adjacent girders are mounted to common articulation points which can be remotely actuated to adjust the positions and angles of the girders. Note, however, that the girders cannot be moved independently of one another: moving a single articulation point changes the position of the two girders mounted to that articulation point. Like the JLC-X/NLC structures, the CLIC structures are instrumented to permit measurement of high-order mode amplitude and phase (and thus beam-to-structure offset), with an assumed resolution of 10  $\mu\text{m}$ .

The rf girders are assembled and pre-aligned to the tolerances specified in Table 7.19. RF girders, quadrupoles, and BPMs are installed in the tunnel and final alignment is accomplished with a combination of laser and wire-alignment systems.

Main linac alignment proceeds in several stages. Initially the beam is steered to minimize the RMS of the BPM readings. The quads and BPMs are then ballistically aligned [39], and the rf structures are aligned by moving the rf girders so that the average offset and slope of the readings in the structure's beam position readouts is

minimized. Finally, the emittance growth due to any residual wakefield effects is minimized by measuring the emittance as a function of the vertical position of a selected set of rf structures, and seeking the minimum.

#### 7.3.3.4 Integrated Simulations of Linear Colliders

As stated in Section 7.3.3.3, significant effort has been invested in the simulation of beam-based alignment of the main linacs. Here, all projects foresee to use either dispersion free steering or ballistic alignment (which in the normal conducting machines includes alignment of the rf structures to the beam by use of the internal BPMs) followed by an optimization of the emittance by the use of emittance tuning bumps. In dispersion free steering (DFS), segments with a large number of quadrupoles (about 40 to 50) are corrected by minimizing the difference between the trajectories of two beams with different energies and simultaneously minimizing the absolute offsets of the beams in the quadrupoles. In the ballistic method a ballistic beam is used to align a number of consecutive BPMs (typically 12 to 16) and when the quadrupoles are switched on again, they are aligned in a second step to restore the ballistic trajectory.

Cross-checks of the simulations performed for the different projects are necessary to establish the validity of the results. The two main programs used in this review to simulate the correction in the main linac are LIAR [40] and PLACET [41]. The comparison of the results was difficult because LIAR used dispersion free steering while PLACET used ballistic alignment. In the framework of this review it was possible to include dispersion free steering in PLACET. While some effort was made to ensure comparability, details of the methods simulated still differ.

LIAR has been used to simulate the effect of dispersion free steering in NLC and TESLA; the resulting emittance growth (before application of the emittance tuning bumps) in the main linac was found to be 20% for NLC [42] and 143% for TESLA [43]. In comparison, one of the models of dispersion free steering implemented in PLACET yielded emittance growths of 13% for NLC and 110% for TESLA. While the agreement is not completely satisfactory, we feel confident that the remaining differences can be resolved. They are likely due to the mentioned details of the methods simulated. These comparisons were made to verify that the implementation of similar correction algorithms yields similar results in the different programs. The very implementation chosen for this comparison is not necessarily the best choice for all of the machines.

Earlier studies of TESLA's beam-based alignment algorithm indicated that the emittance growth at the end of the linac would be at the level of 22%, that the primary source of emittance dilution was wakefields from misaligned rf cavities, and that nearly all of the emittance growth could be cured through use of dispersion-free orbit bumps in the linac [44]. Those studies neglected the effects of pitched rf cavities, which are an additional source of dispersion; including the cavity pitch angles results in a substantially larger dispersive emittance growth at the end of beam-based alignment. An example of a simple modification of the algorithm that can lead to significantly smaller emittance growth is the following. These studies require that the position and angle of the beam be fitted at the entrance to each correction bin using BPMs; the limited precision of this operation degrades the quality of the DFS fit, which contributes significant additional emittance growth [45]. This part of the growth can be avoided, if either the fit is not performed (which requires a

stable incoming beam) or if the BPM resolution is improved by a factor of 2 (which one may be able to achieve by averaging over multiple bunches).

No direct comparison could be made to cross-check the simulations of the ballistic alignment. Since both methods, dispersion free steering and ballistic alignment, correct the dispersion quite well, one would expect that the remaining emittance growth is dominated by the wakefields. In this case it should be the same for both methods. Indeed, simulations for CLIC using PLACET showed that they yield very similar results with both methods, after application of the emittance tuning bumps. Also in the case of TESLA, simulations of ballistic alignment have been performed; they resulted in a growth of about 50% before application of the tuning bumps [45]. This is similar to the value obtained by dispersion free steering, assuming a stable beam. These results give some confidence in the implementation of the methods.

Further study is needed to understand the remaining differences between the programs. The actual implementation of dispersion free steering in the SLC proved to be difficult, likely because of the presence of systematic errors [46]. Therefore an in-depth discussion of all relevant error sources and their inclusion in the simulations has to take place; the impact of dynamic errors on the beam-based correction is of special concern. This will require significant further effort.

### 7.3.3.5 Multibunch Emittance Growth Due to Structure Offsets and Other Imperfections

Long-range wakefield deflections within a bunch train can be caused not only by coherent betatron oscillations (BBU as discussed in Section 7.3.2.2), but also by offsets of the rf structures or an imperfect trajectory. The multibunch emittance growth has been calculated with realistic offset errors and the design long-range wakefields, as summarized in Table 7.20. The growth is small for all proposals.

TABLE 7.20

Multibunch growth in normalized vertical emittance due to trajectory offsets in the rf structures with realistic machine imperfections. The NLC result [47] assumes 30  $\mu\text{m}$  rms structure-to-structure offsets on a girder as the dominant error source. The TESLA result [48] assumes 500  $\mu\text{m}$  rms structure-to-structure offsets. The CLIC result is from [49].

Machine Design	$\Delta\gamma\epsilon_y$ [nm·rad]
JLC-X/NLC	1
TESLA	0.6
CLIC	0.1

In the case of structures which rely, wholly or in part, upon detuning for wakefield control, there are additional tolerances on the pitch angle of the structure with respect to the beam trajectory, on the straightness of the structure, and on achieving the correct higher order mode frequencies. These tolerances are particularly relevant for TESLA and JLC-X/NLC; the CLIC structures rely much more heavily on damping of higher order modes, and less heavily on detuning, which makes them less sensitive to errors in these parameters.

In a pitched structure the modes in the front and back of the structure are excited with the wrong phase relation for cancellation via detuning or “beating” of the modes. This contribution was quantified for the JLC-X/NLC case with the old 1.8 m long structure, where vertical emittance growth of 1.6 nm-rad is predicted due to the long-range wakefields which result from 50  $\mu$ rad random structure tilt errors. This is a purely multibunch effect, and it is in addition to the single-bunch emittance growth from structure tilt errors discussed in Section 7.3.3.3. The contributions should be properly evaluated for all LET designs based on their present structure configurations.

Structures that rely upon detuning must also achieve tolerances on structure straightness, since cell-to-cell deformations of the structure, like structure pitch angles, can cause a breakdown in the “beating” of modes which reduces the overall wakefield. This error can be more significant than the structure-to-structure alignment tolerance: for example, the JLC-X/NLC structure-to-structure alignment tolerance for 2 nm-rad worth of multibunch vertical emittance growth is 42  $\mu$ m, while the cell-to-cell tolerance for the same quantity of emittance growth is only 20  $\mu$ m [47]; again, this emittance growth is in addition to the single-bunch growth reported in Section 7.3.3.3. Since several JLC-X/NLC prototype structures achieved cell-to-cell construction tolerances which were approximately 2  $\mu$ m, we conclude that this source of emittance growth can be essentially eliminated.

A third issue for structures which rely upon detuning is that structure fabrication errors can lead to an unacceptable wakefield, depending on the distribution of the errors. In the case of JLC-X/NLC, it has been shown that a 3 MHz RMS error in frequency can cause an emittance growth of more than 50 nm-rad if (a) the error is not correlated from cell to cell in a given structure, and (b) the errors are repeated exactly from structure to structure. Other error modes, such as errors which are random cell-to-cell and also structure-to-structure, are far less critical. Gradual changes in the structure wakefield due to aging, sagging, or damage during fabrication or installation must also be considered. Similarly, the TESLA wakefield assumes 1 MHz RMS dipole mode variation randomly distributed over the ensemble of cavities, and assumes that the limited precision of cavity fabrication is sufficient to guarantee this variation. If the cavity fabrication process does not yield the desired distribution of higher order mode frequencies, then the resulting wakefield could be more severe than is presently anticipated.

The multibunch effects of structure misalignments and fabrication errors are nearly static. Consequently, it is possible to carefully measure the bunch-by-bunch offsets within a bunch train at a few locations and correct these offsets via feedback. The feedbacks in question are both “slow” (in the sense that they apply nearly the same correction to each bunch train) and “fast” (in the sense of using high bandwidth deflectors to shape the bunch trains). All designs can profit from intra-train feedbacks, and improvements in multibunch emittance dilution of up to a factor of 10 [50] or even more [48] are predicted.

In summary, multibunch emittance growth due to structure offsets is for all designs small compared to single bunch effects. This statement is true if the design long-range wakefields are achieved (see comments on multibunch BBU in Section 7.3.2.2). We note that the quoted results have been obtained without emittance bumps for TESLA and the NLC. The effect from emittance bumps should be included in the multibunch simulation. As multibunch effects depend strongly on the structure deformation, further beam dynamics studies should be performed once structure designs are finalized and more operating experience is available for prototype structures.

### 7.3.4 Dynamic Misalignments

The small vertical emittance and nanometer-size beam at the interaction point (IP) necessarily lead to tight stability tolerances on the components of the LET. The previous section discussed beam-based alignment methods to achieve these tight tolerances starting from more realistic installation errors. This section discusses how well those tolerances can be maintained over time in the presence of ground motion and vibration. Element motion can degrade the luminosity through two mechanisms: separation of the beams at the IP and emittance growth, both caused by trajectory changes.

Beam separation occurs on a faster time scale than emittance growth, so fast that it would be impossible to maintain luminosity for more than a few seconds without beam-based feedback. All linear colliders will rely on the beam-beam deflection signal to maintain collisions with a feedback similar to that pioneered at the SLC. For JLC-X/NLC and CLIC, the primary IP feedback system operates at the machine repetition rate (*i.e.*, train to train), analogous to the SLC system. Both machines plan additional mechanical stabilization of the final doublets (FD). TESLA plans to use fast kickers within the long ( $\sim 1$  ms) bunch train to correct the offset based on the signal from the first few percent of the bunches. Because of the large capture range of this feedback, further stabilization of the FD is not currently foreseen.

The second loss mechanism, emittance growth, is driven by the slower drift of the orbit in the upstream sections of the LET, resulting in spurious dispersion, coupling, *etc.* Feedback is necessary to maintain the “gold orbit” established by the initial tuning. This feedback operates train to train and hence, the warm machines have an advantage because of their higher repetition frequency. For both the IP offset and beam size stabilization, TESLA has the tightest tolerances due to the large vertical disruption parameter (see Section 7.3.2.9). For a 10% luminosity loss, TESLA must achieve a beam-beam offset less than 0.8 nm ( $0.16\sigma_y$ ), compared with 2 nm for JLC-X/NLC ( $0.67\sigma_y$ ) and 1.2 nm for CLIC ( $0.8\sigma_y$ ). TESLA is also very sensitive to longitudinal correlations within the bunch (“banana effect”), which coupled with the low repetition rate of the feedback, makes it difficult to maintain the orbits to the required tolerance.

Long term stability on time scales of hours to months can have a significant impact on integrated luminosity performance as it determines the frequency of invasive tuning. This has been studied extensively for both the linac and beam delivery system using a slow diffusive ground motion model. The studies concluded that the luminosity would be stable for extended periods providing the gold orbit was maintained by feedback or corrections, and the BPM offsets are stable.

Although a large number of studies have been done over the years, and as part of this review, the results presented have all come from simulations. The ground motion models are based on data derived from measurements at various sites but a complete representation of an actual site is very difficult. For example, although many noise sources were identified, the SLC beam jitter was never fully understood. These simulations are indicative of the expected performance but they have not been benchmarked against real machines.

### 7.3.4.1 Ground Motion Models

It is important to model element motion in both the spatial and the frequency domain to properly understand its impact. The frequency spectrum is important when considering the feedback performance, and spatial information is important for correlation effects. For example, even large amplitude motion which is spatially correlated does not affect collider performance. Sources of motion include natural ground motion, human-produced “cultural noise” and noise sources on the support girders themselves (*e.g.*, cooling water flow). In addition, the girders may amplify existing noise sources.

Ground motion amplitudes vary significantly from site to site, and depend on many conditions. Fast vibration can range from sub-nanometer to hundreds of nanometers. The coherence of the motion depends on geology (*i.e.*, sound phase velocity) and on the spatial distribution of the noise sources. Slow motion depends mostly on natural (human independent) phenomena and parameters, such as rigidity and homogeneity of the rock, underground water flows, rain, depth, and atmospheric pressure variation.

Several comprehensive studies of ground motion have been made and more are in progress. Different types of motion (slow diffusive ATL motion, systematic motion, elastic waves, vibration, *etc.*) have been identified and characterized and their properties studied. These studies, both experimental and theoretical, have been used to create quantitative models of ground motion which include both natural and man-made sources that are typically present in the tunnels of large accelerators. To span the intrinsic variability of the phenomena and of site conditions, three models of ground motion were considered.

Three noise models (**A**—“Low,” **B**—“Intermediate,” and **C**—“High”) were used to cover a wide range of conditions. These models are based on measurements on the tunnel floor of LEP and at representative sites in California for **A**, at the SLAC tunnel and the Aurora mine near Fermilab for **B**, and on the tunnel floor of HERA for **C**. (Section 7.3.4.6 contains more discussion on expected noise for the different LC projects.) For this study, the ground motion models were considered project independent. Additional contributions coming from noise generated on the girder or amplified by imperfect girders are project specific and are evaluated separately for each machine. Another potentially important source of noise is the experimental detector which affects the stability of the final doublet (FD). This FD noise is assumed to be project independent (although different technical solutions are envisioned for CLIC, JLC-X/NLC and TESLA as discussed later).

The spatial and temporal properties of ground motion may be described by a 2-D power spectrum. The traditional 1-D power spectra for absolute motion and for relative motion between two separated points can be obtained from the 2-D spectrum, and an example is shown in Figure 7.14 for the three models studied. The models include a contribution from diffusive (“ATL”) motion that dominates at low frequencies and vanishes for high frequencies, and a contribution from isotropically distributed plane waves propagating in the ground which represent fast motion including cultural noise. Details of the models and relevant parameters can be found in [52]. To simulate the effects of ground motion on collider performance, the models were implemented in the codes Matlab-LIAR and PLACET.

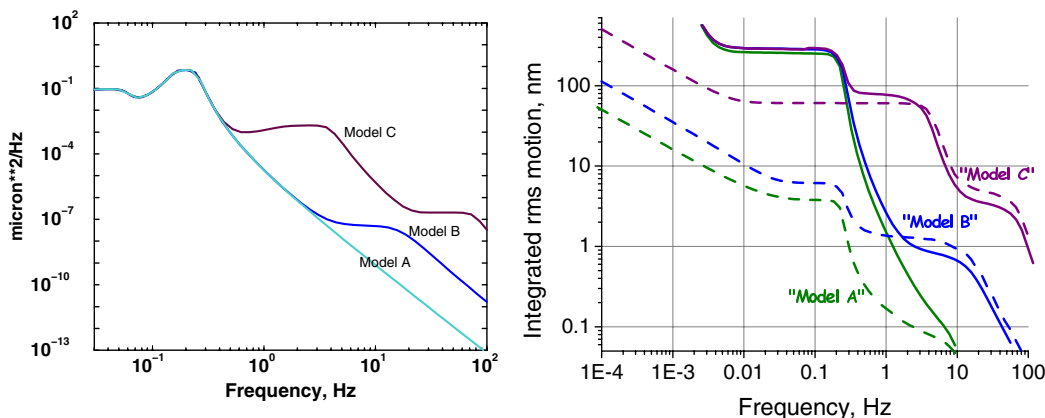


FIGURE 7.14. Ground motion model spectra. The absolute spectra (left), the integrated absolute spectra (right, solid lines) and the integrated relative (for  $\Delta L=50$  m) spectra (right, dashed lines).

### 7.3.4.2 Detector Noise and Active Stabilization

Any additional vibration introduced by the experimental detector is a specific concern since the final doublets (FD) may be partially supported by the detector, and they have the tightest jitter tolerances. Unlike ground motion, which has been studied extensively, little data is available on the motion of elements inside the detector. Some measurements were made at SLD in 1995 [51] and in 2000, and the 1995 measurements are shown in Figure 7.15. The data indicate about 30 nanometers of final doublet relative motion due to detector vibration from measurements made under less than optimal conditions. At HERA differential motion across the IR hall was measured to vary from 100 nm to 200 nm depending on conditions, but this hall is situated in a very noisy location [53]. These measurements are not really indicative of what can be achieved as neither detector was designed to minimize vibration. Data taken in the detector hall of OPAL at LEP showed integrated ground motion of only 0.7–1.2 nm rms above 5 Hz. This would be relevant if the FDs were cantilevered from the tunnel rather than partially supported by the detector (as for SLD). The optimal support system for the FDs is still under study. At the stability level required for the warm machines (nanometers above 5–10 Hz), mechanical resonances of the magnet itself or other effects which can move the magnetic center are concerns and require further study.

Given the uncertainties in detector noise, we have assumed a project independent model for detector vibration, based loosely on the SLD measurements, and shown in Fig. 7.15 (left). In a properly designed site, one could expect a lower value to be achieved. This amplitude of FD motion would require active stabilization for the warm machines. JLC-X/NLC and CLIC propose to use a combination of laser interferometers and/or mechanical motion detectors as sensors driving piezoelectric or electrostatic mechanical actuators or dipole correctors to adjust the position of the FD magnetic center. This approach can optimally

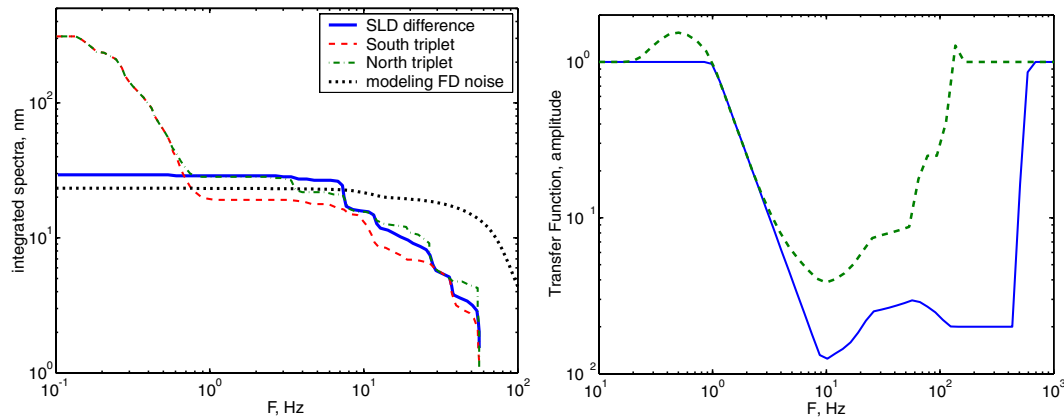


FIGURE 7.15. Results of 1995 vibration measurements on the SLC detector [51] (left plot). The integrated spectra show that the difference of the motion (solid line) of the South triplet (dashed curve) and the North triplet (dash-dot curve) is about 30 nm, as measured by two STS-2 seismometers installed on the triplets. The black dotted line shows an approximation for the FD noise used in the integrated simulations, which extends to higher frequencies to represent more accurately the expected spectrum after low frequency detector modes have been suppressed. The right plot shows the modelling transfer functions used in simulations to represent FD stabilization (dashed: already achieved; solid: expected performance with new sensors).

be applied to magnets which are stiff and light in weight, such as permanent magnets, but compact superconducting magnets may also be a possibility. In recent studies, a CLIC electromagnet has been stabilized to 0.9 nm above 4 Hz, a factor of 10 reduction with respect to the supporting ground [54]. Continuing such studies and demonstrating the performance of a full system is an important R&D item.

For TESLA, with an intratrain feedback capture range of about 100 nm, there would be no need for additional FD stabilization even under SLD conditions. However, differential motion at the level measured at HERA could pose a problem for TESLA and would be prohibitive for a warm machine.

### 7.3.4.3 Simulation Results

To study the effects of ground motion and its interaction with feedback systems, new integrated simulations of fast (train-to-train) luminosity stability were performed as part of this review. The simulations included the three ground motion models and detector noise model just described, a realistic model of train-by-train and an idealized model of intratrain IP collision feedback, and an idealized model of active stabilization of the final doublets. The train-by-train feedback, based on the NLC design [55, 56, 57], was reoptimized for each vibration assumption. The intratrain feedback was simulated in a “simple” version where the average position and angle offset was simply zeroed, and latency was ignored. For TESLA, a “full optimization” version was also studied which varied the offsets during the train passage to find maximum luminosity. This is useful because the banana effect can

cause the optimal offsets to change on a train-to-train basis. The doublet stabilization was modelled by the idealized transfer function shown in Figure 7.15 (solid) and for some cases with a more realistic curve (dashed). The former represents expected performance with new sensors being developed, the latter what has been already achieved.

As a starting point, the machines were misaligned and then a simple one-to-one trajectory correction was applied to mimic a “tuned” collider. In addition to quad and structure offsets, structure tilts must be included, as their effect is significant and had been omitted from some previous studies. The rms magnitudes of the misalignments were chosen to produce nominal luminosity on average and to reproduce approximately the expected amount of  $yz$  and  $y'z$  correlation along the bunch to realistically account for the banana effect (see [58] and [57]). In all cases, the time-dependent luminosity was calculated for 256 trains at the machine repetition rate, corresponding to an elapsed time of 51 s for TESLA, 2.1 s for JLC-X/NLC and 1.3 s for CLIC. For TESLA, this time is long enough to see a slow degradation in luminosity from emittance growth due to orbit errors in the BDS, and consequently requires the inclusion of an upstream orbit feedback, not needed on a 1–2 s time scale. The simulations were done with Mat-LIAR and PLACET, with good agreement between the codes for the cases cross checked. Both used GUINEA PIG for a full simulation of beam-beam effects. The Mat-LIAR simulations alone required over half a year of CPU time. For these studies, only one bunch was tracked, and bunch-to-bunch effects were ignored. Figure 7.16 is an example of results showing luminosity as a function of train number for each project.

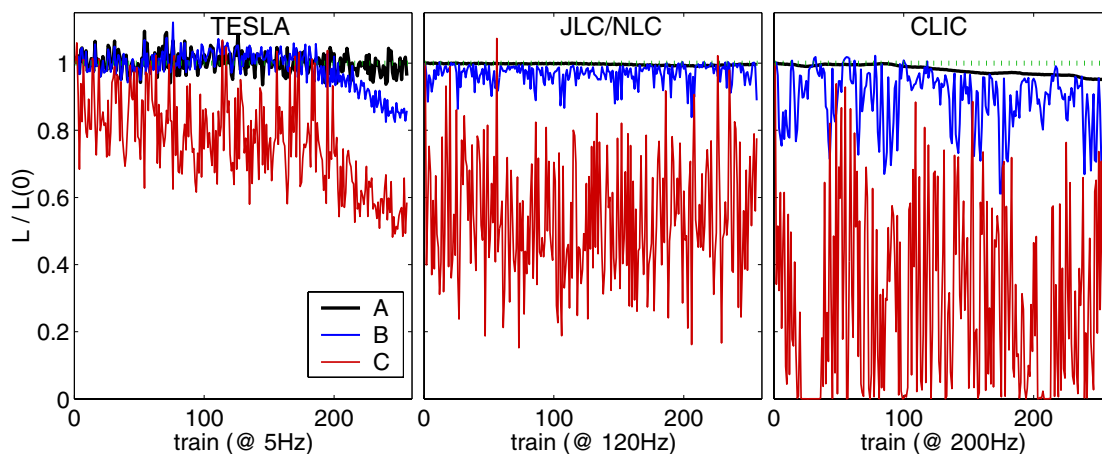


FIGURE 7.16. Example of simulations of TESLA, JLC-X/NLC and CLIC for three models of ground motion with simple intratrain IP feedback for TESLA and train-to-train feedback for the others. The final doublet follows the ground with no additional vibration due to the detector.

The simulation results are summarized in Figure 7.17 showing the percentage of luminosity obtained for each LC under GM models **A** through **C**, with and without additional final doublet vibration induced by the detector, and with different combinations of IP feedbacks and FD stabilization. Each point represents three different seeds for the machine and for

## LUMINOSITY PERFORMANCE WORKING GROUP ASSESSMENTS

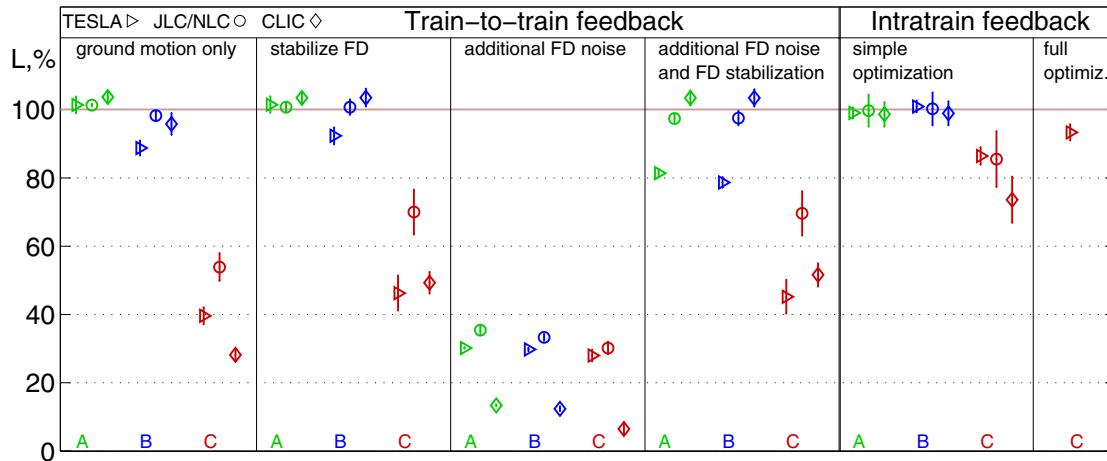


FIGURE 7.17. Percentage of luminosity obtained for each LC with ground motion models **A**, **B**, **C**, with and without additional vibration of FD, and with different combinations of IP feedbacks and FD stabilization. With the intratraining feedback, neither FD noise nor stabilization was included. The results are averaged over 256 trains (50 for TESLA). The error represents the statistical variation in mean luminosity.

the ground motion. The results are averaged over 256 trains (50 for TESLA). From these studies, one can draw the following conclusions:

- For ground motion models **A** and **B** with no additional detector noise, all designs maintained nominal luminosity with the specified beam-based IP feedback alone (simple intratraining for TESLA, train-by-train for the others).
- If a pessimistic estimate of detector noise is included, then the luminosity for JLC-X/NLC drops to  $\sim 35\%$  and for CLIC to  $\sim 12\%$ , independent of ground motion model. Doublet stabilization effectively recovers full luminosity, but only for models **A** and **B**. For TESLA, the intratraining feedback is expected to compensate for detector noise.
- For ground motion **C**, there was a significant deterioration of the luminosity. Even without detector noise, the luminosity dropped to below 30% for CLIC and below 60% for JLC-X/NLC. Doublet stabilization only improved this to 50–70%, independent of whether detector noise was included. For TESLA, the luminosity was 85% assuming a simple intratraining angle and offset feedback. This could be raised to 95% with the intratraining luminosity maximization.

For completeness, TESLA was also simulated using only a 5 Hz train-to-train feedback, without the planned intratraining system. For the worst case of model **C** with additional detector noise and no stabilization, the luminosity dropped to about 30%.

In addition to ignoring multibunch effects, a number of other potentially important issues were either not included or considered in too idealized a fashion. Realistic effects of the intratraining position and angle kickers were not included, but are being studied [59]. The

results for the intratrain IP feedback would indicate that it can be quite effective for all designs, but this is misleading as the feedback latency was not included in the simulations and is significant for the warm machines. For more pessimistic assumptions on FD stabilization, (Figure 7.15 right plot, dashed line) less FD vibration can be accommodated without degrading the luminosity, although for the case of NLC, model **B**, SLD noise and poorer stabilization, the luminosity loss was only 25%. Another concern is jitter amplification, due either to wakefields in the post-linac collimation system (see Section 7.3.2.6), or to multibunch beam-beam effects with a crossing angle (see Section 7.3.2.10). The interplay of different feedback systems with different time scales has not been considered in sufficient detail. Hardware imperfections have also been omitted such as beam losses affecting position monitors or finite resolution of the fast luminosity monitors. These studies also did not evaluate the effect of stabilizing other quads in the linac or beam delivery system, which could improve performance.

#### 7.3.4.4 Impact of Jitter on Slow Tuning

The stability results quoted in the previous section assume that a machine has been tuned to peak luminosity at time zero. This is a valid approach to investigate the stability of the luminosity, but the effectiveness of the initial tuning itself (outlined in Section 7.3.3.4) will also be influenced by the dynamic errors. If train-to-train luminosity variation is significant, then the tuning will need to average many trains, increasing the “tuning” time. However, the tuning will only converge if it can be completed before any uncompensated slow drifts can accumulate. Results from the previous section’s stability studies suggest typical RMS train-to-train luminosity variation should be  $<10\%$  for models **A** and **B**, and as large as 25–30% for model **C**. For TESLA with simple intratrain feedback, this can be reduced to  $\sim 15\%$ , and to  $\sim 8\%$  with the full feedback. Figure 7.18 shows simulations of TESLA with ground motion **C** and the full feedback, where the optimal vertical offset and angle found by feedback can vary between trains by 36% of the nominal beam size.

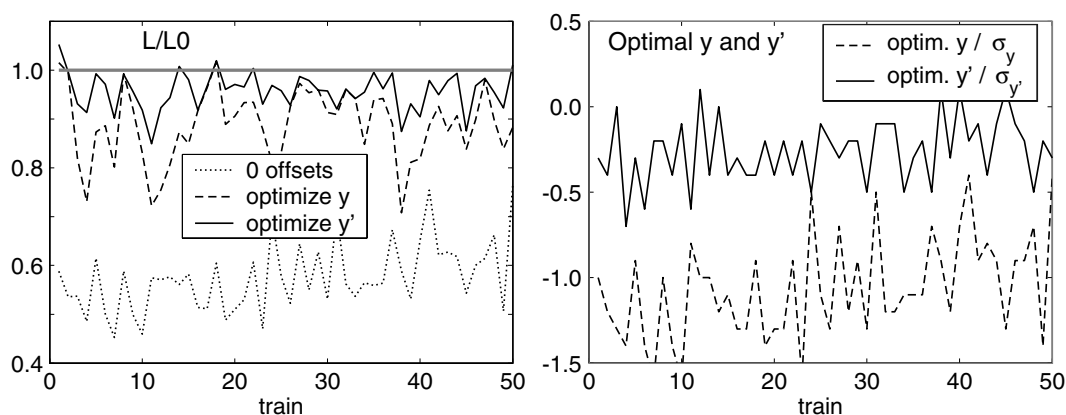


FIGURE 7.18. TESLA simulations with ground motion **C** and intratrain IP feedback with full optimization. Left: Normalized luminosity. Right: Optimal  $y/\sigma_y$  and  $y'/\sigma_{y'}$  with respect to zero offsets. Only one seed is plotted.

Luminosity variability is not the only issue of importance for tuning. Train-to-train position or energy jitter throughout the LET can cause train-to-train changes in the beam size and shape, as well as backgrounds. These all impact the accuracy of the beam size and position diagnostics required to tune up the machine. Experience at the SLC would indicate that an untuned machine can be more unstable than a tuned machine, making it difficult for the procedures to converge.

Additional technical sources of noise, not included in these simulations, can potentially increase the train-to-train jitter. Extreme care should be taken not to allow machine components to introduce noise above the bandwidths of the various feedbacks (for TESLA this includes high-frequency noise within the bunch train). Obvious candidates for potential “white noise” sources are damping ring extraction kickers, rf systems, and any other pulsed systems. TESLA is especially sensitive here, due to the tight beam-beam tolerances set by the high disruption parameter. At some point, the jitter will become a significant hindrance to the tuning. An averaging over several trains, to reduce the impact of luminosity fluctuations on slow tuning, will be more efficient in warm machines due to their higher repetition rate. In TESLA the intra-train feedback and the possibility of performing some tuning scans within a single bunch train may improve the situation; the extent to which this compensates the lower repetition rate, and the implications for hardware performance, remain to be studied in detail.

The impact of ground motion and technical noise on the tuning is extremely important for all machines. Until these effects are evaluated, it is difficult to quantify with confidence the achievable luminosity.

### 7.3.4.5 Effects on Longer Time Scales

The previous discussion covered motion on the very fast time scale. On a very long time scale, ground motion (for example, diffusive motion, ground settling, seasonal or diurnal drifts, *etc.*) will gradually degrade the linac alignment, and decrease the luminosity. Many of these effects are modelled by the ATL law or, for systematic motion, with the ATTL law, but typically under the assumption of uniform geology. Care must be taken to ensure that natural geologic discontinuities and non-uniformities do not break the expected correlations of the motion.

Projects foresee different strategies for dealing with these effects. TESLA assumes that the trajectory will be sufficiently stable to be corrected by dipoles located at the quadrupoles. Component realignment would be limited to the yearly shutdowns. JLC-X/NLC and CLIC plan to use active mover systems to quasi-continuously align the components onto the beamline. If the BPM electronics are stable, then invasive beam-based alignment (discussed in Section 7.3.3.3) should not be needed during the course of a run.

For the ground motion models considered, the impact on integrated luminosity should be minimal. In the intermediate time scale, accumulated misalignments will first appear as aberrations in the beam delivery system, which should be curable by BDS orbit correction and slower tuning knobs. The interplay of the BDS orbit correction and IP feedback needs to be studied, especially for TESLA, given its low repetition rate and tight sensitivity to beam-beam offsets. There are also still outstanding questions about the details of the orbit correction implementation that require further study.

### 7.3.4.6 Assessment of Site and LC Technological Noises

To assess the expected vibration levels at various proposed sites, it is important to consider not only external site and geology dependent noise, but also internally generated noise from collider components. The internal sources depend on the technology chosen but may be almost site independent. The following is a discussion of issues affecting stability conditions for various tunnel and collider configurations, attempting to classify them in comparison with models **A**, **B**, **C**.

If a linear collider is built in a deep tunnel in competent rock, then the noise from external sources when measured on-the-floor will be close to ground motion model **A**. This model was based on data from the LEP tunnel at CERN (about 100 m depth) and similar behavior can be expected in a deep tunnel in Illinois, California or Japan (given appropriate geology). Measurements suggest that surface activity does not greatly influence the noise level in the tunnel.

If a linear collider is built in a shallow tunnel, but on a layer of competent rock, then the noise from external sources is expected to be between ground motion model **A** and model **B**, assuming that the site is sufficiently remote and nearby surface activity is limited. (An issue for further R&D is to clarify requirements on noise sources). An example might be a cut-and-cover tunnel on one of the California sites.

If a linear collider is built in a shallow tunnel in a sedimentary layer with considerable on-surface urbanization and activity, then the noise from external sources when measured on-the-floor may reach or exceed ground motion model **C**. An example would be an LC constructed in the vicinity of DESY in a HERA-like tunnel, for the portion lying under an urbanized area. The more rural part of the tunnel where the IR would be located should be quieter. Further R&D is required to estimate noise levels (issues such as resonances of the top sedimentary layers need to be understood) and measurements are planned. The same estimates would apply to shallow tunnels at KEK or near Fermilab. In general, a shallow tunnel in unfavorable geology and/or in an urbanized area represents the greatest uncertainty and risk in estimating noise levels, and requires extremely careful study.

Technology-generated internal noise will be different for warm and cold machines. One category is the noise generated by machinery (such as cryo systems, water pumps, *etc.*) and power supplies located in parallel utility tunnels or on the surface and transmitted to the collider components through the ground. Such noise sources are of concern (an item for further R&D), and no detailed evaluation is available for either technology. However, such noise sources can likely be suppressed by proper design and vibration isolation (to avoid transmission to the ground), as successfully done in industry and in other projects such as LIGO. Noise sources (*e.g.*, power supplies, electronics with fans, *etc.*) located in the tunnel present another challenge which must be evaluated and their effects minimized (R&D item).

Another category of project-specific internal noise is vibration generated by components located on the support girders. For warm machines, the main issues are vibration generated by cooling water and mechanical coupling from pulsed rf sources to the structures. The linac quadrupoles typically have separate supports and are coupled to the structures only via the ground, and possibly via the beampipe bellows if the BPMs are fixed to the quadrupoles (as for NLC). NLC studies have shown that, while vibration of rf structures due to cooling water can be several hundred nanometers (which is tolerable for them), the coupling to nearby quadrupoles is only about a percent [60], *i.e.*, several nanometers.

Vibration due to cooling water in the quadrupoles was measured to be only on the nanometer scale [61]. Taken together, these considerations suggest that in favorable tunnel and geology, the vibration of linac quadrupoles for warm machines can be as small as the level of the ground motion model **B**, and pessimistically, within a factor of 2–3. Further R&D is needed to demonstrate that the stability of the quadrupoles is sufficient in the full scale final design of the warm machines.

To reach multi-TeV energies, it may be necessary to reduce component motion to somewhat below the level of model **B**. If passive stabilization is not sufficient, then active methods may be used. Recent stabilization studies at SLAC and CERN [62] indicate nanometer stability may be feasible. In CLIC studies, vertical vibration in a water-cooled stabilized linac quad was found to be 0.9 nm without and 1.3 nm with nominal water flow above 4 Hz [63]. Further R&D is needed both to demonstrate a full scale system and to study compatibility with operation of the collider.

For TESLA, possible sources of internal vibration are the rf pulse in the cavities (due to Lorentz forces, piezo-tuners, and microphonics, the first of which is known to cause longitudinal contraction of the cavities by several microns [64, 65]), as well as coupling from the cryogenic systems (pumps, *etc.*). The superconducting TESLA linac quadrupoles are in the same cryomodule as the cavities and supported via a common “girder” (the 300 mm gas return pipe). An important design issue is to ensure that the quadrupoles are sufficiently decoupled from vibration sources in the cryostat. In the latest generation of cryomodule, the quadrupole is mounted directly under a support structure at the center of the module. This location was chosen to maintain static alignment tolerances during pumping and cooldown in spite of the large asymmetrical forces [66], and it may also help reduce vibrations. Both the quadrupoles and the cavities are mounted between bellows to decouple motion through the vacuum chamber, but neither the vibration modes of the quadrupole nor the coupling to the cavities have been quantitatively analyzed.

The first cryomodules installed at TTF in 1995 were equipped with a large number of vibration sensors [67], but no reliable measurements of quadrupole vibration are available and serious investigations have started only recently. Both experimental studies and numerical analysis need to be urgently pursued in order to ensure that the quadrupole vibration amplitudes are not significantly larger than anticipated.

This discussions has focused primarily on the main linacs, where there are hundreds of sensitive components. The beam delivery system has elements with tighter tolerances, but they are sufficiently few that they do not pose a major risk even if individual stabilization were required.

### 7.3.5 Other Time-Dependent Sources of Error

Although vibration and ground motion are the most important sources of time-varying performance in the LET, they are not by any means the only ones. The remaining time-dependent sources of error are summarized here.

### 7.3.5.1 Magnet Strength Jitter and Drift

The limitations on magnet strength variation are primarily set by the collision-steering requirements of the linear collider, rather than the emittance control requirements. The RMS beam-to-quad offsets in the quadrupoles after all steering and alignment is complete will typically be tens of micrometers for JLC-X/NLC and CLIC, and hundreds of micrometers for TESLA. These values are large compared to the tolerances established in Section 7.3.3.3 because DF steering tends to result in large but correlated beam-to-quad offsets that cancel one another out over one or two betatron wavelengths. In order to limit the amount of unwanted beam steering occurring in an inter-train period, the fast variation in quad strength must be on the order of  $100 \times 10^{-6}$  for JLC-X/NLC or CLIC, and  $250 \times 10^{-6}$  for TESLA. In the case of TESLA, the tolerance depends upon the IP collision feedback to remove the cumulative effect of the LET quads upon the beam-beam offset; JLC-X/NLC and CLIC tolerances do not rely upon such a feedback. None of the tolerances listed above particularly challenge the state of the art for magnet power supplies. The fast strength variation in permanent magnet quads has not been quantified at this level, but is expected to be acceptable.

Since the TESLA dipole correctors will be used to move the effective quad centers by a similar distance (hundreds of micrometers RMS), their fractional tolerance is comparable to the quad tolerance. Similarly, the horizontal bending magnets can steer the beam at the IP and will demand very tight control of their strength. In many cases, this tolerance can be relaxed by powering bend magnets in series from one  $\eta = 0$  point to the next. This tolerance has not recently been evaluated for any of the designs. Another tolerance of some concern is the strength of the vertical bend magnets used to transport the TESLA beam from the damping ring (at tunnel ceiling elevation) to the main linac (at tunnel floor elevation).

Magnets in the beam delivery area also have a strength tolerance based on IP spot size dilution. This topic has been studied in great detail [68, 69]; in general, stability at the  $100 \times 10^{-6}$  level is acceptable for most beam delivery quads,  $10\text{--}50 \times 10^{-6}$  is required for several others, and the final doublet magnets have relatively severe tolerances, often as tight as  $1 \times 10^{-6}$ . These tolerances are relevant for a time period between optimizations of the waist position (typically performed by maximizing luminosity), which can be up to a few hours. These tolerances might be of some concern in the case of a crossing angle: inhomogeneous heating of the doublet magnets by time-varying beam tails in the neighboring extraction line may cause unacceptable variation in the strength and/or center position of the final lenses, especially in the case where the latter are permanent magnets. The strength tolerance on strings of bend magnets in the final focus may also be unusually tight, since these magnets can move the beam horizontally in the strong sextupoles of the final focus, which would cause a shift in the longitudinal position of the focal point.

### 7.3.5.2 Relative Arrival Time

If the beams do not collide at the correct longitudinal position, then the luminosity will be reduced due to the hourglass effect. Estimates based on linear optics give a tolerance of approximately  $0.2 \beta_y^*$  for the permissible error in the  $z$  position of the collision [70]. Although in principle such a path length difference could be caused by a betatron oscillation, the amplitude of the oscillation would have to be of the order of centimeters to

make up a path length change at the level of  $100 \mu\text{m}$ ; we therefore discount such a possibility. Other potential sources of IP arrival time variation are tidal effects and timing system jitter. For all these reasons, it is probably essential to have an arrival-time monitor near the IP. In addition, TESLA will probably require some form of chicane for path-length control, since the phase relationship between the electrons and positrons is locked by their positron production and damping ring designs.

### 7.3.5.3 RF Amplitude and Phase

The relevance of main linac rf amplitude and phase jitter to luminosity performance has not been studied in great detail, primarily because the simple studies which have been performed have shown that, so long as the beam energy at the IP remains within the system bandwidth, these jitters have no impact on luminosity. In general, the tolerances implied by the IP energy stability needs of the experimenters are far tighter than any luminosity tolerance.

This is not true for the bunch compressor rf systems, which manipulate the longitudinal phase space. Table 7.21 shows the tolerances on bunch compressor amplitude and phase which lead to: (a) change in longitudinal IP position of  $0.2 \beta_y^*$ ; (b) change in bunch length of 5%; (c) change in centroid energy of 0.2%; (d) change in RMS energy spread by 25%. If one accepts that the four tabulated sensitivities are equal in their importance to luminosity performance, then the tolerances on bunch length and longitudinal position of the collision point will set the tolerances on the bunch compressor rf systems.

The studies described have all been performed on perfect lattices. Preliminary studies with tuned lattices indicate that no additional difficulties will arise in this case, although this cannot be entirely ruled out without further studies.

The amplitude and phase stability tolerances for the bunch compressor rf systems shown in Table 7.21 are somewhat tighter than the requirements on the main linac systems. These tolerances should nonetheless be achievable with a careful design, which should be possible given the relatively small number of bunch compressor systems.

JLC-X/NLC and CLIC have an additional rf-related tolerance: specifically, the amplitude and phase tolerance for the crab cavities near the IP. The phase difference between the two cavities,  $\phi_{e^+} - \phi_{e^-}$ , must be stable to approximately  $0.025^\circ$  in the case of NLC (assuming a crab cavity which operates at S-band); this is also discussed in Section 7.4.3.2. The relative phase tolerance for the CLIC crab cavity is comparable, assuming a similar frequency. This tolerance corresponds to a 2% luminosity loss due to horizontal beam offsets at the IP. The other crab cavity tolerances, such as voltage and absolute phase, are much looser and not expected to pose a problem [71].

### 7.3.5.4 Linac Energy Management

The energy profile along a linac is not constant. The accelerating voltage seen by the beam is a function of the klystron output voltage, the transmission into the structure, the phase between the beam and the rf, and the setting for the rf phase (as a function of BNS damping and bunch charge). All these might change with time, resulting in a varying acceleration from structure to structure. In addition, some accelerator sections can be

TABLE 7.21: Performance sensitivity of bunch compressor rf parameters.

Parameter	TESLA			NLC					
	$\phi$ [°]	Ampl. [%]		L-Band		S-Band		BC2 X-Band	
				$\phi$ [°]	Ampl. [%]	$\phi$ [°]	Ampl. [%]	$\phi$ [°]	Ampl. [%]
$\Delta z = 0.2\beta_y^*$	0.1	0.5		0.2	2.3	5.5	0.3	0.4	3.0
$\Delta\sigma_z/\sigma_z = 5\%$	4.6	1.4		0.6	2.6	2.4	0.3	7.0	1.4
$\Delta E/E = 0.2\%$	1.7	6.4		0.5	4.2	5.4	0.8	0.8	7.5
$\Delta\sigma_E/\sigma_E = 25\%$	2.0	3.0		1.2	6.0	3.6	0.6	2.0	2.7

switched off completely, due to klystron problems, *etc.* As a consequence, the energy at a given linac point is usually different from its design value. The mismatch between beam energy and linac magnet strength will induce optical errors and can severely deteriorate the emittance optimization in the linac. This was strongly experienced at the SLC, where a change in klystron complement could severely reduce the achievable luminosity. In practice, this means that the quadrupoles must either be rescaled when the klystron complement changes, or else that the lattice must be designed so that the emittance dilution which occurs when the complement changes is tolerably small.

The optical mismatch induced by energy errors is usually not severe, causing a multiplicative emittance growth. This was studied for the NLC, showing that a maximum emittance increase of 5 nm-rad can be expected [72]. Expected effects should be quantified for all proposals, though no major problem is expected.

The robustness of the linac emittance optimization algorithms against energy errors is expected to be more critical. This is most obvious for emittance bumps, which depend on phase advances and beta functions at the locations of errors (anywhere) and the location of correction (bump). Any changes in the Twiss functions can deteriorate the efficiency of correction. This was studied for the corrected NLC linac, but without emittance bumps [72]. A peak emittance growth of 16 nm-rad is predicted, with a typical value of 4 nm-rad. It was observed in the simulation that seeds which experienced a large emittance growth also experienced a large increase in the RMS orbit as reported by the beam position monitor system, which suggests that the emittance degradation was caused by a betatron oscillation that was permitted to propagate freely down the length of the linac. If this is the case, then the inclusion of train-by-train steering feedbacks in the simulation would likely reduce the resulting emittance degradation.

Expected energy errors due to regular imperfections and klystron failures should be included into the simulations of all projects. The change in emittance should be calculated, in order to establish sufficient robustness of correction algorithms against energy errors. If a lattice re-scaling is required, then scaling algorithms should be included into the machine designs and their performance should be quantified. This seems especially important for NLC where permanent linac magnets are used with mechanical strength tuning. The problem of klystron failures does not apply for the CLIC drive beam concept, where luminosity can in any event only be delivered with all drive beams operational.

### 7.3.5.5 Beam Position Monitor Offset Stability

As discussed in Section 7.3.4, slow ground motion will gradually drive a linear collider out of alignment, and re-steering will be required to recover full luminosity. Re-steering to a particular set of BPM readings (“gold orbit”) will succeed only if the BPM offsets do not vary dramatically once the “gold orbit” has been empirically determined. If the offsets do vary, then a more laborious and invasive tuning procedure is required to generate a new “gold orbit.” If this procedure needs to be repeated too frequently, then luminosity will never be delivered.

The linac beam-to-quad sensitivities in Table 7.19 also constitute permissible BPM offset changes in the linac after the invasive alignment procedure is complete. The stability requirement for TESLA is therefore approximately 11  $\mu\text{m}$  RMS, which is comparable to the

estimated stability of the LEP BPM system [73]. The NLC requirement is  $1.3 \mu\text{m}$  RMS; in addition, because the NLC design anticipates that the BPMs will be rigidly mounted to quads which are on movers, the NLC quadrupole centers must be stable to this level as well. Stability of BPM electrical offsets at this level has been demonstrated over a 1 week timescale [74], but the larger picture—stability of BPMs and, in the case of NLC, quad centers over months—has not been demonstrated at this level. The CLIC requirement of  $0.9 \mu\text{m}$  is in a similar situation.

These numbers correspond to the required stability of the main linac BPMs. At this time, no similar specifications are available for the BPMs in the beam delivery regions, which may have even tighter requirements. It is also important to note that poor BPM stability can be partially compensated by more aggressive use of global tuning knobs throughout the LET. This option has not been adequately studied at this time.

#### 7.3.5.6 Time-Dependent Stray Fields

At this time, none of the LET designs has a specification of any sort on time-dependent stray fields in the accelerator housing. The consensus of the reviewers is that this phenomenon will not be a significant problem for any of the designs.

### 7.3.6 Luminosity Issues Related to Energy Upgrades

The most obvious luminosity impact of an energy upgrade in a linear collider is that the normalized emittance dilution in the bend magnets of the beam delivery system scales with the sixth power of the beam energy. In the case of TESLA, horizontal emittance growth increases to  $0.01 \mu\text{m}\cdot\text{rad}$  at 800 GeV c.m., while in the case of NLC it reaches to  $0.04 \mu\text{m}\cdot\text{rad}$  at 1 TeV c.m. The CLIC beam delivery system for 500 GeV c.m. becomes intractable at an energy of approximately 1.25 TeV c.m.; the system has been designed to permit operation at 3 to 5 TeV c.m. after reduction of the bending angles in both the collimation and final focus regions, and realignment of the other magnets to the new line formed by the bends—no change in the system length is required. The NLC system is similarly designed to operate at energies above 1 TeV c.m. with a geometry change. In both the NLC and CLIC cases the geometry change can be accommodated in a tunnel of reasonable cross-section. The chromatic breakdown due to synchrotron emissions in the 500 GeV c.m. final doublet would increase to unacceptable levels in all three designs; thus, in each design a longer final doublet is envisioned for energies significantly above 500 GeV c.m., except in CLIC, where the doublet length is already sufficient for 3 TeV c.m. Since a longer final doublet introduces more chromaticity, this modification implies somewhat tighter tolerances on the final focus, and can lead to a reduction in bandwidth. Finally, in all cases the vertical beam size is reduced at higher energy, due to adiabatic damping of the emittances and also, in some cases, due to reduced normalized emittances and/or  $\beta^*$  values; this will make the collision stabilization problem more difficult.

In addition to these general issues, each energy upgrade plan has unique features which will impact the luminosity performance. These are summarized here.

## LUMINOSITY PERFORMANCE WORKING GROUP ASSESSMENTS

**TESLA:** The TESLA energy upgrade parameters call for:

- A reduction in linac repetition rate from 5 Hz to 4 Hz, which will reduce the effectiveness of train-by-train feedbacks
- An increase in the number of bunches to 4886 per train, and reduction of inter-bunch spacing to 176 ns, which may have some impact on the intra-train feedback; in principle, reduction of the inter-bunch spacing could also increase the severity of long range wakefields, but in practice this does not appear to be the case for the TESLA design wake
- Reduction in single-bunch charge to  $1.4 \times 10^{10}$ , which will reduce the influence of single-bunch transverse wakefields, although this is already not much of a problem for TESLA
- Reduction in damping-ring normalized emittances from  $8 \mu\text{m}\cdot\text{rad} \times 20 \text{ nm}\cdot\text{rad}$  to  $6 \mu\text{m}\cdot\text{rad} \times 10 \text{ nm}\cdot\text{rad}$ , and in IP normalized emittances from  $10 \mu\text{m}\cdot\text{rad} \times 30 \text{ nm}\cdot\text{rad}$  to  $8 \mu\text{m}\cdot\text{rad} \times 15 \text{ nm}\cdot\text{rad}$ ; preserving the smaller emittances may imply improved performance from the beam instrumentation

**NLC:** The NLC energy upgrade parameters call for:

- Installation of an additional 6.5 km of accelerator structures and FODO lattice in the section of the tunnel presently occupied by the bypass line, which may lead to additional wakefield emittance growth.
- Increase in  $\beta_x^*$  from 8 mm to 13 mm, which will modestly loosen the beam delivery system tolerances.

**CLIC:** It should be noted here that the CLIC design and research effort has been targeted at the requirements of the 3 TeV c.m. configuration; the resulting parameters were then scaled appropriately to the 500 GeV c.m. energy of the reference design. By comparison to the latter set, the CLIC energy upgrade calls for:

- Addition of over 11 km of 30 GHz linac per side, which may lead to significant additional wakefield emittance growth; it is anticipated that several additional emittance bumps are required per main linac to manage this source of luminosity degradation
- Reduction in  $\gamma\epsilon_x$  at damping ring extraction from  $1.6 \mu\text{m}\cdot\text{rad}$  to  $0.45 \mu\text{m}\cdot\text{rad}$ , and a reduction in the same parameter at the IP from  $2.0 \mu\text{m}\cdot\text{rad}$  to  $0.68 \mu\text{m}\cdot\text{rad}$ ; this may make the emittance preservation problem more severe, and will further constrain synchrotron radiation emittance growth in all parts of the LET
- Reduction in linac repetition rate from 200 Hz to 100 Hz, which will make train-by-train feedbacks less effective
- Reduction in  $\beta_x^*$  from 10 mm to 6 mm, which will make the final focus more difficult to tune and stabilize, and will lead to increased synchrotron radiation emittance growth in the final doublet; increase in  $\beta_y^*$  from  $50 \mu\text{m}$  to  $70 \mu\text{m}$ , which will ease all of the same issues.

The CLIC upgrade from 500 GeV c.m. to 3 TeV c.m. is foreseen to proceed in stages, so that no single step of the upgrade process becomes intractable. One can nonetheless anticipate that the performance requirements of CLIC beamline devices at the final stage may be substantially stricter than those at the initial stage.

Finally, another option for high-energy operation for all LET designs is to operate the 500 GeV c.m. configurations with reduced current. This permits operation at a higher gradient, hence higher energy, but with a reduced luminosity due to the reduced beam current. The detailed luminosity implications of this option have not been evaluated.

### 7.3.7 Conclusions

The working group on the Low Emittance Transport (damping ring exit to IP) has studied the designs for the TESLA, JLC-X/NLC, and CLIC LET regions. The studies have included luminosity issues in an error-free LET, as well as luminosity degradation that arises from static and dynamic misalignments and errors, and has also briefly considered the issues relevant to higher-energy operation of each system.

The consensus of the working group is that **from the point of view of luminosity performance, the feasibility (as defined in Section 7.1.3) of each LET design has been established.** Our additional major conclusions are as follows:

- The basic, error-free designs of each LET are in a mature state. Decks exist for all important beamlines, and the fundamental design issues for a linear collider LET have been properly addressed. These issues include but are not limited to: synchrotron radiation, transverse wakefields from accelerator structures, optical aberrations in the final focus and elsewhere, and severity of the beam-beam interaction.
- The simulation codes used to assess the performance of the LET have been checked and carefully cross-compared for the case of the error-free designs, and in general agreement between the codes is good; this leads to confidence in the results of tuning or dynamic simulations performed using the same codes. Similarly, multiple codes were used in the study of dynamic misalignments, and their results were generally in good agreement.
- Simulations of main linac alignment and tuning were performed on multiple simulation codes. The results agree at the level of approximately a factor of 2 in the worst case; it is believed that the discrepancies are due to differences in the details or assumptions of the algorithms, and will be resolved presently. The linac simulations show performance that is consistent with achieving the luminosity goals of the different designs, although much remains to be done.
- A significant gap in current understanding of LET performance is the absence of detailed, integrated simulations of both initial tuning and ongoing operation of each design.
- A site with ground motion comparable to models **A** or **B** would be an acceptable situation for all LET designs. A site with motion comparable to model **C** would permit TESLA to deliver 90% of its “vibration-free” luminosity, and would limit

## LUMINOSITY PERFORMANCE WORKING GROUP ASSESSMENTS

JLC-X/NLC and CLIC to 70% to 80% of “vibration-free” luminosity, if aggressive measures were taken to combat the loss due to element motion. There is significant concern that the good operating conditions present in simulation, and required if the aggressive measures are to succeed, can be achieved in real life.

- All LET designs, regardless of ground motion conditions, will require some form of IP collision feedback based upon the beam-beam interaction; either intra-train or train-by-train operation can be considered. This implies that one or several BPMs which are critical to the operation of the LET have to be placed in the pathological near-detector environment, in which radiation levels and BPM backgrounds will be high.
- In the presence of significant detector noise which is coupled to the final doublet magnets, active stabilization of the final doublets is essential for JLC-X/NLC and for CLIC. For TESLA it is expected that an intra-train collision feedback could be used rather than magnet stabilization, although use of the latter technology as well is not ruled out.
- In order to ensure compliance with system vibration tolerances, it is important to accurately determine the degree and character of noise sources in the tunnel, and in particular those on the beamline itself. None of the designs have a girder prototype which has been fully characterized in terms of vibration.
- Train-to-train luminosity fluctuations due to element motion may be on the order of 10%. Such large variations will impact the convergence speed of tuning which is based on maximization of the luminosity signal, and in severe cases may prevent convergence altogether. In general, the performance of the slow or near-static tuning algorithms in the presence of ground motion, luminosity variations, and other dynamic effects is an area which requires considerable further study.

### 7.3.8 Concerns

In addition to these conclusions, the working group notes a number of particular concerns related to luminosity performance of the LET designs. From highest to lowest priority, these concerns are:

- All of the LET designs rely on beam instrumentation performance that meets or exceeds the state of the art. Some key examples from the various designs include: stable, high precision BPMs; BPMs incorporated into accelerator structures; BPMs in the IR for train-by-train or intra-train collision feedback; laser wires with high resolution and signal/noise ratio; fast and precise luminosity monitors; and diagnostics for the longitudinal phase plane.
- The simulations of static tuning are not yet complete: the main linac simulations need to completely converge, and similar exercises must be carried out for bunch compressor and beam delivery regions. The impact of dynamic effects during the process of static tuning must be evaluated.

- A more complete evaluation of in-tunnel noise sources, both “cultural” and “technical,” is required. Recent experiments at Fermilab have demonstrated the difficulty in assessing the impact of these sources [75].
- The present designs include an uncomfortably large jitter amplification due to collimator wakefields in the vertical plane. Recent measurements of collimator wakes indicate that the theory may overestimate the effect by as much as a factor of 2, which indicates that the desired accuracy of theoretical predictions (approximately 10%) is not yet achieved.
- The final doublet technology selected for JLC-X/NLC or CLIC must meet stringent requirements on stability in position and focusing gradient. At this time, it is not possible to make a convincing argument that an engineering solution for this problem is in hand. Note that, in the case of TESLA, it is expected that the desired gradient stability will be provided by the large inductance of the proposed superconducting magnet design, and the position stability is addressed through use of an intra-train collision feedback.
- More studies on the beam-beam “banana” instability are required to ensure that the intra-train collision feedback and luminosity optimization proposed for TESLA will function properly in practice. This is also a concern for the JLC-X/NLC and CLIC intra-train feedbacks, but the issue is less severe in these cases because train-by-train feedback and final doublet active stabilization are expected to provide most of the collision stabilization needed for luminosity.
- In the case of JLC-X, because of the small crossing angle (7 mrad) and short inter-bunch interval (1.4 ns), the parasitic collisions make the luminosity very sensitive to relatively small beam offsets at the IP. This sensitivity can be mitigated through the use of an electromagnetic shield between the incoming and outgoing beams, but this shield must intrude quite far into the IR to reduce the luminosity loss to a level comparable to what is foreseen for NLC or CLIC. The issues of acceptable luminosity loss, required shielding, and the machine-detector interface implications of the shielding must be carefully considered for JLC-X with a 7 mrad crossing angle.
- Although the “as-designed” long-range wakefields are quite acceptable from the point of view of achieving luminosity with long bunch trains, any error in the construction of the structures that changes the wakefields can exert tremendous leverage on the luminosity performance. It is important to ensure that the structures can be manufactured with wakefields which are acceptably close to the “as-designed” ideal, and that the error models used to simulate manufacturing defects reflect reality.
- The CLIC bunch compressor design is not quite complete, and a full estimate of the emittance growth induced by coherent synchrotron radiation has not yet been performed.

### 7.3.9 Phenomena That Were Not Reviewed

There were several areas in which a potential luminosity issue was identified, but insufficient information existed to quantify the performance risk. These areas are:

- Ion and electron cloud effects in the single-pass LET
- Dark current as a source of long-range wakefields, or a source of background for the instrumentation
- Beam halo, which can drive similar effects to the dark current, and which was poorly modelled and understood in the SLC
- Stray fields, in particular their impact on the tuning procedures
- Variation in the charge extracted from the damping rings

### 7.3.10 Items for Further R&D

We present here the suggested R&D items for the LET designs. The items have been ranked in their importance according to the ranking scheme described in Section 7.1.3.

#### 7.3.10.1 Ranking 1

No Ranking 1 items were found in this review. It is the consensus of the reviewers that, from the point of view of luminosity performance, the feasibility (as defined in Section 7.1.3) of each LET design has been established.

#### 7.3.10.2 Ranking 2

- Complete the static tuning studies described in Section 7.3.7 and Section 7.3.8.
- Develop the most critical beam instrumentation, including the intra-train luminosity monitor required by TESLA, the train-by-train luminosity monitor required by JLC-X/NLC and CLIC, and ensure that an acceptable laser-wire profile monitor can be provided where needed in each design.
- Perform the calculation of coherent synchrotron radiation in the CLIC bunch compressor.
- Develop a sufficiently detailed prototype of the main linac module (girder or cryomodule with quadrupole) to provide information about on-girder sources of vibration.

#### 7.3.10.3 Ranking 3

- Estimate the technical noise level which will be present at the beamline due to klystrons, pumps, and other sources which are necessarily close to the accelerator.
- For JLC-X/NLC, demonstrate the magnetic center stability (at the 1 to 10  $\mu\text{m}$  level) required in LET quadrupoles over the relevant time scale of minutes to days.

- Perform collimator wakefield measurements which are relevant to the LET designs, and investigate other solutions to the beam halo problem which would permit relaxation of the collimation aperture in the event that the wakes turn out to be as large as presently anticipated.
- Develop the BPMs required for emittance preservation and operation of the beam-beam collision feedback.
- Compute the detailed tolerances for fast vibration, magnet strength stability, rf stability, *etc.*, and verify that static tuning will converge in the presence of these dynamic errors.
- Estimate the robustness of tuning algorithms in the presence of malfunctioning BPMs, correctors, and element translation stages.
- Characterize the likely cultural noise at any prospective LC site.
- Design the “pre-LET” collimation systems which are intended for use between the damping ring extraction and the LET.
- Estimate electron/ion effects in the LET.
- Demonstrate the mechanical alignment techniques which will be used prior to commissioning.
- Complete calculations of the multibunch wakefield effects in the pre-linac and bunch compressor regions.

#### 7.3.10.4 Ranking 4

- Study the implications of reducing the value of  $D_y$  for TESLA, in the event that such a reduction is desired in order to ease the tolerances on the “banana” instability.
- Perform further simulations and studies of the formation of beam halo in the LET.
- Perform further studies on the impact of dark current on the LET.
- Demonstrate the feasibility of an intra-train feedback which operates within the short time required for JLC-X/NLC and CLIC.

## 7.4 MACHINE-DETECTOR INTERFACE

The present section is organized as follows.

The main issues affecting the baseline designs are outlined in Section 7.4.1 and discussed in detail in Section 7.4.2 to Section 7.4.7. The luminosity performance of the collider, as well as some of the essential design choices, are deeply related to the impact of the beam-beam interaction on the center-of-mass (c.m.) energy spectrum, on the phase space of the outgoing beam, and on the collision backgrounds (Section 7.4.2). All of these affect the IR layout and the spent-beam extraction scheme (Section 7.4.3), as well as some of the

final-doublet specifications (Section 7.4.4). The interrelated subjects of beam halo, collimation and machine protection are considered in Section 7.4.5, followed by a comparative overview of accelerator-induced backgrounds (Section 7.4.6). The location of the beam energy and polarization measurements (Section 7.4.7) is intimately linked to the crossing-angle issue. Energy tunability and upgradability are briefly discussed in Section 7.4.8, and the main conclusions are regrouped in Section 7.4.9.

Where appropriate, recommendations for further R&D are regrouped at the end of each section, ranked according to the definitions of Section 7.1.3; within each ranking category, the items are listed in order of decreasing importance.

### 7.4.1 Overview

Many of the critical issues in the Beam Delivery system: optical design, beam dynamics, tuning algorithms, beam-line diagnostics, and halo collimation, are largely generic across Linear Collider designs. Except for collimation, all of them are discussed elsewhere in this report. The discriminating issues affecting the design and performance of the Interaction Region (IR) and Machine-Detector Interface (MDI) are fundamentally related to the choice of linac rf technology through the time structure of the colliding beams.

First, the short interbunch separation (0.7–2.8 ns) in the warm-machine designs requires the beams to collide with a crossing angle (7–20 mrad) to avoid multiple collisions: their horizontal separation at parasitic crossings must be sufficient to suppress the multibunch kink instability. In contrast, the ability of superconducting-rf systems to sustain a long train of widely spaced bunches allows the beams to collide head-on. This has several consequences.

- The non-zero crossing angle of the warm designs complicates their IR layout. The main issues here include the need for crab crossing (Section 7.4.3.2) and for separate incoming and outgoing transport lines, as well as tougher technological requirements on the final-doublet (FD) quadrupoles (Section 7.4.4).
- The head-on geometry of the TESLA design constrains the layout of the spent-beam extraction line (Section 7.4.3.3), with implications in the areas of FD aperture, masking, accelerator backgrounds, machine protection, and hardware reliability. It also limits the availability, and perhaps the performance, of beam-energy and -polarization diagnostics (Section 7.4.7).

Second, warm and superconducting rf systems are naturally optimized for bunch trains of very different length and repetition rate, resulting in contrasting sensitivities to, and cures for, collision jitter and vibration throughout the machine (Section 7.4.4).

- The high repetition rate ( $\sim 10^2$  Hz) of the warm machines makes it possible for train-to-train collision-feedback systems to compensate for magnet vibrations (and other rapidly varying sources of luminosity loss in the BDS) up to about 10 Hz. Higher-frequency vibrations must be damped by proper design of supports, and/or actively compensated. Depending on the actual ground-motion and magnet-motion spectrum, satisfactory performance of these feedback and stabilization techniques may prove essential in achieving the luminosity goals.

- In TESLA, the large number of bunches per train, combined with the wide bunch spacing, allows for an intra-train collision feedback that devotes the first few percent of every train to restoring collisions between two trains initially separated by potentially large transverse offsets. This technique significantly relaxes the tolerances on ground motion and other sources of vibration throughout the machine.

Finally, the time structure of the beam impacts the design of the machine-protection and collimation systems (Section 7.4.5), as well as the sensitivity of some particle detectors to beam-induced backgrounds (Section 7.4.6).

- In the case of an errant beam pulse, the post-linac collimation section must gracefully handle an entire bunch train in JLC, NLC or CLIC. But it is only required to withstand at most two bunches in TESLA<sup>4</sup> where the long spacing between bunches allows an emergency-extraction kicker to direct the remainder of the beam onto the main dump before it can damage the beam line. This feature reduces by a factor of 40 (compared to NLC) the amount of beam that may be accidentally lost in the TESLA BDS in case of a major hardware fault in the linac, albeit by shifting part of the emphasis onto the reliability of the machine-protection system. In all machines however, the critical issue in collimator design remains single-bunch damage.
- The sensitivity of individual experimental subdetectors to machine-induced backgrounds may favor one or the other time structure, depending on their time resolution and integration window. However, the predicted background levels appear sufficiently moderate that differences between machines can be mitigated by adjustments in detector design: this issue is not considered critical, at the present level of understanding, for any of the linear-collider concepts.

## 7.4.2 Beam-Beam Effects, Luminosity Spectrum, and Collision Backgrounds

In all designs, the luminosity goals lead to IP beam sizes small enough for each bunch to generate an intense electromagnetic field which focuses the opposite bunch, leading to an increase in total<sup>5</sup> instantaneous luminosity, but also to a significant broadening of the angular spread of the outgoing beam (200–400  $\mu\text{rad}$ ) and to the emission of beamstrahlung (Figure 7.19). Each primary-beam particle radiates, on the average, one to two photons with a typical energy of several GeV. This process dilutes the luminosity spectrum toward lower  $e^+e^-$  c.m. energies (Figure 7.20), and is an abundant source of backgrounds ( $e^\pm$  pairs, minijets, and backscattered secondaries).

Analytical treatment of the beam-beam interaction is not possible, so one has to resort to simulations. Two widely used packages are CAIN [76] and GUINEA-PIG [77]. Their predictions of the beamstrahlung flux and of the total energy carried by the pairs were compared for TESLA parameters, showing very good agreement [78]. GUINEA-PIG estimates of the luminosity enhancement expected at SLC for different beam parameters also agreed well with actual measurements [79]. One can therefore consider these simulations as quite reliable.

<sup>4</sup>At least for fast energy errors. Other fault scenarios are discussed in Section 7.4.5.2.

<sup>5</sup>That is, integrated over the entire energy spectrum

## LUMINOSITY PERFORMANCE WORKING GROUP ASSESSMENTS

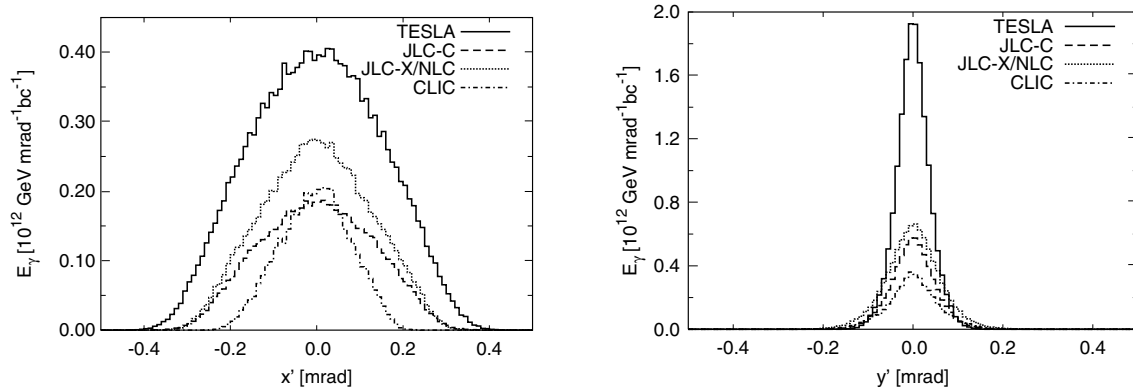


FIGURE 7.19. Angular distribution of beamstrahlung photons in the horizontal (left) and vertical (right) planes, for TESLA (top curve), JLC-C and JLC-X/NLC (middle curves) and CLIC (bottom curve). The flux predictions assume perfectly centered collisions of ideal gaussian beams, and correspond to the parameters listed in Table 7.22.

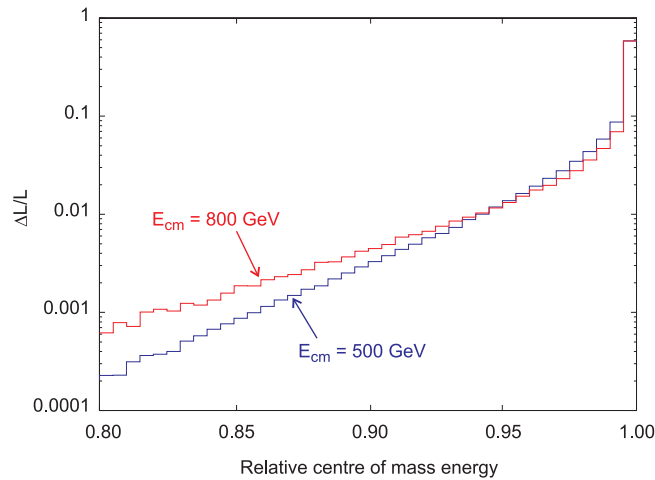


FIGURE 7.20. Luminosity spectra for 500 GeV and 800 GeV c.m. energy (TESLA parameters).

### 7.4.2.1 Luminosity Spectrum

The predicted c.m. energy distributions are fairly similar in all designs. At  $\sqrt{s}=500$  GeV, the average energy loss per beam particle  $\delta_B$  ranges from 3–5%, with about 65% of the total luminosity at c.m. energies above 99% of the nominal value, and 85–90% of the luminosity within 5% of the nominal c.m. energy (Table 7.22). The degradation of the spectrum by beamstrahlung is found to be comparable to that due to initial-state radiation. In all machine designs it is possible (if so required by the experimental program) to sharpen the energy spectrum at some cost in luminosity.

TABLE 7.22: Linear colliders: beam delivery system and interaction point parameters

	TESLA			JLC-C			JLC-X/NLC <sup>a</sup>			CLIC	
	500 GeV	800 GeV	500 GeV	1000 GeV	500 GeV	1000 GeV	500 GeV	1000 GeV	500 GeV	3000 GeV	3000 GeV
Beam delivery system length <sup>b</sup> [km]	3.2			3.8			3.8			5.2	
Collimation system length <sup>b</sup> [km]	1.4			1.4			1.4			4.1	
Final Focus system length <sup>b</sup> [km]	1.2			1.6			1.6			1.1	
$\gamma\epsilon_x^* / \gamma\epsilon_y^*$ [m-rad $\times 10^{-6}$ ]	10 / 0.03	8 / 0.015		3.6 / 0.04			3.6 / 0.04			2.0 / 0.01	0.68 / 0.01
$\beta_x^* / \beta_y^*$ [mm]	15 / 0.40	15 / 0.40	8 / 0.20	13 / 0.11	8 / 0.11		13 / 0.11			10 / 0.05	16 / 0.07
$\sigma_x^* / \sigma_y^*$ [nm] before pinch <sup>c</sup>	554 / 5.0	392 / 2.8	243 / 4.0	219 / 2.1	243 / 3.0		219 / 2.1			202 / 1.2	60 / 0.7
$\sigma_z^*$ [ $\mu\text{m}$ ]	300		200	110			110			35	
$\sigma_{\Delta E/E}^d$ [%]	0.14 / 0.04			0.25			0.25			0.25	0.35
Distance between IP and last quad	3.0		4	3.5			3.5			4.3	
Crossing Angle at IP [mrad]	0			7			7 (20)			20	
Disruptions $D_x / D_y$	0.23 / 25.3	0.20 / 28.0	0.29 / 17.5	0.10 / 10.3	0.16 / 13.1	0.10 / 10.3	0.16 / 13.1	0.10 / 10.3	0.04 / 6.4	0.07 / 6.3	
$\Upsilon_0$	0.05	0.09	0.07	0.28	0.13		0.28			0.25	5.0
$\delta_B$ [%]	3.2	4.3	3.4	7.5	4.6		7.5			4.4	21.1
$n_\gamma$ [number of $\gamma$ s per $e$ ]	1.56	1.51	1.36	1.30	1.26		1.30			0.75	1.53
$N_{\text{pairs}} (p_T^{\text{min}} = 20 \text{ MeV}/c, \Theta_{\text{min}} = 0.2)$	39.4	37.3	10.7	15.0	11.9		15.0			7.2	43
$N_{\text{hadron events/crossing}}$	0.248	0.399	0.075	0.270	0.103		0.270			0.066	2.26
$N_{\text{jets}} \times 10^{-2} [p_T^{\text{min}} = 3.2 \text{ GeV}/c]$	0.74	1.90	0.23	2.27	0.36		2.72			0.29	150.5
Geometric Luminosity <sup>e</sup> [ $10^{33} \text{ cm}^{-2} \text{ s}^{-1}$ ]	16.4	28.1	8.76	18.5	17.7 (14.2)		18.5 (22.2)			16.0	47.0
$H_D$	2.11	1.90	1.61	1.42	1.49		1.42			1.42	1.70
Luminosity dilution for tuning [%]		0		5			5			10	0
Peak Luminosity <sup>e</sup> [ $10^{33} \text{ cm}^{-2} \text{ s}^{-1}$ ]	34.5	53.4	13.6	24.9	25.1 (20.1)		25.0 (30.0)			21.0	80.0
$L_{99\%}$ [%]	66	62	67	58	64		58			71	41
$L_{95\%}$ [%]	91	86	90	86	85		77			87	53
$L_{90\%}$ [%]	98	95	97	87	94		87			93	62

<sup>a</sup>Numbers in ( ) correspond to US site with 120 Hz repetition rate.

<sup>b</sup>System length includes both incoming beamlines.

<sup>c</sup>For all designs except CLIC, the IP spot sizes are calculated as usual from the emittances and beta functions. With the design emittances in CLIC, nonlinear aberrations in the final focus system increase the final spot size by 20 to 40%.

<sup>d</sup>Energy spread is for electrons / positrons if different.

<sup>e</sup>For the sake of uniformity, the geometric luminosity is simply defined as  $N^2/4\pi\sigma_x^*\sigma_y^*$  times the number of crossings per second, and in all cases assumes head-on collisions, no hour-glass effect and no pinch. The peak luminosity is calculated using the Guinea Pig program and incorporates all the effects, including the pinch enhancement, hour-glass, and crossing angle where applicable, plus any additional IP dilutions that may be expected.

## 7.4.2.2 Beam-Beam Backgrounds

**7.4.2.2.1 Bremsstrahlung and Pair Production** Bremsstrahlung photons are emitted at small angles (Figure 7.19) with respect to the incoming-beam direction, and can easily be extracted from the detector. But their interaction with beam particles or photons from the opposite bunch constitutes one of the main background sources, through the abundant production of low-energy  $e^+e^-$  pairs. The dominant processes are  $\gamma\gamma \rightarrow e^+e^-$ ,  $e\gamma \rightarrow ee^+e^-$  and  $ee \rightarrow eee^+e^-$ . The previously mentioned simulation packages calculate the pair-production rate using the beamstrahlung photons and replacing the primary electrons and positrons with equivalent virtual-photon spectra. The resulting final-state particles are then tracked through the electromagnetic field of the bunches as it evolves during the collision. The energy and transverse-momentum distributions computed in this approximation for the  $ee \rightarrow eee^+e^-$  process have been compared [80] to a more complete Monte Carlo written by Vermaseren [81]. The two calculations show reasonable agreement, but at large transverse momenta, differences of up to a factor of 2 were found.

Because of their low momenta, the pair-produced electrons and positrons are strongly deflected by the field of the beams, resulting in a strong correlation between their polar angle  $\theta$  and the maximum transverse momentum  $p_t$  (Figure 7.21). The sharp  $\theta$ -dependent cutoff reflects the fall-off of the electromagnetic field of the bunch at large radial distances. The detector solenoid maps the  $p_t$  cut-off into two “stay-clear cones,” the apex of which lies at the IP and which contain most of the pair-produced background flux. Only a small—albeit somewhat uncertain—fraction of the pairs is produced with large enough initial angle and/or transverse momentum to escape the cones. While  $e^\pm$  pair-production constitutes a potentially serious background source for the vertex detector, appropriate combinations of solenoid field strength, extraction-line aperture, mask angular coverage and vertex-detector radius have been shown to result in tolerable occupancy levels (Section 7.4.6).

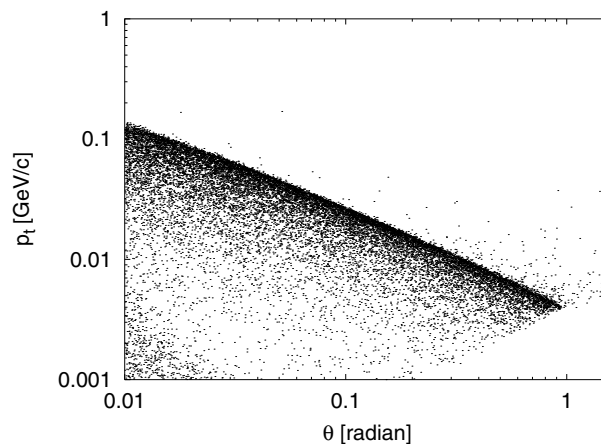


FIGURE 7.21. Polar-angle and transverse-momentum distribution, after the collision, of  $e^\pm$  from incoherent pair production. This particular simulation uses CLIC parameters, but such behavior is generic across projects.

The pairs created at the IP are channelled by the solenoidal field to the pair luminosity monitor, the extraction-line chamber, or the first extraction-line quadrupole. The total energy carried by the pairs is quite large. A substantial fraction of these particles will be lost in the spent-beam channel before it leaves the detector (see Figure 7.22 and Section 7.4.3.3), resulting in:

- A significant backscattered neutron flux (Table 7.23)
- Secondary photons from which the detector must be shielded
- Charged electromagnetic-shower debris which are scattered back toward the IP. These soft  $e^\pm$  follow the field lines of the solenoid which channels them back toward the vertex detector, potentially increasing the background by an order of magnitude.

TABLE 7.23

Neutron hit density in the proposed vertex trackers, in units of  $10^9$  n/(cm<sup>2</sup>×yr) at 500 GeV c.m. energy. The numbers reflect the different masking and extraction-line geometries as optimized by the individual machine and detector study groups. LD and SD refer to the two NLC detector models mentioned in Section 7.4.3.1. Neutron-flux predictions are not yet available for CLIC.

	TESLA [82]	NLC (LD) [83]	NLC (SD) [83]	JLC-X [84]
Pair-induced	1.0	1.8	0.5	0.03–0.13
Backscattered from dump(s)	negligible	0.1	0.1	0.03–0.05

Backgrounds from backscattered debris have been largely mastered in all machine designs. Masking schemes (Figure 7.23 through Figure 7.25) have been devised to shield the detector from backscattered electromagnetic debris and to deplete the neutron flux. The corresponding backgrounds in the tracking detectors have been reduced to acceptable levels. The pair-induced neutron flux, however, remains of concern for some vertex-detector technologies (Section 7.4.6).

LUMINOSITY PERFORMANCE WORKING GROUP ASSESSMENTS

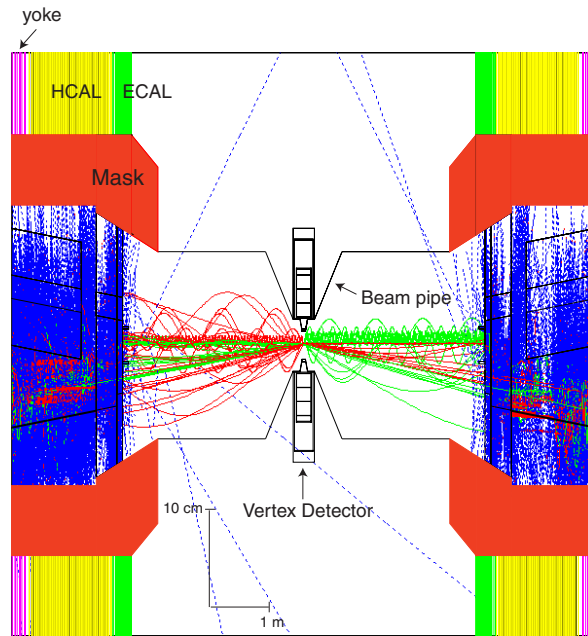


FIGURE 7.22. Simulated beam-beam backgrounds at the IP, showing the trajectories of  $e^\pm$  pairs and electromagnetic shower debris (x-z view). The dashed blue lines represent photons, red solid lines electrons, and green lines positrons. The incoming  $e^-$  beam comes in from the left. High-energy  $e^\pm$  debris roughly follow the initial beam direction into the extraction line, while lower-energy products spiral along the solenoid field lines and hit the front face of the luminosity monitor. Note that pair-induced low-energy  $e^-$  traveling to the left (the right) are defocused (focused) by the incoming  $e^-$  ( $e^+$ ) beam (and similarly for positrons). This particular simulation reflects the NLC IR layout and beam parameters, but similar features are found in all projects.

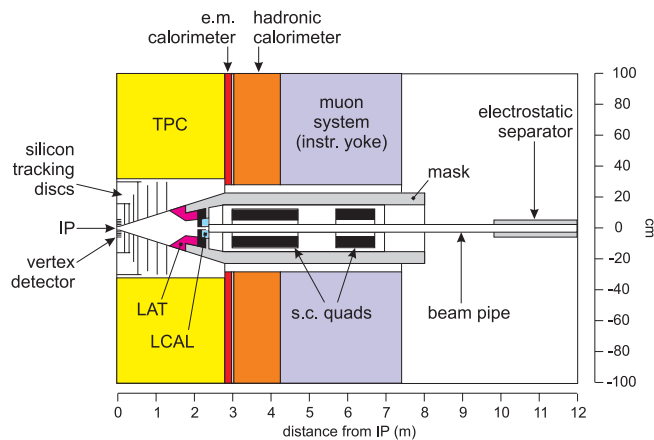


FIGURE 7.23. IP masking and spent-beam extraction in the TESLA design (y-z view).

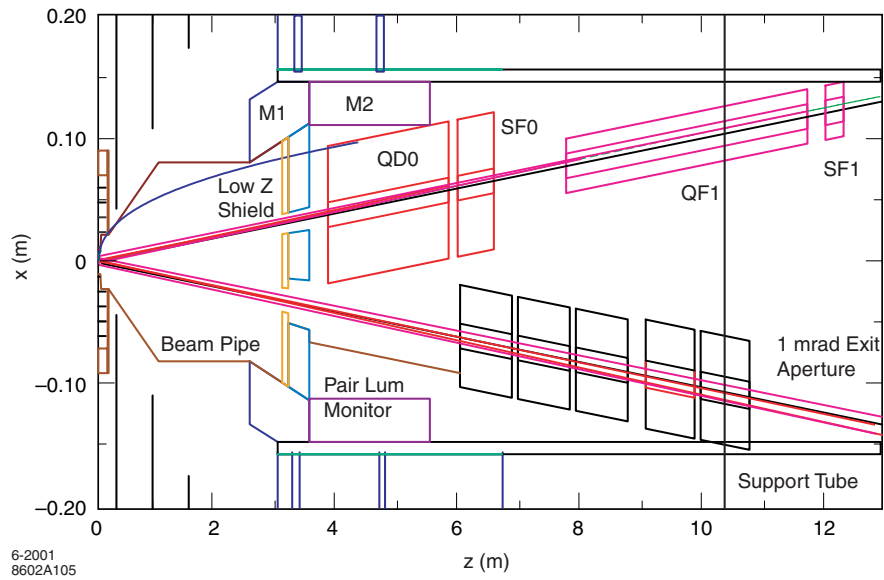


FIGURE 7.24. NLC IR layout (LD detector model, x-z view). M1 and M2 are detector masks, QD0 and QF1 are the final doublet, and SF0 and SF1 are chromaticity-correcting sextupoles.

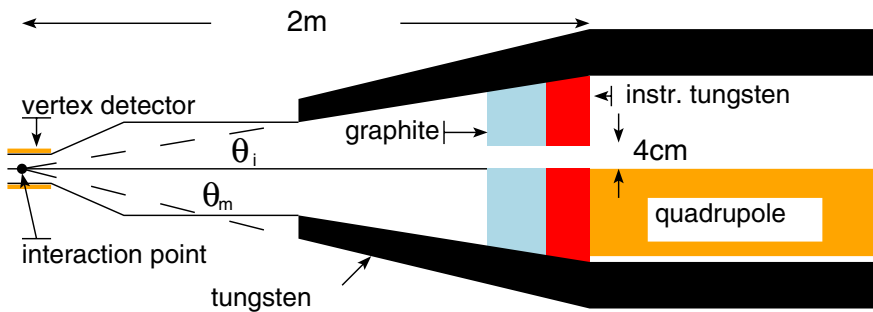


FIGURE 7.25. View from above of the CLIC mask design. The sketch is stretched in the vertical direction. Care has to be taken that no particles are backscattered through the hole in the mask.

**7.4.2.2.2 Hadronic Backgrounds** The total hadronic cross section in two-photon collisions is poorly known at high energies. The expected number of events with a two-photon c.m. energy above 5 GeV is given in Table 7.22. This comparison is based on the parameterization of Reference [85]; other parameterizations [86] agree to better than a factor of 2 at  $E_{cm}=500$  GeV.

A fraction of the hadronic events are relatively hard and contain so-called minijets. They are due to direct production of quark pairs ( $\gamma\gamma \rightarrow q\bar{q}$ ), direct-photon scattering off a parton in a resolved photon (“once-resolved” process:  $\gamma q \rightarrow gq$ ,  $\gamma g \rightarrow q\bar{q}$ ), or parton-parton scattering if both photons are resolved (eight different “twice-resolved” subprocesses in all)<sup>6</sup>. Table 7.22 lists the predicted number of minijet pairs per bunch crossing with a transverse momentum above 3.2 GeV/c using the parameterization of Reference [87] implemented in GUINEA-PIG; comparable results are obtained if one uses Reference [88] instead. Their potential impact on detector performance is briefly touched upon in Section 7.4.6.

## 7.4.3 Interaction-Region and Extraction-Line Layout

### 7.4.3.1 IR Layout

The main characteristics of the proposed IR layouts are as follows:

- TESLA: The beams collide head-on and are separated electrostatically after they exit the detector (Figure 7.23). The final-focus quadrupole doublets are superconducting. The TESLA detector design has a 4 T solenoid field.
- JLC: The beams collide with a crossing angle of 7 mrad. The final-focus quadrupole is a conventional iron magnet surrounded by a superconducting solenoid compensator, where the beams exit through the coil pocket of the quadrupole. The JLC-X detector design has a 3 T solenoid field. No detailed detector or IR design exist for the JLC-C option.
- NLC: The beams collide with a 20 mrad crossing angle and exit past the outer radius of the final quadrupoles (Figure 7.24) into an extraction line. The final-focus quadrupole doublets use permanent magnets (PM), or possibly a compact superconducting design. NLC is considering two detector options: “Large” (LD) and “Silicon” (SD), which use, respectively, a 3 T and a 5 T solenoid field.
- CLIC: The beams collide at a 20 mrad crossing angle (Figure 7.26). The baseline final-doublet system uses PM quadrupoles; a compact superconducting quadrupole is under study. The CLIC detector design has a 4 T solenoid field.

All designs incorporate conical masks to shield the detector from the secondary particle debris produced when the pairs interact. The outer parts of the mask, which must lie outside the pair stay-clear, are instrumented as a Si/W calorimeter and serve as a low-angle tagger (LAT). The inner part, which shadows the face of the quadrupole, is subjected to a high flux of particles from pair creation (several TeV per crossing). Backscattering of

<sup>6</sup>Measuring the total cross-section of the latter two will be an interesting experiment at a future linear collider.

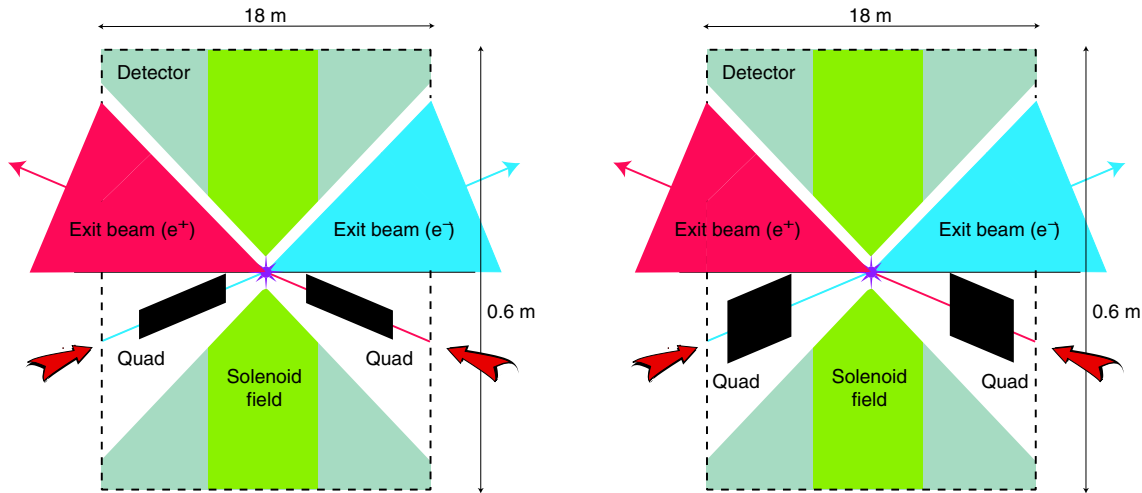


FIGURE 7.26. Top view of the CLIC IP region with the detector, the colliding beams, and the final quadrupoles for the base-line (left) and the compact final-focus optics (right) at 3 TeV. Scales are indicated. The transverse size of the detector is about 17 m.

low-energy secondaries is prevented by a covering layer of low-Z material. This section of the mask is instrumented as a luminosity monitor that measures the number of beam-beam induced  $e^\pm$  pairs [89].

**7.4.3.1.1 Evaluation** The interaction region design must provide for: support (and possibly active stabilization) of the final focus quadrupoles; masks for synchrotron radiation, and for photons and neutrons produced by pairs; beam position monitors and feedback kickers; and luminosity and (possibly) beam-size monitors. Almost all of these elements are tightly packed up against (or penetrate) the detector and the solenoid yoke.

The TESLA, JLC-X, and NLC interaction region designs are reasonably mature and contain all of the elements needed in a geometry that is consistent with the detector, solenoid, and return yoke. The CLIC IR design is not as completely developed and cannot be evaluated, but it should be similar to that of NLC.

For the head-on collisions at TESLA, the beam pipe must have a large aperture to accommodate the disrupted beam. Only superconducting (SC) magnets can provide the necessary combination of gradient and aperture. For designs with a crossing angle, the final doublet must be compact to allow the extracted beam to pass outside the quadrupole (NLC, CLIC), or must have some provision for the spent beam to be extracted through a field-free region of the magnet (JLC-X). Since the incoming beam pipe is small, PM quadrupoles can be used. These are rigid and free from external water or power connections, which can be an advantage in suppressing vibration; but they are tunable over a narrow range only.

A comparison of the angular acceptance of the present detector models is presented in Table 7.24. The low-angle coverage, which is important in some SUSY searches, is similar in TESLA (where the mask dimensions are determined by the size of the SC quadrupoles and their cryostat) and in NLC (here the magnet envelope is specified to be within the cone of

TABLE 7.24

Detector polar-angle coverage. All numbers are in mrad and refer to the 500 GeV designs except for CLIC. In the crossing-angle designs, the pair monitor must allow for the passage of both the incoming-beam and the spent-beam pipes, which causes a  $\sim 10\%$  gap in azimuthal coverage for  $\theta < 30$  mrad.

	TESLA	NLC (LD)	JLC-X	CLIC (3 TeV)
Main detector	>83	>52	>200	>120
LAT (instrumented mask)	27–83	32–52	150–200	40–80
Luminosity (pair) monitor	5.5–28	6.4–32	50–150	10–40

the pair stay-clear to maximize the detector acceptance). In JLC-X the mask dimensions are determined by the large size of the iron quadrupoles and their compensating solenoid. In CLIC at 3 TeV, the acceptance is limited by the pair stay-clear; no optimization has been done yet for the 500 GeV CLIC design.

An important difference between the designs is in the support system for the final doublets, where differential motion of the doublets can cause the beams to miss each other at the IP. TESLA plans to compensate for such motion with intra-train feedback and thus uses conventional separate supports. JLC-X proposes a single carbon-fiber reinforced tube which extends through the detector and supports both doublets. In NLC, each doublet would be mounted inside a cantilevered support tube; a number of different configurations are under study, combined with a feedback system to provide active stabilization of the relative magnet positions using inertial sensors and/or an optical-anchor interferometer [90].

### 7.4.3.2 Impact of Crossing Angle on Nominal Luminosity

**7.4.3.2.1 Horizontal Beam-Beam Overlap** In the normal-conducting designs, the crossing angle is large enough to degrade the nominal luminosity by a factor<sup>7</sup> of 4–6, unless compensated by a crab-crossing system as planned for NLC, CLIC and probably JLC. The transverse alignment tolerances of the crab cavities are quite loose. However, there are tight roll tolerances ( $\sim 0.4$  mrad for a 2% luminosity loss), which means that the cavity must be mounted on a mover system and adjusted.<sup>8</sup> The structures themselves are not an issue; an actual S-band version will be installed at the TTF and used to measure bunch length. The tolerance (see also Section 7.3.5.3) on the relative phase stability of the two cavities ( $0.025^\circ$  of S-band) is challenging: some R&D is still needed here, but the engineering appears feasible (the cavities can be driven from a single klystron and one can use the reflected power signal to adjust the relative phases).

**7.4.3.2.2 Solenoid-Steering Effects** The transverse component of the detector solenoid field present in any crossing-angle configuration shifts the positions and angles of the beams at the IP, as well as the outgoing-beam trajectory, by energy-dependent amounts. While small variations in nominal beam energy may be accommodated by steering correctors and/or quadrupole trim windings, covering a wide c.m. energy range

<sup>7</sup>Including the loss of pinch enhancement ( $H_D \rightarrow 1$ ).

<sup>8</sup>The roll control also allows efficient removal of any residual  $y - z$  wakefield correlations at the IP.

may require realigning several components in the extraction line, an operational overhead. This has been studied for a 6 T detector at NLC and the shift was less than 1 mm between 90 GeV and 1 TeV. With a 1 cm aperture extraction line, this may be acceptable; alternatively, the aperture could be increased or the magnets could be equipped with movers as elsewhere throughout the complex.

**7.4.3.2.3 Dispersion and Emittance Dilution** With a non-zero crossing angle, synchrotron radiation emission and dispersion due to the solenoid and fringe fields can cause vertical beam size growth at the IP. The increase in vertical beam size was found to be negligible [91] for three different solenoid designs considered for the NLC. Simulations for CLIC at 3 TeV, which used a simplified model of the solenoidal field, indicated an acceptable spot size growth [92]. Because the vertical beam size growth is a rapidly increasing function of the transverse component of the solenoid fringe field, it is prudent to make detailed calculations using realistic solenoid field maps as these become available for each machine.

### 7.4.3.3 Spent-Beam Extraction

The spent-beam extraction line must satisfy a number of difficult constraints. The main dump must gracefully handle both the nominal, highly disrupted charged beam, and a low-emittance outgoing beam for the case when no collision has occurred. At  $\sqrt{s}=500$  GeV, 180–360 kW of beam power (assuming nominal conditions and a static, perfect machine) are radiated as photons, which must be absorbed in a straight-ahead dump. Spent-beam losses must be kept at a moderate level, to limit heat deposition and component activation, and to avoid production of excessive backgrounds in the physics detector (and in the post-IP beam instrumentation). The geometry is further complicated by the presence of the incoming beam, whether in a separate beam line or not. The dumps are typically located a substantial distance from the IP to allow the low-emittance beam to expand in size before striking the dump window, and to reduce the neutron backshine. Since the beam power to be absorbed is large for both the neutral and charged beams, it is desirable to minimize the number of expensive, water-cooled dumps.

The main characteristics of the proposed extraction lines are as follows.

- TESLA uses two separate dumps for the beamstrahlung and for the charged spent beam, housed in the same shielded dump hall located 240 m from the IP. The outgoing charged beam is vertically deflected immediately downstream of the IR doublet using a combination of an electrostatic separator and of a superimposed magnetic field (the two fields cancel for the incoming, oppositely charged beam). A thin-bladed septum magnet then separates the spent beam from the incoming beam into two distinct vacuum chambers before the first parasitic crossing (about 50 m from the IP). A large-aperture lattice transports the spent beam to the dump with minimal particle losses. The beamstrahlung dump, located directly above the main charged-particle dump, requires a small aperture to allow passage of the incoming charged beam (Figure 7.27). The current design has an aperture of 20 mm diameter, allowing some 40 kW of beamstrahlung power through to a second dump located after the first dipole bend. Secondaries from the charged-beam dump cannot reach the

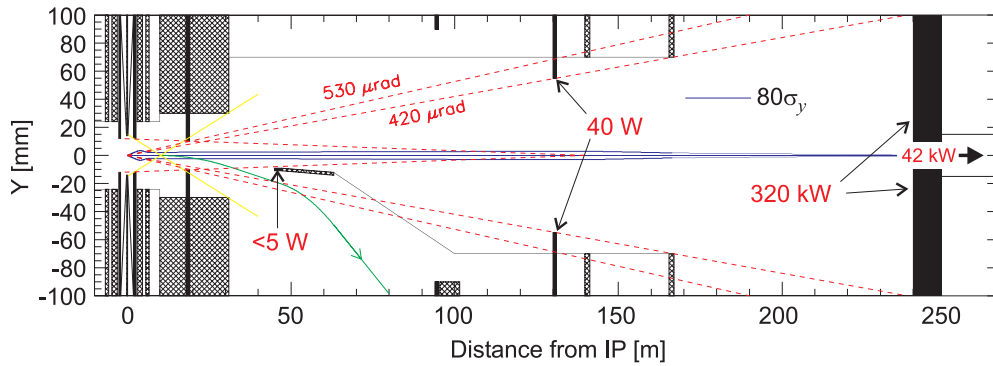


FIGURE 7.27. Vertical layout of the TESLA final-transformer region, as presented in Section II-7.6.2 of Reference [93]. The beamstrahlung power levels are for the 500 GeV machine under ideal conditions.

vertex detector on a straight-line trajectory, but the smaller number from the beamstrahlung dumps can.

- NLC uses a single dump located 150 m from the IP for both the neutral and charged particle beams. The 20 mrad crossing angle allows the outgoing beam to exit in a separate beam pipe, with flexibility in the choice of optics. The first quadrupole is 6 m from the IP. A chicane separates the neutral and charged beams to allow energy and polarization diagnostics at an image point of the IP. The dump is on-axis to accommodate the neutral beam, and a 1 mrad beamstrahlung stay-clear is enforced. Back-scattered secondaries from the dump can reach the vertex detector on a straight-line trajectory, but the distance and apertures limit the solid angle to an acceptable level.
- JLC-X plans to use two separate dumps. A beamstrahlung dump is located 300 m from the IP, while the charged beam is bent toward a separate dump.
- CLIC plans an extraction line similar to that of NLC, but no detailed layout is available yet.

**7.4.3.3.1 Evaluation** In TESLA, where the outgoing neutral beam and the incoming charged beam share the same vacuum pipe between the IP and the dump, a narrow compromise has to be found between conflicting requirements. The incoming-beam aperture needs to be restricted by masks that protect the detector from synchrotron radiation (SR). The outgoing beam requires a large stay-clear for outgoing SR-photons and beamstrahlung-photons to limit backscattered backgrounds and to avoid excessive heat deposition in the superconducting final doublets. In addition, the low-energy particles in the outgoing beam are overfocused by the strong final doublets, leading to large quadrupole apertures and precluding most extraction-line diagnostics.

The tightest apertures for the outgoing photons are a 10 mm radius SR mask located 18 m from the IP, the extraction-septum blade at 45 m (in the vertical only), and a 55 mm-radius collimator at 130 m that protects the intermediate doublet. The resulting stay-clear angle

of  $420 \mu\text{rad}$  (neglecting the septum blade, discussed further below) seems marginal for the neutral beam, as it is barely larger than the expected angular spread of the beamstrahlung fan (Figure 7.19) assuming nominal conditions, centered collisions and zero beam-beam deflections.

An area of particular concern is that of the extraction septum. Such magnets are delicate to build and subject to failure, especially in as hostile an environment as that of a 11 MW disrupted beam passing a few mm away from a thin blade. In addition, the edge of this septum, located at  $\theta_y \sim -200 \mu\text{rad}$  (Figure 7.27), further restricts the vertical photon stay-clear.<sup>9</sup> It is highly likely that pulse-to-pulse jitter, ground motion, or diagnostic beam-beam scans will repeatedly induce vertical beam separations that translate into deflections of  $100\text{--}300 \mu\text{rad}$ . While beam separation by a few  $\sigma$  suppresses luminosity, beamstrahlung emission persists, potentially sweeping the full photon fan along the septum magnet for at least a fraction of a bunch train.<sup>10</sup> More importantly, time-dependent errors in the linac and the BDS may result in rapidly varying bunch-shape distortions that significantly enhance beamstrahlung production. Recent simulations of such effects [95] suggest that the total radiated beamstrahlung power may exceed 500 kW (compared to 360 kW under ideal conditions), and that photon losses at the septum could average 2–3 kW during routine operation, with rapid fluctuations up to about three times the average value. The resulting neutron flux reaching the detector may be significant because of the proximity to the IP. None of these effects have been taken into account in the present extraction-line and IR designs. Assuming that the septum can be built to safely handle the average loss rate, protecting that area against excessive power deposition will further complicate the machine-protection system. More generally, the tightness of this (and other) extraction-line aperture(s) will no doubt impact the operational flexibility, and therefore the running efficiency, of the TESLA BDS as currently designed.

Another critical component is the electrostatic separator. It is based on a design used at LEP which reached the 50 kV/cm field needed at  $\sqrt{s}=500 \text{ GeV}$ , but which exhibited frequent arcing (1 trip/hour) when illuminated by synchrotron radiation. Given the more hostile radiation environment of the TESLA extraction line, this problem must be solved in order not to become a serious reliability issue.

The use of a single dump for both neutral-particle and charged-particle beams also constrains the design of the NLC extraction line. Because the dump has a direct line-of-sight to the IP, it should be located as far downstream as possible to limit the backscattered neutron flux. However, the 1 mrad beamstrahlung stay-clear sets an upper limit on the distance from the IP if the dump window is to have a reasonable size. Since the beamlines are separate, the outgoing aperture does not affect incoming-beam collimation. The outgoing beam size is similar to that for TESLA and the factor of 3 larger beamstrahlung stay-clear appears sufficiently generous to accommodate all possible circumstances (vertically offset beams, large deflections, beam shape fluctuations).

---

<sup>9</sup>The outer edge of the septum blade is radially constrained by the charged spent-beam stayclear. In the TDR design, the blade is 2 mm thick and its inner edge lies at  $y=-9 \text{ mm}$ ; it is protected by a “septum-shadow mask,” about 1 mm thick and 1 m long. The nominal charged-beam losses in that area amount to  $\sim 1 \text{ kW}$  [94]. A more recent study envisages to thicken the magnet blade to 5 mm, leading to an even tighter photon stay-clear.

<sup>10</sup>Until either the beam-beam feedback recenters collisions, or an MPS interlock fires the emergency-extraction kicker.

## LUMINOSITY PERFORMANCE WORKING GROUP ASSESSMENTS

The optics of the TESLA and the NLC extraction lines have been carefully optimized to minimize charged-beam losses. Both designs achieve a wide momentum bandpass and deliberately concentrate the losses (which mostly occur in the low-energy tail of the spent beam) at one or two locations sufficiently distant from the detector. The losses depend on the disrupted particle distributions at the IP, which are affected by the interplay of various incoming-beam errors with the beam-beam interaction. For instance, while horizontal separation of the beams by a few  $\sigma$  at the collision point has little impact on extraction-line radiation levels, vertical separation enhances disruption (as well as beamstrahlung production) and significantly increases spent-beam losses (Table 7.25). The predicted losses appear manageable at this stage of the design. It should be pointed out, however, that only primary particles were considered in these simulations, and that the predicted beam losses may increase once ground motion and machine imperfections are taken into account. The NLC momentum bandpass appears sufficiently wide ( $\sim 70\%$ ), and the total power deposition low enough (about 700 W for the worst-case  $20\sigma_y$  separation) to provide ample margin, at least at  $\sqrt{s}=500$  GeV. This needs to be further reviewed in the TESLA case: the extraction-line optics are constrained by the incoming beam, the total power scraped from the charged beam is an order of magnitude larger than in NLC, and the range of beam-beam offsets considered in Reference [94] is somewhat restricted.

TABLE 7.25

Predicted charged-beam losses in the TESLA and NLC extraction lines at  $\sqrt{s}=500$  GeV. All numbers are in % of the incoming-beam population unless specified otherwise. The maximum loss occurs for a vertical separation of  $2\sigma_y$  in TESLA and  $20\sigma_y$  in NLC.

Vertical IP separation ( $\# \sigma$ )	0	2	10	20
TESLA [94] (Peak losses)	0.12	0.15 (0.12 at mirror-quad collimator, 90 m from the IP)	0.10	not evaluated
NLC [96] (Peak losses)	<0.002	$\sim 0.002$	0.012	0.030 (140 W/m, 100 m from the IP)

The neutron flux backscattered from the beam dump(s) into the vertex detector has been computed for each of the IR layouts (Table 7.23). Most designs successfully reduced this flux to an order of magnitude below that of the pair-induced neutron flux, whether or not there is a direct line of sight from the main dump to the detector. This conclusion is sensitive to the details of the extraction-line geometry and to the vertex-detector radius. In NLC for instance, the hit rate from backscattered dump neutrons would increase by a factor of 40 if the inner radius of the vertex detector were halved [83]. However, the minimum

achievable detector radius is effectively limited by synchrotron radiation and beam-beam pairs, as well as by these neutrons. The NLC VTX radius is currently set at 1.2 cm as compared to 1.5 cm for TESLA.

#### 7.4.3.3.2 Open Issues and Items for Further R&D

- TESLA: the trade-offs between head-on and crossing-angle collisions, and in particular the implications of the present extraction-line design, should be thoroughly revisited (Ranking: 2). This internal review should include (but not necessarily be limited to):
  - A more realistic estimate of beamstrahlung and spent-beam losses in simulated imperfect machines with dynamical errors
  - A systematic study of the impact of a partially shared beam line on SR masking. Recent simulation results (discussed in Section 7.4.5.1) suggest that in order to effectively collimate the incoming SR fan, the aperture of the mask located 18 m from the IP needs to be such that it intercepts a sizeable outgoing SR flux, potentially resulting in a dangerous background of backscattered, penetrating SR photons
  - A reassessment of the required stay-clear for the outgoing charged and neutral beams. Are the magnitude and the longitudinal distribution of both average and occasional losses tolerable from the viewpoints of thermal effects (SC quadrupoles, septum magnet), neutron background, and performance of crucial instrumentation (BPMs, possibly also beam-energy monitors)? Are the required stay-clear apertures compatible with effective masking of incoming SR?
  - A failure analysis that examines the potential operational impact of large orbit excursions, frozen feedbacks, and septum-blade protection interlocks

In addition, the following engineering R&D is necessary for the successful operation of the head-on scheme as currently proposed (Ranking: 3):

- Demonstrate separators with high enough reliability in the predicted radiation environment, and with high enough gradient to operate at  $\sqrt{s}=500$  GeV
- Design an extraction-line septum that can safely withstand realistic beamstrahlung and spent-beam losses
- All projects: because the fringe field of the detector solenoid has a radial component,  $\mu\text{m}$ -level vibration of the solenoid field with respect to the beam will induce nm-level jitter of vertical beam position at the IP. The detector and magnet design must ensure correspondingly adequate mechanical stability of the solenoid windings and return yoke (Ranking: 3).
- CLIC: no extraction-line design is available as of this writing (Ranking: 3).

### 7.4.4 Assessment of Final-Doublet Issues

#### 7.4.4.1 Stabilization

The beams must collide head-on to avoid significant luminosity degradation. This requires limiting the relative transverse beam-centroid jitter at the IP to about one nm.

For TESLA at the DESY site, vibration of the linac and beam-delivery quadrupoles is expected to be sufficiently large that the beams would separate by many  $\sigma$  from one train to the next, independently of doublet motion. The large number of bunches per train (2820), combined with the wide bunch spacing (337 ns), allows for an intra-train collision feedback based on beam-beam deflection and luminosity signals, that devotes the first few % of every train to restoring collisions. This straightforward technique significantly relaxes the tolerances on ground motion and other sources of vibration at the IP (Section 7.3.4.3). The TESLA TDR [93] relies on this feedback alone to guarantee collision stability.

Because of their much shorter bunch trains (100–300 ns), the warm-rf machines cannot rely on intra-train feedback alone. They must be located on a site where ground-motion amplitudes are small enough that vibration of the linac quadrupoles is not an issue. The faster repetition rate ( $F_{\text{rep}}=100\text{--}200$  Hz) allows pulse-to-pulse trajectory and collision feedbacks to compensate for “slow” motion, *i.e.*, at frequencies up to approximately 10 Hz.<sup>11</sup> The remaining concern is fast motion of the final doublets. Ground-motion amplitudes at sites such as the LEP or SLAC tunnels can be low enough without further stabilization. Unfortunately, cultural noise generated by the accelerator or detector will almost certainly produce vibrations in excess of the tolerance (Section 7.3.4.6), and additional stabilization will be needed.

It is critical that the LC detectors at a warm-rf machine be designed to minimize vibrations since the FDs will be partly mounted on the detector. Several active measures are being developed for CLIC and JLC-X/NLC to provide the necessary relative stability between the FDs. These include mechanical stabilization of magnet position via feedback and correction of the magnetic-center position with dipole coils via feedforward. Both methods would rely on inertial measurements of the FD motion by seismometers (“inertial anchor”), and/or on optical interferometric measurements of their position with respect to each other or to stable ground (or a stabilized mirror) under the detector (“optical anchor”). Bench tests of both the inertial sensor and the optical anchor have already demonstrated a sensitivity close to what will eventually be required [90]. CERN and SLAC are presently developing a nonmagnetic inertial sensor and a prototype overall integrated system. Subnanometer position stabilization has been routinely achieved in industry. At the IP of a linear collider, however, it is a major challenge, because of the cramped space available, the presence of the detector solenoid field, the magnetic forces induced by the solenoid on the FDs and the interaction with other feedback systems.

The intra-train deflection-feedback technique is actually also applicable to warm machines, but the much shorter duration of the train implies exacting processing speeds and limits its effectiveness to compensating for residual small offsets not corrected by the techniques outlined previously. Development of such a fast system at SLAC and elsewhere [97, 98] shows promise as an additional safety factor for collision stability.

The impact of the stabilization systems on the hermeticity and the coverage of the detector will require careful consideration. The optical anchor would require optical paths from each FD to stable locations outside the detector, enclosed in an evacuated or sealed pipe to prevent refractive-index fluctuations. While not totally negligible, the radius of such pipes

---

<sup>11</sup>Beam-beam feedback cannot suppress noise sources at frequencies higher than about one tenth of the signal sampling rate. For instance, random amplitude jitter from upstream sources or magnetic-center vibration of the final doublet could not be effectively compensated for if occurring above about 300 kHz in TESLA (bunch-to-bunch) or 10 Hz in JLC-X/NLC (train-to-train).

would be sufficiently small ( $<5$  cm) that the impact on detector coverage would be moderate. The compactness of the inertial sensors currently under consideration suggests that by themselves, they would not require significant space beyond the blind spot arising from pair stay-clear and masking. The choice of FD support technology, however, may have a larger impact. Two approaches are under study: spring-mounted soft supports with active vibration damping, or rigid supports possibly associated with a larger array of vibration sensors to detect internal vibration modes of the FDs. The choice of support scheme is partially linked to the choice of FD technology (PM or superconducting) and to the stabilization method(s) adopted (mechanical feedback or feedforward-stabilization of magnetic centers). A detailed evaluation will only be possible once designs are more advanced.

#### 7.4.4.1.1 Items for Further R&D

- It is essential for any warm-rf linear collider project to demonstrate FD stabilization in an environment that adequately reproduces the system constraints of an actual detector and IR (Ranking: 3).
- The current TESLA design relies entirely on the intratrain IP feedback to guarantee collision stability. Although a similar technique has been used routinely at SLC, PEP-II and KEKB, its success is crucially dependent on the performance of the corresponding instrumentation (BPMs, pair luminosity monitor) in a high-disruption, high-radiation environment. It may be prudent to incorporate some form of FD stabilization in the baseline design to anticipate unexpectedly large vibration problems (Ranking: 3).
- The detector implications of the proposed support and stabilization scheme(s) should continue to be investigated as part of these studies (Ranking: 4).

#### 7.4.4.2 Magnet Technologies

**7.4.4.2.1 Requirements** The final-focus quadrupole doublet faces a number of challenging requirements. The doublet must be placed a few meters from the IP, develop a high gradient, accommodate the spent-beam channel, and be mechanically and electromagnetically stabilized. It must be able to operate, with long-term field stability, within a harsh radiation environment.

In addition, it is advantageous if the magnetic field of the doublet is adjustable to accommodate energy-tuning of the collider. This would also permit beam-based alignment.

**7.4.4.2.2 Technology Choices and Assessments** Table 7.26 presents the details of the baseline design choices for the final focus doublet for each linear collider project.

- TESLA's choice of superconducting technology [99] takes advantage of the lack of a crossing angle: the large mechanical envelope of the doublet and the fringe field present no problem for the extraction line. The aperture must be large enough to accommodate the spent beam and its beamstrahlung. This leads to a high-field

LUMINOSITY PERFORMANCE WORKING GROUP ASSESSMENTS

TABLE 7.26

Summary of baseline FD magnet parameters. In the last column, the length refers to the magnet adjacent to the IP.

Project (beam energy)	Technology	Field Gradient [T/m]	Radial Aperture [mm]	Pole Tip Field [T]	Width [mm]	Length [m]
TESLA (250 GeV)	Iron-free superconducting, Nb <sub>3</sub> Sn at 1.8 K	250	28	7	355	1.7
NLC (250 GeV)	SmCo <sup>5</sup> permanent magnet	144	10	1.44	56	2.0
JLC-X (250 GeV)	Resistive iron electromagnet, with SC shield	188	6.9	1.3	20	2.4
CLIC (1.5 TeV)	Sm <sup>2</sup> Co <sup>17</sup> permanent magnet	388	3.8	1.5	43	3.5

magnet, not unlike an LHC quadrupole, but with the significant complication of the presence of the 4 T detector solenoid field, which requires the use of Nb<sub>3</sub>Sn as the superconductor. The required critical-current performance of the cable is demanding but has been reached in R&D samples. The resulting large Lorentz forces on the coils present mechanical design challenges, particularly since the conductor is relatively brittle. The amplitude of magnetic-center vibrations produced by vibrational coupling from the cryosystem (or by cooling fluids) should be estimated to check that they remain within the correction capability of the feedback system. The field strength is fully adjustable over a large dynamic range.

- With a 20 mrad crossing angle, NLC has chosen a PM solution (SmCo<sup>5</sup>) as its baseline; a compact superconducting magnet for NLC is also under study at BNL. The compact size eases the mechanical stabilization issues and allows a simple design for the extracted-beam channel. Although there is no magnetic shield in the baseline design, depolarization of the PM material in the solenoid field has been studied and found not to be a concern [100]. Because of the dependence of the remanence on temperature, there are tight overall temperature stability requirements (driven by overall field strength changes) and very tight thermal gradient requirements (driven by shifts of the magnetic center). Such thermal gradients might be generated by, for example, asymmetric energy deposition in the FD pole tips. The overall temperature or thermal gradient variations will very likely be slow, and their effects should be compensated by the inter-train feedback system. It may be possible to adjust the field strength over a limited range [101].
- JLC's baseline solution [102] is a small-aperture resistive-iron electromagnet, protected from the solenoid field by a superconducting shield. The problem of the large size of the device is solved by using the coil pocket for the spent-beam channel. Significant issues in this design are possible mechanical vibrations due to cooling water, and perturbations to the spent-beam transport due to fields in the coil pocket. The field strength is adjustable. However the highly saturated pole tip will limit the dynamic range over which adequate field quality can be maintained.

- Like NLC, CLIC uses a compact REC PM design, which can be mechanically stabilized and accommodates a separate spent-beam channel.  $\text{Sm}^2\text{Co}^{17}$  is chosen for its radiation hardness. The 3 TeV design [103] uses a short doublet which does not overlap with the solenoid field but requires in addition a very strong PM sextupole. It also has tight overall temperature stability requirements and very tight thermal gradient requirements. The 500 GeV design needs a field gradient roughly six times smaller, and an inner radius of 6.6 mm. The field-strength adjustability has not been studied.

#### 7.4.4.2.3 Items for Further R&D

- The availability of compact SC final-doublet quadrupoles, with adequate vibration characteristics, would greatly improve the operational flexibility of crossing-angle machines. R&D on this topic should be vigorously pursued (Ranking: 3).
- Adjustability, over a wide range, of the strength of PM FD quadrupoles is highly desirable. R&D on this topic is ongoing, and is strongly encouraged (Ranking: 3).
- For the PM designs, one of the issues is the tight temperature stability and thermal gradient requirements (Ranking: 3). Estimates should be made to ensure that the thermal time constants are sufficiently long for feedback to be useful, and to determine whether there is a risk to develop thermal excursions large enough for them to exceed the range of the feedback systems. If a problem is found, then the use of a temperature-compensated material can be considered.
- For the resistive design, the dynamic range should be evaluated, and the effect of vibrations induced by water cooling on the motion of the magnetic center should be investigated (Ranking: 3).

### 7.4.5 Beam Halo, Collimation, and Machine Protection

Control of detector backgrounds originating from the accelerator itself is an important concern for luminosity performance. The peak luminosity—often taken as the figure of merit for performance—is useless if the detector is simultaneously blinded by unacceptable background.

Incoming-beam backgrounds can be loosely categorized into two related topics: the beam halo, which can extend many standard deviations beyond the beam core; and the generation of muons from halo particles that are intercepted by physical apertures. All machine designs realized early the need to remove the halo to a certain depth. This “collimation depth” is generally set by the synchrotron-radiation fan generated by the halo particles in the last few magnets close to the IP: by definition, all particles within the collimation depth generate photons that should pass cleanly through the IR.

Halo particles outside of the required collimation depth are removed by physically intercepting them with mechanical “collimators,” which are formed by a thick absorber of many radiation lengths ( $X_0$ ), placed in the optical shadow of a thin ( $0.25$ – $1 X_0$ ) spoiler. The spoiler is necessary to protect the absorber from a direct hit by the beam, the multiple

Coulomb scattering in the thin spoiler being sufficient to reduce the peak energy density on the face of the absorber to below damage threshold. By definition, the spoilers are the smallest apertures in the machine (relative to the beam size) and therefore likely to be the first aperture hit by a wayward beam. For this reason, machine protection is a significant design constraint for a collimation system. In the following sections only the thin “spoilers” are referred to, as their apertures generally define the collimation depth. It is generally implicit that a spoiler shadows an associated thick absorber, as described previously.

In principle, the loss of particles from the halo should be at controlled points along the lattice (*i.e.*, at the absorbers and spoilers). These locations then become sources of muons. How many of these muons eventually reach the detector depends on many factors: distance from source to the IP, beam-line layout, tunnel geometry and the use of “muon spoilers” or “tunnel fillers.”

#### 7.4.5.1 Halo and Collimation Efficiency

The current collimation systems for TESLA, JLC-X/NLC, and CLIC have been outlined in the machine overviews. They share the following common features:

- A pre-linac (low-energy) collimation system to remove beam tails (halo) generated primarily in the damping ring
- A post-linac momentum collimator system
- A post-linac multistage betatron collimation system

These systems exist (at least conceptually) in all the designs, but the level of detailed design work differs across projects. An actual design for the pre-linac low-energy collimation system does not exist, although space has been allowed for it in all machines. In the remainder of this section we will attempt to highlight the differences between the current approaches to post-linac high-energy collimation (Table 7.27), which poses the more difficult problem. It should be noted that, with the exception of the TESLA emergency-extraction scheme, none of the collimation schemes currently being discussed are specific to the machine design, and all are to a certain extent interchangeable (although implementation details would differ).

It is not possible to stop all the halo particles: edge scattering, non-linear fields at high particle amplitudes, *etc.* tend to repopulate the phase space outside the collimation depth. The effectiveness of the collimation system can be defined in terms of either:

- The fraction of initial halo particles that survive (or are rescattered out of) the primary collimation system, and hit secondary collimators or other aperture limitations closer to the IP. This “primary-collimation efficiency” is relevant when estimating muon backgrounds.
- The number of halo particles that lie outside the collimation depth when they reach the final doublet. This parameter is relevant when estimating synchrotron-radiation backgrounds (as well as the rate of lost-particle hits close to the detector, if any).

TABLE 7.27

Main parameters of the post-linac primary collimation system ( $\sqrt{s}=500$  GeV); the full list is available in Reference [104].  $\sigma_{x,y}$  are the horizontal and vertical beam sizes at the spoiler (including the dispersive contribution);  $\sigma_{x,y}^\beta$  refer to the betatron contributions alone. The quoted muon rates include those produced in the collimation section as well as further downstream in the BDS. In some cases, the spoiler settings must be tighter than the effective collimation depth (at the final doublet) because of dispersive or higher-order effects.

		TESLA	JLC-X/NLC	CLIC
Nominal collimation depth	# $\sigma_{x,y}^\beta$ at spoiler	12, 74	11, 31	9, 65
Momentum collimator	x gap [mm]	$\pm 1.50$	$\pm 3.20$	$\pm 1.60$
	$\sigma_{x,y}$ [ $\mu\text{m}$ ]	154, 4.5	534, 29	814, 38
Betatron collimator				
Final-doublet phase	x, y gaps [mm]	$\pm 1.50, \pm 0.50$	$\pm 0.30, \pm 0.20$	$\pm 0.34, \pm 0.20$
	$\sigma_{x,y}$ [ $\mu\text{m}$ ]	129, 7	28, 6.5	38, 3
IP phase	x, y gaps [mm]	$\pm 1.50, \pm 0.50$	$\pm 0.30, \pm 0.25$	$\pm 0.30, \pm 0.20$
	$\sigma_{x,y}$ [ $\mu\text{m}$ ]	128, 7	16, 0.8	22, 3
Primary-collimation efficiency		0.01	$< 1 \times 10^{-5}$	$< 3 \times 10^{-4}$
Muons reaching IR (single beam)	for $10^{-3}$ halo (per 150 bunches)	10–100	1–10 (per train)	50–500 (per train)
Effective collimation depth	# $\sigma_{x,y}^\beta$ at FD	13, 80	15, 31	11, 100

All machines currently have a dedicated primary collimation system located upstream of the final focus system (FFS). Additional secondary or “clean-up” collimators are located in the FFS. The maximum number of halo particles that may be intercepted in this secondary system is limited by the IP muon flux the detector can tolerate. The primary system—which intercepts most of the halo—should have high enough an “efficiency” to reduce the losses in the secondary system to acceptable levels. At the same time, the combination of primary and secondary collimation must bring the halo population outside the collimation depth in the final doublets within tolerance. It is typically required that no SR photon (whether produced by the beam core or by the halo) be allowed to hit any detector or machine component between the entrance to the final doublet on the incoming beam side to the exit of the other doublet on the outgoing side. In addition, no charged halo particles are allowed to hit the beam pipe in the same region.

Whether or not the quoted efficiencies are sufficient depends not only on the tolerance of the detector to the different backgrounds, but also on the population (density) of the actual halo entering the BDS. Analytical estimates of the halo population have been made for all the machine designs [105, 106, 107], and all quote conservative estimates on the order of  $10^4$  particles per bunch outside the collimation depth, corresponding to a fraction of about  $10^{-6}$  of the total bunch charge. Sources of halo considered were the damping ring, residual gas scattering, wakefields and linac dark current. There is general consensus that the damping rings are a significant source of halo, and that a pre-linac collimation system with an efficiency of better than  $10^{-3}$  is required (the previously quoted halo estimates assume the existence of such a system).

The NLC design<sup>12</sup> uses five betatron spoilers in the primary system placed alternately at the IP phase and at the final-doublet phase, the latter being the most critical. A separate momentum spoiler is located downstream of the betatron spoilers at a high dispersion point

<sup>12</sup>The version discussed here [104] differs from that described in Reference [108] only by the location and/or aperture of some of the spoilers and SR masks.

( $\sim 200$  mm). Three additional “clean-up” spoilers are located in the FFS. The primary system allows for a collimated halo population of up to  $\sim 10^9$  particles per bunch train ( $10^{-3}$  of the full beam current) and achieves a collimation efficiency significantly better than  $10^{-5}$ , resulting in less than  $10^4$  particles per train being lost in the secondary system (Figure 7.28, left). Simulations of muon production and tracking indicate that a loss rate of  $10^9$  particles in the primary collimation system produces a few muons in the detector (assuming two magnetized “tunnel-fillers” between the collimation system and the IR). A loss of  $10^6$  particles in the secondary system produces one muon in the detector, which, given the high efficiency of the primary system, translates into less than 0.01 muon per bunch train. The tolerable loss rate in the primary system, which is three orders of magnitude larger than the analytical estimates of the halo population, allows for a considerable safety margin: this conservative approach is inspired by the SLC experience, where the measured detector backgrounds vastly exceeded predicted levels. In addition, the NLC has implemented a novel non-linear optical scheme<sup>13</sup>, in which octupole doublets placed in the FFS “fold” the halo particles into the required collimation depth. These doublets, which work most efficiently only in a final focus system with local chromaticity correction, loosen the required physical apertures of the collimators by a factor of 2–4 compared to those quoted in Table 7.27, reducing the amount of halo that needs to be intercepted.<sup>14</sup>

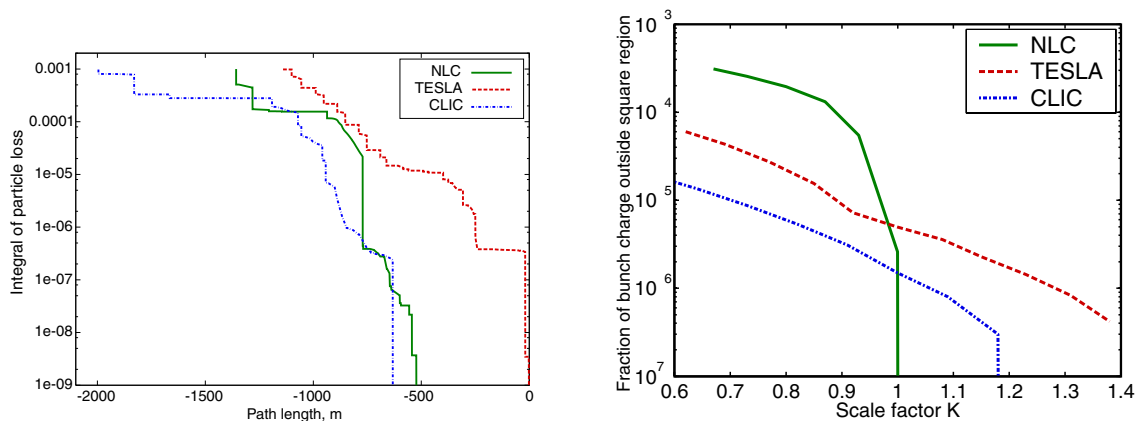


FIGURE 7.28. Collimation-system performance [104] assuming an incident fractional halo of  $10^{-3}$ . Left: fractional loss of charged-halo particles, integrating back, starting at the IP, and normalized to the nominal bunch charge. The horizontal scale shows the distance from the IP. The upstream edge of the secondary-collimation system is located at  $-543$  and  $-583$  m in NLC and TESLA respectively. In CLIC, the last betatron absorber is located at  $-632$  m. Right: number of charged-halo particles per bunch, normalized to the nominal bunch charge, in a rectangular  $x-y$  window at the entrance to the final doublet, as a function of the collimation depth. The scale factor  $K$  defines the window dimension: for  $K=1$ , the window size corresponds to the effective collimation depth listed, for each machine, in Table 7.27.

<sup>13</sup>This concept has also been proposed independently by the TESLA group but is not included in their present design [93].

<sup>14</sup>The collimation-efficiency figures quoted here do not assume the use of tail-folding octupoles.

The TESLA system is somewhat different: five pairs of x-y spoilers are separated by a phase advance of about  $\pi/4$ , forming an octagon in phase space (the first and last spoilers are degenerate in phase). The first spoiler has a non-zero horizontal dispersion (100 mm) and acts as the primary momentum collimator. There are four additional “clean-up” collimators in the FFS itself. Recent simulation results have shown that with the primary collimation as currently designed, the loss rate in the secondary system amounts to about 1% of the initial halo population. Because the TESLA bunch spacing is longer than the entire bunch train for the warm machines, TESLA generally quotes background rates per bunch crossing. However the subdetector most sensitive to muon background (the TPC) integrates over 150 bunches, so that for the same assumed incident halo fraction of  $10^{-3}$ , the effective halo population becomes similar to that of NLC. TESLA has proposed not to use the tunnel-filler approach to suppress the muons from the primary collimation system, opting instead for smaller magnetized toroids. These have a length of 10 m, diameters between 0.5 m and 1.0 m, and a field of 10–14 kG. Simulations have shown that twenty such toroids distributed in the lattice between the collimators and the IR can reduce the muon rate by three orders of magnitude, allowing a particle loss of  $\sim 10^8$  in the primary system for one muon in the detector. Again assuming a collimated halo of  $10^{-3}$ , this translates into up to 30 muons in the detector for 150 bunches. Muons from the secondary system close to the IR must also be considered. Typically  $10^6$  particles lost in this region generate one muon. With the previously quoted primary-collimation efficiency, the remaining halo in the secondary system amounts to  $3 \times 10^7$  particles/150 bunches, resulting in  $\sim 30$  additional muons reaching the detector.

For the purposes of this review, the CLIC-500 collimation system is taken to be a scaled version of the 3 TeV variant. The 3 TeV requirement is primarily reflected in the system length (over 2 km per side, compared to less than 1 km for the NLC and TESLA systems); shorter layouts are currently being investigated. The system consists of an energy-collimation section followed by a betatron-collimation section. The design of the momentum-spoiler optics is primarily driven by spoiler-survival considerations, and is characterized by a single dispersive peak ( $D_x \sim 500$  mm) with a large vertical  $\beta$ -function ( $\sim 100$  km) which increases the design beam size at the spoiler to a safe value ( $\sqrt{\sigma_x \sigma_y} \sim 180 \mu\text{m}$ ). The downstream betatron system consists of four spoilers at alternating IP and final-doublet phases with much smaller beta functions. Muon studies have been performed for the 3 TeV center of mass case: using three tunnel fillers, the loss rate per muon reaching the IP typically amounts to  $3 \times 10^5$  particles [109]. At 500 GeV c.m. energy, the tolerable rate should be an order of magnitude higher; a reference fractional halo of  $10^{-3}$  would then result in  $\sim 250$  muons per bunch train in the detector.

Computations of the collimation efficiency at the final doublet, and of the resulting halo-induced SR backgrounds, are still in progress for the various designs. Recent calculations [104] that include charged-particle tracking (both of halo primaries and of shower secondaries) as well as SR photon production in non-linear magnetic elements, are illustrated in Figure 7.28 (right).

- The design of the NLC collimation system is well advanced. The edge of the collimation depth is sharply defined; but for no halo photons to hit the beam pipe near the IP, rather tight collimator settings ( $\pm 0.2$  mm) are needed (in the absence of tail-folding octupoles only).

- In TESLA, the boundary of the collimated halo is barely visible, in spite of several tight collimator settings, in particular in the secondary-collimation system. A large number of halo particles ( $\sim 10^5$  per bunch) enter the final doublet outside the collimation depth.<sup>15</sup> The simulations also indicate that with the collimator configuration simulated here (which corresponds to that of Reference [93]), some SR photons from the halo ( $\sim 2 \times 10^4$   $\gamma$ 's per bunch) do hit the detector mask located 3 m from the IP; their total energy (150 GeV per bunch) is however small compared to that of beam-beam induced pairs. More importantly perhaps, the same study also shows a sizeable outgoing photon halo ( $\sim 1.2 \times 10^5$  GeV/bunch, corresponding to about  $1.2 \times 10^7$  photons) hitting the downstream SR mask 18 m from the IP: the total energy of the halo photons intercepted by this mask is comparable to that of outgoing SR photons from the beam core hitting the same mask. Finally, about  $10^{10}$  photons/bunch radiated by the core of the incoming beam hit the SR mask upstream of the IP. All of these background sources are cause for serious concern, because the simulations at this stage completely neglect back-scattering and edge-scattering of SR photons off masks and other aperture limitations. It should be noted that the relative intensity of the background sources is extremely sensitive to the interrelated aperture settings necessary to simultaneously accommodate an incoming and an outgoing beam. While it is plausible that the effectiveness of the collimation system may be further improved, these results underscore the urgent need for more detailed studies.
- Detailed simulations of the 500 GeV CLIC system are only beginning, and the collimator configuration is still very much in flux.

#### 7.4.5.2 Machine-Protection Issues

Hardware survival is an integral part of the design of the collimation system. Although the thin spoilers are designed to protect the downstream absorbers from a direct hit from the beam, the extremely high bunch charge densities require protection of the spoilers themselves.

TESLA has the advantage of a long bunch train and large bunch spacing. In the event of a failure, the bunch train can be “kicked out” of the machine and sent to the main dump. This fast-extraction system is located upstream of the momentum spoiler. BPMs strategically placed a few meters upstream identify off-axis or off-energy bunch trains and fire a bank of 40 fast kickers which extract the remainder of the bunch train to the main dump via a dedicated beamline.<sup>16</sup> The system is designed to allow at most two bunches through before firing, at least for the most frequent failure type (a fast energy or betatron error that occurs on the time scale of the interbunch separation). Faults such as power supply failures or shorting magnet coils anywhere along the machine, are expected to develop on a sufficiently slow time scale for BPMs to detect dangerous orbit drifts, or for

<sup>15</sup>The apparent contradiction with Figure II.7.5.3 of Reference [93], in which no particles are found outside the collimation depth, remains to be resolved.

<sup>16</sup>In addition to firing the kickers, a signal is sent to the damping-ring extraction system which aborts the pulse: given the linac length, this corresponds to about 340 bunches which need to be handled by the fast extraction system.

beam-inhibit watchdogs to abort the next pulse whenever a hardware fault is detected in the 200 ms between bunch trains.

The nominal beam size at the downstream momentum spoiler is sufficiently large (even for the worst-case  $e^+$  beam) that it should survive a direct hit from one bunch (possibly two). In the current TESLA design, a further protection for the momentum spoiler is provided by the magnetic energy spoiler (MES), a non-linear optics module which increases the vertical beam size in the event of an energy error, allowing the mechanical spoiler to survive 4–6 bunches. Since the non-linear system also reduces the momentum bandpass (Section 7.3.2.4), its use is still under review. The rationale behind the additional protection of the momentum spoiler reflects the philosophy that fast energy errors are expected to be significantly more frequent than pure orbit errors (with an amplitude large enough to strike the spoilers). The TESLA system reduces the spoiler protection issue to that of single-bunch damage, but at the same time shifts the emphasis onto the reliability of critical MPS components (fast kickers, BPMs, hardware watchdogs, etc).

A TESLA-style fast extraction system is not possible for NLC or CLIC because of the much shorter bunch spacing and bunch train. Here the spoilers must deal with the entire bunch train ( $\sim 10^{12}$  particles, compared to  $\sim 10^{10}$  for a single TESLA bunch). Both NLC and CLIC have adopted the philosophy of passively protecting the momentum spoilers by placing them at locations of larger horizontal dispersion and vertical  $\beta$ -function. Table 7.28 lists the nominal beam parameters relevant to spoiler survival. The critical figure of merit is the peak particle density, which is proportional to the total number  $N_p$  of particles striking the spoiler, and inversely proportional to the area of the beam spot ( $\sigma_x\sigma_y$ ).

TABLE 7.28

Spoiler-survival parameters for the momentum and betatron spoilers ( $\sqrt{s}=500$  GeV). For TESLA,  $N_p$  is twice the single-bunch population, while for CLIC and NLC it refers to that of the entire bunch train.  $\sigma_x$  and  $\sigma_y$  are the horizontal and vertical beam size at the spoiler (including the dispersive contribution).

		$N_p [\times 10^{10}]$	$\sqrt{\sigma_x\sigma_y} [\mu\text{m}]$	$N_p/(\sigma_x\sigma_y) [\mu\text{m}^{-2}]$
Momentum	TESLA	4	26	$5.8 \times 10^7$
	NLC	144	124	$9.4 \times 10^7$
	CLIC	62	176	$2.0 \times 10^7$
Betatron (FD / IP phase)	TESLA	4	30 / 31	$4.6 \times 10^7/4.2 \times 10^7$
	NLC	144	13.4 / 3.5	$8.0 \times 10^9/1.2 \times 10^{11}$
	CLIC	62	10.9/8.3	$5.2/9.0 \times 10^9$

Estimates based on instantaneous temperature rise and ultimate tensile strength suggest<sup>17</sup> that  $N_p/(\sigma_x\sigma_y)$  should remain below  $2\text{--}3 \times 10^7$  for Cu, and below  $1\text{--}3 \times 10^8$  for Ti. Table 7.28 indicates that the Ti TESLA spoilers lie comfortably below damage threshold. The CLIC momentum spoiler is below the Cu threshold, while the NLC one is not. For the betatron spoilers, both CLIC and NLC significantly exceed the quoted limit. The NLC design

<sup>17</sup>These threshold values are based on the initial energy loss, and are therefore valid for thin spoilers only. For “thick” spoilers, the thresholds are further reduced by the shower development.

philosophy assumes that a direct hit will locally damage the spoiler, and proposes either “consumable” (or “reparable”) spoilers [110], which can be rotated to offer a new undamaged (or reconditioned) spoiler edge to the beam. The current NLC prototype design for the consumable spoiler has the capacity to withstand approximately 1000 damaging pulses before being replaced. The advantage here is the short length and relatively small  $\beta$ -functions of the collimation system, leading to looser tolerances and better wakefield performance; this is offset to some degree by the complexity of the spoiler design itself.

CLIC studies of various linac failure modes suggest that a beam with a betatron amplitude large enough to strike a spoiler, will have its emittance diluted by the strong linac wakefields by as much as two orders of magnitude [111]. But failures causing a significant energy deviation are not necessarily accompanied by a large beam-size increase at the momentum collimator, and some energy errors are small enough for the beam to hit the betatron collimators located further downstream [112]. CLIC is therefore also considering the use of consumable spoilers.

### 7.4.5.3 Other Considerations

**Wakefields:** The control of transverse wakefield kicks from the relatively narrow spoiler and absorber gaps must also be considered. All machines propose to use spoilers with long tapers to reduce the effect of the geometric-wakefield kick. The current design of the consumable spoiler for NLC uses tapers constructed from beryllium, which will have a 1  $\mu\text{m}$  copper coating to reduce the resistive-wake effect [110]. The NLC group, in collaboration with other laboratories, has also carried out wakefield tests, using the SLAC linac beam on several different spoiler geometries and materials to cross-check theoretical calculations. The potential impact of collimator wakefields on luminosity has been discussed in Section 7.3.2.6.

**Mechanical Design:** The gaps of both spoilers and absorbers need to be remotely adjustable so that they can be (i) fully opened during commissioning, and (ii) adjusted during background tuning. The NLC has the most advanced design for the consumable collimator, where a prototype has been successfully constructed and tested: with a few minor engineering modifications it is thought that the design will achieve the required tolerances [110]. R&D is still on-going on the copper coating for the beryllium taper. At other machines, the static-jaw type of collimator is more in keeping with existing designs, although tolerances are tighter. It should be noted that R&D into novel materials and designs for collimators is on-going (for example at LHC), the results of which are also likely to be of benefit to the LC designs. There is clearly room for more work on these topics.

### 7.4.5.4 Summary and Items for Further R&D

**7.4.5.4.1 Collimation-System Concepts** Collimation-system concepts appear feasible, be it in terms of optical layout, primary-collimation efficiency, spoiler and absorber design, or machine protection. But the designs are not mature yet: in some areas, substantial uncertainties persist, or realistic performance margins remain to be incorporated.

- The tight aperture settings needed to achieve satisfactory collimation efficiency, coupled with significant beam jitter, can lead to a substantial luminosity degradation by wakefields. (See Section 7.3.2.6). Tail-folding octupoles appear very promising to significantly relax the collimation requirements, but this technique is not yet integrated in all BDS designs. If collimator wakefields are eventually measured to be as large as predicted by current models, then the experimental validation of the tail-folding technique becomes an important R&D topic (Ranking: 3).
- The level of halo SR intercepted in the IR area is of some significant concern in the TESLA case, and its implications for detector backgrounds must be thoroughly investigated. A careful review of the SR flux produced by the core of the beam is also clearly required for all projects. This flux is one to two orders of magnitude larger in TESLA than in NLC (because of stronger bends and quadrupoles). Even though in both cases beam-core photons appear adequately intercepted by the SR masks located 10–20 m from the IP, more sophisticated computations of potential SR backgrounds, that include tip-scattering and back-scattering from all aperture limitations, are highly necessary (Ranking: 3).
- The available halo-related background simulations suggest that the collimation systems as designed would yield, at  $\sqrt{s}=500$  GeV, 1–10 muons per effective bunch train into the NLC detector, and approximately ten (fifty) times more at TESLA (CLIC), pessimistically assuming a collimated halo of  $10^{-3}$  of the bunch charge. While considered tolerable (Section 7.4.6.1), the predicted muon rates are sensitive to both the tunnel and the machine geometry: the numbers quoted previously should only be considered as order-of-magnitude estimates (Ranking: 3).
- Background simulations: a great deal of work has been done to understand the halo and its impact on the detector performance. However, given the statistics of the problem (a few particles in  $10^{10}$  can cause an enormous increase in detector backgrounds), there is clearly scope for further studies. Simulation tools are currently being developed to enable better tracking of both primary and secondary particles, while the models of the machines and their environment (*e.g.*, tunnel layout) become increasingly detailed. Studies of “tuned” machines which include errors are also required, to better understand the interaction between luminosity and background tuning (Ranking: 3).

**7.4.5.4.2 Machine Protection** As some details of the designs continue to evolve, a thorough and recurring review of potential failure modes is mandatory (Ranking: 3). In TESLA for instance, recent simulations show large halo-induced losses [104] early in the collimator section, confirming a risk of beam-induced damage in this area: an additional protection collimator may be required at a high-dispersion point further upstream. Another example concerns the warm machines. It is assumed that the single-bunch damage threshold is independent of whether or not there are following bunches. There could be cases, however, where material survives a single bunch because the beam is blown up, but the total heat deposited by the train causes a problem.

## 7.4.6 Detector Backgrounds

Several detector designs are being pursued [113]. Proceeding radially outward from the IP, a generic layout contains a silicon vertex detector, main tracker, electromagnetic calorimeter, hadronic calorimeter, solenoid coil, iron yoke and muon system. In general the physics requirements lead to detectors somewhat larger than at LEP/SLC and with much stronger magnetic field ( $\geq 3$  T) in order to handle the higher energies and more intense backgrounds. This activity is now generating extensive R&D on subdetector technology [114].

While the designs are primarily driven by physics performance, there remains leeway in the choice of subdetector technologies, and it is equally important to ensure robustness against accelerator-induced backgrounds. Their potential impact falls in two categories:

- Degraded performance (tracking efficiency, pattern recognition, energy resolution, background rejection). Tolerance criteria are briefly discussed in Section 7.4.6.1. The expected background rates have been evaluated in a fair amount of detail [83, 115, 116, 117, 118, 119] as part of the IR-design optimization process, and are reviewed in Section 7.4.6.2 to Section 7.4.6.4.
- Radiation damage. This is an issue mainly for CCD-based vertex detectors (Section 7.4.6.4).

### 7.4.6.1 Detector Tolerance to Backgrounds

The detector tolerance can be quantified by comparing the “pain threshold” (defined as the background level where the performance of a subdetector starts being compromised) to the background level predicted in that same subdetector under nominal operating conditions.

It is typically assumed that a 1% occupancy limit in a tracker is conservative. However this can translate into rather different tolerance levels, depending on the chosen detector technology. The TESLA TPC, for instance, integrates over about 150 bunches, but its exquisite three-dimensional granularity makes it highly background-tolerant: a 1% limit translates into 2550 muons per 50  $\mu$ s [120]. More generally, the time structure of the beams and the sensitivity window of each subdetector must be taken into account when computing the effective occupancy. Overall, the estimated occupancies in tracking detectors appear moderate even when integrated over the full bunch train of the warm machines.

Tolerable background levels in calorimeters are harder to quantify in a general way, as their impact depends not only on the fraction of cells above threshold, but also on the actual amount of energy deposited and on the physics channel under study. TESLA states [120] that all its subdetectors have higher safety margins than the TPC, and that the whole detector is robust against background underestimations. One could envisage [120] a criterion similar to that of the tracking systems, requiring for instance that less than 1% of the calorimeter cells contain an energy deposition comparable to that of a minimum ionizing particle. Given the high granularity ( $10^4$ – $10^5$  cells) and the integration time (100–200 ns) of the calorimeters currently under study, this translates into a tolerable muon rate of a few per train in the warm machines, equivalent to about 600 muons per 50  $\mu$ s in TESLA. The same criterion leads to tolerable total energy depositions (excluding the low-angle calorimeters) of the order of a few hundred GeV (per train in warm machines, per

pulse in TESLA). But these are only rough estimates, that need to be validated by physics-performance studies.

### 7.4.6.2 Beam-Beam Backgrounds

**7.4.6.2.1 Pairs** The dominant background source is that of incoherently produced  $e^\pm$  pairs which stem from the conversion of beamstrahlung photons in the strong electromagnetic field of the colliding bunches (Section 7.4.2.2). The overall pair-production rate (Table 7.29), as well as the number of  $e^\pm$  reaching a “generic” vertex detector (Figure 7.29), are largest in TESLA because of the larger bunch population and larger number of beamstrahlung photons per electron.

TABLE 7.29

Number and energy of pairs produced at  $\sqrt{s}=500$  GeV, computed with GUINEA-PIG.

	TESLA	JLC-C	JLC-X/NLC	CLIC
Number of pair particles/crossing	152,000	44,000	52,000	32,000
Number of pair particles/sec	$2.1 \times 10^9$	$0.84 \times 10^9$	$1.2 \times 10^9$	$0.99 \times 10^9$
$E_{tot}/\text{crossing}$ [TeV]	354	117	185	153
$\langle E(e^\pm) \rangle$ [GeV]	2.3	2.7	3.6	4.8
Number of pair particles/crossing ( $p_t > 20$ MeV/c, $\theta > 200$ mrad)	39	11	12	7.2

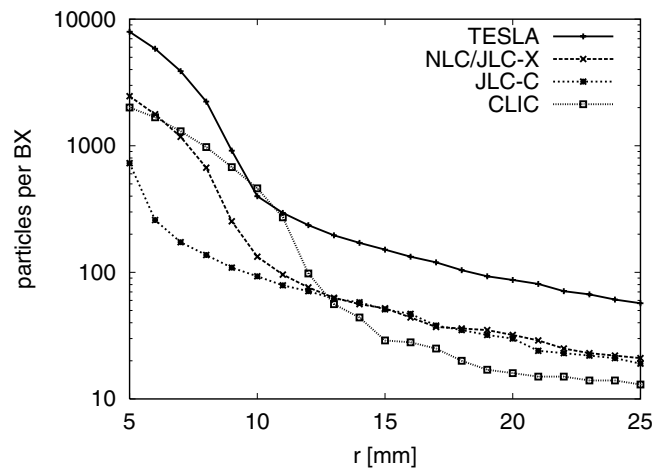


FIGURE 7.29. Number of particles per bunch crossing that hit the innermost layer of the vertex detector. The same solenoidal field  $B_z=4$  T and angular coverage  $|\cos \theta| \leq 0.98$  has been assumed for all machines. The radial edge of the stay-clear cone is apparent.

GEANT-level simulations of the optimized IR configurations<sup>18</sup>, including beamstrahlung photon and pair production, as well as scattering and transport of secondaries in the presence of masks and detector elements, yield the background estimates listed in Table 7.30 to Table 7.31. The occupancy is far below critical levels in the vertex detectors.<sup>19</sup> The TPC occupancy remains well below the 1% tolerance. The calorimeter occupancy appears of no concern in the TESLA case because of the long bunch spacing. The short trains of the warm machines, however, result in cumulative background energy depositions which may be an issue for some physics topics. The time resolution of the calorimeters will strongly influence the background rejection capability and is an important design consideration.

**7.4.6.2.2 Hadronic Events** The rate of two-photon hadronic events (Section 7.4.2.2) predicted by GUINEA-PIG for the various machines is listed in Table 7.32 for several sensitivity windows. The resulting charged-hit density in the vertex detectors lies two to three orders of magnitude below that induced by the pairs. Assuming a mean charged-hadron multiplicity of 10–20 particles per event above  $p_T$  threshold, a few ten charged tracks would cross the volume of a TPC during the integration time of that detector. While these could in principle fake interesting physics events because they all originate from the nominal IP, the time resolution of the TPC should allow disentangling them from interesting processes, at least in the TESLA case. The energy deposited in the calorimeters is comparable to, or slightly larger than, that from the  $e^\pm$  pairs.

### 7.4.6.3 Single-Beam Backgrounds

**7.4.6.3.1 Muons** The estimated muon flux at the detector has been reported in Table 7.27. At  $\sqrt{s}=500$  GeV and assuming the use of some kind of “muon spoilers,” the predicted rates remain, in all designs, one to two orders of magnitude below the critical level in the tracking systems (provided the detector granularity is large enough). The rates remain acceptable for the calorimeters, albeit by a narrower margin. As discussed in Section 7.4.5.1, these safety factors remain subject to sizeable uncertainties: population of the incoming halo, tunnel and beam-line geometry, longitudinal distribution of secondary-particle losses, collimation and muon-spoiler efficiencies, *etc.* But the assumptions used in designing the collimation system appear sufficiently conservative to provide a satisfactory margin on muon backgrounds.

**7.4.6.3.2 Synchrotron Radiation** Synchrotron radiation is produced by the incoming beams in the fields of the last bending magnets and final quadrupoles (as well as by the outgoing beam in the TESLA FD). The collimation systems have been designed so that all SR photons should pass cleanly through IR without striking any part of the detector [121]. Recent comparisons [104] of SR backgrounds in TESLA and NLC demonstrate that

<sup>18</sup>The CLIC simulation reported here actually uses the 3 TeV detector model, but with a reduced vertex-detector inner radius.

<sup>19</sup>provided the readout of the TESLA CCD can be shortened appropriately, as assumed in Table 7.30. Since the CCD readout is slow, it typically integrates over a whole train for the warm-machine designs. Applying a similarly “conventional” CCD technology to TESLA would result in occupancies of  $100 \text{ mm}^{-2}$  and  $8.7 \text{ mm}^{-2}$  in layers 1 and 2 respectively. Thus the CCDs must be read out much faster so as to only integrate over about 150 bunches. For this eventuality a “column-parallel” readout is being designed for the CCDs. Other vertex-detector technologies are also being considered [113].

TABLE 7.30: Pair-induced occupancies in the TESLA subdetectors, including secondaries ( $e^\pm, \gamma$ ) [83, 116], at  $\sqrt{s}=500$  GeV. The vertex detector is primarily sensitive to charged hits. The sensitivity window is the subdetector integration time.  $R_V$  is the radius of the vertex-detector layer. The solenoid field strength is 4 T.

Subdetector	Hits or energy per Crossing	Sensitivity		Effective		Comment
		Window	# Bunches	Occupancy	Occupancy	
VXD (layer 1)	$3.6 \cdot 10^{-2} \text{ mm}^{-2}$ (340 hits total)	50 $\mu\text{s}$	148	$5.3 \text{ mm}^{-2}$	$R_V=1.5 \text{ cm}$	
VXD (layer 2)	$3.1 \cdot 10^{-3} \text{ mm}^{-2}$ (126 hits total)	250 $\mu\text{s}$	742	$2.3 \text{ mm}^{-2}$	$R_V=2.6 \text{ cm}$	
TPC	1336 $\gamma$ , 5 trks	55 $\mu\text{s}$	160	Few per mil		
ECAL	1176 $e^\pm, \gamma$ ( $E_{th} > 10 \text{ keV}$ )	150 ns	1	1.92 GeV		
(Barrel + Endcap)	192 $\gamma$ , 1.92 GeV ( $E_{th} > 3 \text{ MeV}$ )			( $E_{th} > 3 \text{ MeV}$ )		

Subdetector	Hits or Energy per Crossing	Sensitivity		Effective		Comment
		Window	# Bunches	Occupancy	Occupancy	
VXD (layer 1)	$3.8 \cdot 10^{-2} \text{ mm}^{-2}$	train	192	$7.3 \text{ mm}^{-2}$	$R_V=1.2 \text{ cm}$	
VXD (layer 2)	$3.1 \cdot 10^{-3} \text{ mm}^{-2}$	train	192	$0.6 \text{ mm}^{-2}$	$R_V=2.4 \text{ cm}$	
TPC	1377 $\gamma$	train	192	Few per mil		
ECAL	1741 $\gamma$ , 2.53 GeV	train	192	486 GeV		
(Barrel + Endcap)	( $E_{th} > 10 \text{ keV}$ )			( $E_{th} > 10 \text{ keV}$ )		

TABLE 7.31: Pair-induced occupancies in the CLIC subdetectors, including secondaries ( $e^\pm, \gamma$ ) at  $\sqrt{s}=500$  GeV. Only charged hits are counted in the vertex detector. The sensitivity window of all subdetectors is assumed longer than the duration of the bunch train.  $R_V$  is the radius of the vertex-detector layer. The solenoid field strength is 4 T.

Subdetector	Hits or Energy		Sensitivity		Effective		Comment
	per Crossing	Window	# Bunches	Effective	Occupancy		
VXD (layer 1)	$1.0 \cdot 10^{-2} \text{ mm}^{-2}$	train	154	$1.6 \text{ mm}^{-2}$	$R_V = 1.5 \text{ cm}$		
VXD (layer 2)	$1.3 \cdot 10^{-3} \text{ mm}^{-2}$	train	154	$0.2 \text{ mm}^{-2}$	$R_V = 2.5 \text{ cm}$		
Central tracker	$1400 \gamma (E_{th} > 10 \text{ eV})$	train	154				
ECAL	5 GeV	train	154	720 GeV			
(Barrel + Endcap)	$(E_{th} > 10 \text{ keV})$			$(E_{th} > 10 \text{ keV})$			

TABLE 7.32: Beam-beam induced hadronic backgrounds at  $\sqrt{s}=500$  GeV.

	TESLA	JLC-C	JLC-X/NLC	CLIC
	Hadronic events/crossing	0.25	0.076	0.10
$E_{\gamma\gamma-c.m.s.} \geq 5 \text{ GeV}$				
Hadronic events/100 ns	0.25	5.4	7.4	10
Hadronic events/(148 b or train)	37	15	20	10
	(/148 b)	(/train)	(/train)	(/train)
Number of minijet pairs/crossing [ $\times 10^{-2}$ ]	0.74	0.24	0.36	0.29
$p_T^{min} = 3.2 \text{ GeV}/c$				
Number of minijet pairs/100 ns	0.01	0.17	0.26	0.44
Number of minijet pairs/(148 b or train)	1.1	0.45	0.69	0.45
	(/148 b)	(/train)	(/train)	(/train)

reasonable solutions are close. But they suffer from some of the same uncertainties as the muon flux predictions, do not yet take into account backscattered photons and scattering off mask tips (which in existing machines often dominate the flux eventually reaching the detector), and are potentially very sensitive to details of the magnet and mask apertures near the IP. Much more detailed simulations are clearly required to produce a comprehensive and robust picture of SR backgrounds, both from the halo and from the core of the beam.

**7.4.6.3.3 Beam-Gas Backgrounds** The beam-gas rate in TESLA was estimated [116] at  $3 \times 10^{-3}$  electrons/crossing leaving the beam pipe near the IP, for an (easily achievable) residual pressure of  $5 \times 10^{-9}$  mbar. This scales to 0.5 background events per 50  $\mu$ s in the TESLA TPC. Preliminary estimates for the NLC suggest a somewhat larger rate for the same residual pressure, but even then the predicted absolute background level does not pose a significant problem.

#### 7.4.6.4 Neutrons

Neutrons are produced through photo-nuclear reactions by bremsstrahlung photons from electromagnetic showers. Therefore any  $e^\pm$  (from pairs, radiative Bhabhas, or spent-beam losses) or beamstrahlung photon hitting a mask or beam-line element is a potential source of neutrons. The dominant sources are neutron production by beamstrahlung-induced pairs (Section 7.4.2.2) and backscattering from the main dumps (Section 7.4.3.3). The main concern here is radiation damage to the vertex detector. The total flux predicted at 500 GeV c.m. energy is of the order of  $1\text{--}2 \times 10^9$  n/(cm<sup>2</sup>×yr) (Table 7.23), which is comparable to the neutron tolerance of present CCD's (1 to  $10 \times 10^9$  neutron hits/cm<sup>2</sup>) [83, 116, 122]. This may therefore require periodic replacement of at least the innermost layer if this technology is eventually selected. Other vertex-detector technologies are more radiation-tolerant.

#### 7.4.6.5 Items for Further R&D

**7.4.6.5.1 Fluctuations** The background rates quoted in this report assume ideal, static machines and perfectly centered collisions. Because of ground motion and other dynamical effects, both the position and the shape of the colliding beams will fluctuate from train to train, and even from bunch to bunch. Although strongly suppressed by feedback systems, the residual fluctuations will result in rapid variations in the instantaneous luminosity (Section 7.3.4.3), in the flux and the angular distribution of beamstrahlung photons (Section 7.4.3.3), and therefore in the intensity of beam-beam backgrounds. Because the rate of pairs is proportional to the product of the luminosity by the beamstrahlung flux, and because dynamic beam errors tend to lower the former and enhance the latter, the resulting background fluctuations will be smaller than those of the total photon flux; but they might result in a significant increase (50% or more) of the average level of beam-beam-related backgrounds. This effect has been neglected so far in detector studies and warrants further investigation (Ranking: 4).

**7.4.6.5.2 Physics Studies** Detailed studies of the impact of machine backgrounds on physics analysis are only beginning and more work is required for all designs. In warm machines for instance, the time resolution of the calorimeters will strongly influence the background rejection capability and is an important design consideration.

## 7.4.7 Beam Polarization and Energy Measurement

### 7.4.7.1 Polarimetry

The physics requirement for most studies is a measurement of the  $e^-$  polarization to 0.5% or better. For precision measurements at the  $Z$ -pole, the goal is 0.1%. SLD reached 0.5%, which was achieved using a Compton polarimeter downstream of the IP to measure the polarization continuously on every pulse, with about one third of the time spent on diagnostic scans to optimize performance and reduce systematics. An absolute accuracy of 0.25% might be achievable with a redesigned polarimeter, but 0.1% is very challenging.

All LC designs include a Mott polarimeter to monitor polarization at the  $e^-$  source, and a Compton polarimeter before and/or after the IP.<sup>20</sup> At 0.5–1 TeV c.m. energy, the theoretical beam-beam-induced depolarization of on-energy particles is small (<1%). The absolute uncertainty on the predicted, luminosity-weighted depolarization is likely to be a small fraction of the depolarization itself, but the latter will vary with beam-beam conditions (it can be as large as 10% for the low-energy tail of the luminosity spectrum). Ideally, the polarization should be measured both upstream and downstream of the IP to fully characterize this effect. Whether systematic uncertainties will limit the achievable precision if only an upstream measurement is available, remains an open question. A 0.5% accuracy might eventually be achievable under these conditions; but reaching the ultimate accuracy needed at the  $Z$ -pole will no doubt require either a polarimeter both upstream and downstream of the IP, or  $e^+$  polarization.

The TESLA design has a Compton polarimeter 600 m upstream of the IP (the zero-crossing angle makes it difficult to locate diagnostics in the extraction line). This system has been described in detail in Reference [123]. With an appropriate pulsed laser, they estimate a 0.1% statistical measurement in one second and an overall precision of 0.5% as achieved at SLD. The impact of Compton-scattered  $e^-$  on detector backgrounds appears minor.<sup>21</sup>

The NLC, JLC X-band and C-band, and CLIC designs all have a crossing angle with a chicane in the extraction line to separate the spent charged-particle beam from the photons and allow energy-spectrum and polarization diagnostics. The NLC optics provides an image point of the IP mid-chicane where these diagnostics would be located, and beam losses are calculated to be acceptably low (at least at 0.5 TeV), but no detailed designs have

<sup>20</sup>Two other methods for measuring the polarization are the “Blondel” scheme, which requires the  $e^+$  beam to be polarized, and the W-pair method, which improves with  $e^+$  polarization. Both of these accurately measure the luminosity-weighted polarization, but they require  $e^+$  polarization or energy above W-pair threshold, and they require time to integrate an adequate sample.

<sup>21</sup>The rate of scattered electrons has been estimated at about  $10^4$ /bunch, with an almost flat energy distribution between 50 and 250 GeV. Tracking studies suggest that about 80% get lost downstream of the first CCS dipole; the corresponding muon rate is negligible (assuming the use of muon toroids). Another 13% hit a collimator 570 m upstream of the IP. A few tens of electrons per bunch may reach the final doublet outside the collimation depth; their impact on detector background remains to be investigated.

been done. A polarimeter upstream of the NLC IP has been discussed but has not yet been explicitly included.

### 7.4.7.2 Energy Spectrometer

A precise measurement of the beam energy is required for various physics studies. Typical precision goals are  $\sim 40$  MeV for the Top mass,  $\sim 50$  MeV for Higgs production threshold, 2–5 MeV for Giga-Z and  $< 5$  MeV for WW threshold. In addition to the physics analysis, the SLC used the pulse-by-pulse measurement of the beam energy correlated with other machine parameters as a very powerful diagnostic of accelerator performance. The SLC spectrometer measured the distance between synchrotron light fans from two bending magnets in the extraction lines. In principle, this can provide the desired precision, but would be difficult in a higher-energy collider because of the low-energy tail of the luminosity spectrum. Such a device upstream would cause unacceptable emittance degradation. The LEP spectrometer used a dipole magnet between two BPM triplets but high precision requires tight control of the magnetic field and of the BPM stability. It was only able to achieve  $\sim 50$  MeV and it will be difficult to push this technology to the desired level. Some other techniques have been proposed, such as Moller scattering off a gas jet, but none of these have been studied in detail.

All of the LC designs presume some energy spectrometer measurement but have not specified the hardware in detail. NLC also has a wire scanner at the extraction line image point to measure the energy spectrum of the spent beam. There are locations in the TESLA extraction line where the vertical beam profile is dispersion-dominated and where it might be possible to place a profile monitor, but no actual design exists yet. So far, none of the diagnostics discussed achieve the precision desired by the particle physicists (in any of the machine designs).

### 7.4.7.3 Items for Further R&D

- All projects: none of the polarization or energy diagnostics discussed so far achieve the precision desired by the particle physicists (Ranking: 3).
- TESLA: the radiation levels in the extraction line as currently designed appear incompatible with the eventual installation of beam energy and/or polarization diagnostics downstream of the IP. Even though the ECFA study concluded that a downstream polarimeter is not required, it may be prudent for the extraction-line layout to preserve this capability, should it ultimately be required by the particle physics program. This would require reducing the currently predicted radiation levels by at least an order of magnitude (Ranking: 4).

## 7.4.8 Energy Tunability and Upgradability

This chapter has so far dealt exclusively with the reference designs operating at  $\sqrt{s}=500$  GeV. The present section is devoted to the critical issues associated with operation either at lower energies (Section 7.4.8.1), or at the maximum c.m. energy considered, in this

report, by each of the machine design teams (Section 7.4.8.2): 800 GeV for TESLA, 1 TeV for NLC and JLC, and 3 TeV for CLIC.

### 7.4.8.1 Energy Tunability

While it has been argued that physics output is maximized by always running at the highest possible c.m. energy, most scenarios for a linear collider have included high-luminosity running at several different energies. These might include a resonance scan with a range of a few GeV, the top threshold, the Higgs threshold, or the Z pole.

In all machines, large energy changes will occur only rarely, if only because they would involve extensive setup and retuning of the linac and beam-delivery systems. In addition, for the crossing-angle designs, a small repositioning of some extraction-line elements may be required (see Section 7.4.3.2). If PM final doublets are used, then they would restrict the energy range accessible without a complex and time-consuming exchange of these delicate components buried in the detector [101, 124].

The maximum luminosity achievable at low energy will, in all cases, be limited by the BDS optical bandpass. Operational efficiency may also be hampered by the fact that at low energy, the collimation in the BDS must become tighter (in terms of beam size) because the unnormalized emittance (and therefore the beam size in the final doublet) increases. In addition, for TESLA the positron production scheme (necessitated by the large beam power) causes the  $e^+$  yield to drop rapidly as the  $e^-$  energy decreases, further limiting the luminosity achievable at low  $\sqrt{s}$ .

A separate issue is the need for frequent low-luminosity running at the Z pole for detector-calibration purposes. This has been advocated [125] as an important ingredient to extend the discovery reach beyond the maximum machine c.m. energy, via precision electroweak measurements. The minimum luminosity needed would be about  $10^{31} \text{ cm}^{-2}\text{s}^{-1}$ ; it is unlikely that this requirement could be met without exchanging PM final-doublets optimized for higher energies. However, considerations of overall running efficiency are likely to make other detector-calibration methods more attractive. At LEP-2, one of the four detectors requested Z-pole running about every six weeks; the inherent stability of the storage ring made this operationally straightforward, and the amount of retuning required was minimal. The setup and tuning overhead of any linear collider is likely to be much more substantial—even for “low” luminosity.

### 7.4.8.2 Energy-Upgrade Issues

**7.4.8.2.1 Beam-Beam Effects** The beam-beam issues associated with the energy upgrade are qualitatively different for TESLA, NLC and JLC on the one hand, and for CLIC on the other. The ambitious luminosity goal of the 3 TeV project, driven by the rapid fall in cross-section at high energy, forces a significant reduction in the transverse size of the beams at the IP, resulting in a violent increase in the strength of the beam-beam interaction.

- Luminosity spectrum: at higher beam energies a more severe energy dilution is typically accepted in exchange for higher total luminosity. For TESLA or JLC-X/NLC, the average fractional energy loss increases by a factor ranging from

1.3–2.5, resulting in a luminosity spectrum fairly similar to that of the reference designs (Figure 7.20). The CLIC parameters at  $E_{cm}=3$  TeV are optimized for maximum absolute luminosity in the peak; the average energy loss increases from 4% to 21%.

- Photon, pair and hadron production (Table 7.22): the number of beamstrahlung  $\gamma$ 's per electron, the number of  $e^\pm$  pairs, and the number of hadronic events typically increases by factors of 1.5–3 for TESLA and JLC-X/NLC. For CLIC, the pair rate goes up by more than a factor of 10, and the hadronic event rates by two orders of magnitude.

#### 7.4.8.2.2 Accelerator-Induced Backgrounds

- Beam-beam backgrounds: the above increase in production rates is compounded, for all machines, by the higher energy and multiplicity of the shower secondaries, as well as by the doubling of the bunch-crossing frequency in the TESLA case. Comparative NLC studies at 0.5 and 1 TeV [115] suggest that background levels will remain manageable at high energy in all of TESLA, NLC and JLC, but a thorough evaluation has not been attempted by the committee. At 3 TeV c.m. energy, beam-beam backgrounds increase by large factors, and include the appearance of coherently produced pairs. They have been studied in some detail [126, 127]: the regime is very different (the first layer of the vertex tracker, for instance, is now assumed to lie at a radius of 30 mm instead of 15), and the combined IR and detector optimization is more difficult than at 500 GeV. Similar comments apply to the design of the collimation scheme and the minimization of SR backgrounds.
- Muons become both more abundant and more energetic at high energies, making them harder to deflect and almost impossible to range out. The predicted relative increase in muon flux at the IP, from 500 GeV to the highest machine energy, varies (at constant fractional halo) by one to two orders of magnitude depending on the c.m. energy range, the tunnel layout and the shielding scheme. While detailed estimates are not yet fully consistent across machine designs, enough conservatism has been built into the collimation and muon-shielding schemes that a satisfactory solution is likely to be found even at the highest c.m. energy.
- SR background studies are still at an early stage even for the baseline energy. No fundamental problem is expected here, even though the large increase in critical energy may open new issues.

#### 7.4.8.2.3 IP Stabilization

- In all designs, the nominal vertical spot size decreases<sup>22</sup> by about a factor of 2. For the warm-rf machines, this leads to correspondingly tighter stability and feedback requirements at the IP. TESLA is barely affected because of its intratraining feedback capability.

---

<sup>22</sup>both because of deliberate reductions in invariant emittance and/or IP  $\beta$ -function, and because of stronger adiabatic damping of the emittance.

- In TESLA, the 800 GeV parameter set (Table 2.1) calls for the (approximate) doubling of the number of bunches per train.<sup>23</sup>
  - This may have implications for the intratrain feedback. If the kickers can be built such that they turn on once per pulse and stay on for the entire duration of the train (with the kick strength modulated under feedback control), then the system response time (processor speed, signal propagation delays) need not be different from that of the baseline version. However the noise bandwidth would be doubled, which might cause a problem.
  - Because of the head-on configuration, the first parasitic crossing now occurs inboard of the extraction-line septum. The vertical separation at that location is sufficient for the long-range beam-beam deflection not to induce significant high-frequency noise on the vertical position at the IP, provided the bunch-to-bunch charge jitter remains below 5%.

**7.4.8.2.4 Spent-Beam Extraction** In all projects, achieving a satisfactory extraction-line design becomes more difficult at high energy, primarily because of the larger energy spread of the spent beam and of the significantly larger loss rate of both charged and neutral outgoing-beam components.

- NLC: While negligible at 500 GeV for the ideal case (nominal parameters, perfectly centered collisions), the extraction-line loss rate reaches 1.6 kW under equivalent conditions at  $\sqrt{s}=1$  TeV. This is considered too high by the NLC design team for clean enough polarization diagnostics, except for dedicated, non-colliding pulses. A chicane spectrometer might still be able to operate satisfactorily.
- TESLA:
  - Loss-rate predictions at  $\sqrt{s}=800$  GeV are not available in the literature, but they are expected to be considerably larger than those reported in Section 7.4.3.3 for the reference design<sup>24</sup>. Issues fundamentally associated with the head-on configuration, such as beamstrahlung losses on the septum blade or large loss fluctuations at tight aperture limitations, are likely to be exacerbated by the energy upgrade;
  - Either the gradient or the length (or both) of the electrostatic separators need to be increased.

**7.4.8.2.5 Collimation and Machine Protection** The combined effect of invariant-emittance reduction and of the higher beam energy increases the energy density at the spoilers by factors of 1.5, 2.0, and 10 in TESLA, JLC-X/NLC and CLIC, respectively. This brings the TESLA spoilers close to the limit for Ti (see Table 7.28 in Section 7.4.5.2), and makes the specifications of the CLIC spoilers at 3 TeV similar to those of the JLC-X/NLC betatron spoilers at 500 GeV.

<sup>23</sup>Strictly speaking, this is a luminosity-upgrade issue, independent of the actual c.m. energy.

<sup>24</sup>The predicted loss rate in TESLA at  $\sqrt{s}=500$  GeV is a few times larger than that in NLC at 1 TeV, both under ideal conditions.

### 7.4.8.2.6 Summary of Items for Further R&D

- TESLA:
  - Reduce the predicted extraction-line losses at 800 GeV from their present unacceptably high levels (Ranking: 3).
  - Design a collimator and SR-masking configuration compatible with tolerable muon-backgrounds and SR-backgrounds at 800 GeV (Ranking: 3).
  - If the head-on scheme is maintained, then demonstrate electrostatic separator performance (80 kV/cm) and a viable extraction-septum design in the presence of realistic radiation and power losses (Ranking: 3).
- JLC-X/NLC:
  - Reduce the predicted extraction-line losses at 1 TeV from their present unacceptably high levels (Ranking: 3).
  - Demonstrate that muon-backgrounds and SR-backgrounds are tolerable at 1000 GeV (Ranking: 3).
- CLIC:
  - The lack of an extraction-line design is a serious energy-upgrade issue (Ranking: 2).

## 7.4.9 Conclusions

### 7.4.9.1 Feasibility and Risk Assessment

Overall, the feasibility of the proposed designs at the baseline c.m. energy of 500 GeV is on solid ground. The beam-beam simulations that drive the IR geometry and the background suppression are well understood (including the production, transport and masking of secondaries). The layout of the TESLA and NLC IRs, as well as the conceptual (and in some cases, the engineering) design of their crucial components are quite mature. The collimation and machine-protection concepts have been at least partially validated in simulation and/or in actual prototypes (although realistic performance margins remain to be incorporated in many areas). Extensive background-remediation studies result in predicted levels that should be easily manageable in TESLA (thanks to the large bunch spacing); for some of the subdetectors at warm machines, the background levels per train deserve attention (but the question is only one of ultimate performance in specific physics channels, not of overall detector capability).

Concerns remain about some of the extraction-line designs and about final-doublet stabilization; these are detailed here in order of decreasing importance.

### 7.4.9.2 Major Concerns

- **TESLA IR and extraction-line layout.** Both crossing-angle and head-on collisions are feasible in superconducting-rf machines. The latter scheme has been

adopted in the TESLA TDR because of some inherent advantages: simpler IR geometry, looser envelope requirements for the FD quadrupoles, no need for crab-crossing cavities. However, this choice leads to unavoidable compromises in the shared section of the beam line, resulting in:

- Very tight apertures and marginal stay-clear for the outgoing charged and photon beams
- Potentially degraded SR masking
- Overall extraction-line radiation levels significantly larger than in JLC-X/NLC, probably limiting the performance of beam orbit, energy, and polarization diagnostics

In addition, the design of several crucial extraction-line components, as well as their protection in an overconstrained high-radiation environment, constitute a serious engineering challenge.

The combination of these issues raise strong doubts about the operability, reliability, and running efficiency of the extraction line as currently designed. Adopting a crossing-angle geometry would avoid the previously listed difficulties and improve flexibility. There might be implications for the fast-extraction scheme, which would need to be reevaluated. The design of the FD quadrupoles and their support would still be easier than for warm machines because vibration tolerances are looser.

The Working Group recommends that the present extraction-line design be subject to an in-depth internal review along the lines suggested in Section 7.4.3.3, and that until then the possibility of eventually adopting a crossing-angle layout be retained.

### 7.4.9.3 Concerns

- JLC-X/NLC:
  - Relative transverse stability of the two beams at the IP at high frequencies ( $>10$  Hz) is of paramount importance to the performance of warm-rf linear colliders. Extensive laboratory tests of FD stabilization schemes have been successfully carried out, with more planned at CERN, SLAC and elsewhere. These test-bench demonstrations are being backed up by detailed simulations of feedback performance in the presence of ground-motion and other dynamical errors. It remains essential, however, to demonstrate FD stabilization in an environment that adequately reproduces the *system* constraints of an actual detector and IR.
- CLIC:
  - IP stability. The concerns here are similar to those for JLC-X/NLC, compounded by a significantly tighter vertical vibration tolerance at the highest c.m. energy.
  - Extraction-line design. While the NLC extraction-line concept could plausibly be adapted for CLIC at the baseline energy, the very wide momentum bandpass and high energy densities at  $\sqrt{s}=3$  TeV pose a serious design challenge, which remains to be addressed.

- TESLA:
  - IP stability. The TESLA TDR design relies entirely on the intratrain IP feedback to guarantee collision stability. Although a similar technique has been used routinely at SLC, PEP-II and KEKB, its success is crucially dependent on the performance of the corresponding instrumentation (BPMs, pair luminosity monitor) in a high-disruption, high-radiation environment. It may be prudent to incorporate some form of FD stabilization in the baseline design to anticipate unexpectedly large vibration problems.



# BIBLIOGRAPHY for CHAPTER 7

- [1] P. Krejcik *et al.*, “High Intensity Bunch Length Instabilities in the SLC Damping Rings” in *Proc. 1993 Particle Accelerator Conference*, Washington, D.C. (1993) 3240.
- [2] Tanaka *et al.*, NIM A **486** Issue 3, pp521–538
- [3] R. Nagaoka, “Work Carried Out at the ESRF to Characterize and Correct the Coupling,” in *Proc. Seventh European Particle Accelerator Conference*, Vienna (2000) 131.
- [4] S.H. Kim *et al.*, “Investigation of Open-Loop Beam Motion at Low Frequencies at the APS,” in *Proc. 1997 Particle Accelerator Conference*, Vancouver (1997) 745.
- [5] M. Böge, “First Operation of the Swiss Light Source,” in *Proc. Eighth European Particle Accelerator Conference*, Paris (2002) 39.
- [6] K. Kubo, *et al.*, “Beam Tuning for Low Emittance in KEK-ATF Damping Ring,” in *Proc. Seventh European Particle Accelerator Conference*, Vienna (2000) 483.
- [7] K. Kubo and K. Oide, *Phys. Rev. ST Accel. Beams* **4**, 124401 (2001).
- [8] K.L. Bane, *et al.*, in *Proc. 2001 Particle Accelerator Conference*, Chicago (2001) 2955.
- [9] T.O. Raubenheimer, A. Wolski, “Comparison of alignment tolerances in linear collider damping rings with those in operating rings,” LCC-0112 (2003).
- [10] A. Seryi and O. Napoly, *Phys. Rev. E* **53**, 5323 (1996).
- [11] A. Wolski and S. de Santis, “Estimates of Collective Effects in the NLC Main Damping Rings,” LCC-0080.
- [12] A. Wolski, “Electron Cloud in Linear Collider Damping Rings,” *Proc. Mini-Workshop on Electron Cloud Simulations for Proton and Positron Beams (ELOUD’02)*, CERN (2002). Published in CERN Yellow Report CERN-2002-001.
- [13] A. Seryi,  
<http://www.slac.stanford.edu/~seryi/gm/model/>
- [14] T. Imai, *et al.*, “Highly stable beam extraction by double kicker system,” KEK preprint 2002-16, (KEK).

## BIBLIOGRAPHY FOR CHAPTER 7

- [15] T. Imai, *et al.*, “Double Kicker System in ATF,” in *Proc. XX International Linac Conference*, Monterey, CA (2000) 77.
- [16] L. Arnaudon *et al.*, “Effects of Tidal Forces on the Beam Energy in LEP,” in *Proc. 1993 Particle Accelerator Conference*, Washington, D.C. (1993) 44.
- [17] A. Wolski and Y. Wu, “Effects of Damping Wigglers on Beam Dynamics in the NLC Damping Rings,” in *Proc. 2001 Particle Accelerator Conference*, Chicago (2001) 3798.
- [18] A.W. Chao, NIM 180 (1981) 29.
- [19] D.P. Barber, G. Ripken, Handbook of Accelerator Physics and Engineering, A.W. Chao, M. Tigner (editors), World Scientific, 1999, pg. 156–164
- [20] Balakin, V. E. and Novokhatsky, A. V. and Smirnov, V. P., *VLEPP: Transverse Beam Dynamics*, in BATAVIA 1983, Proceedings, High Energy Accelerators, 1983, pp. 119–120.
- [21] Schulte, D., Tenenbaum, P., Walker, N., Wolski, A., and Woodley, M., *Tests of 3 Linear Collider Beam Dynamics Simulation Programs*, SLAC, LCC-Note, LCC-0091, 2002  
[http://www-project.slac.stanford.edu/lc/ilc/TechNotes/LCCNotes/lcc\\_notes\\_index.htm](http://www-project.slac.stanford.edu/lc/ilc/TechNotes/LCCNotes/lcc_notes_index.htm)
- [22] Emma, P., *Zeroth Order Design Report for the Next Linear Collider*, Stanford University, Chapter 5, pp. 268–271, 1996.
- [23] Nosochkov, Y., Raimondi, P., and Raubenheimer, T.O., *Design of Alternative Optics for NLC Prelinac Collimation Section*, SLAC, LCC-Note LCC-0057, 2001  
[http://www-project.slac.stanford.edu/lc/ilc/TechNotes/LCCNotes/lcc\\_notes\\_index.htm](http://www-project.slac.stanford.edu/lc/ilc/TechNotes/LCCNotes/lcc_notes_index.htm)
- [24] Anderson, S. and Shepard, J., *NLC Pre-Linac, 2001 Configuration, Version 2*, April 2001  
<http://www-project.slac.stanford.edu/lc/local/Reviews/Apr2001>
- [25] Oide, K., *Synchrotron Radiation Limit of the Focusing of Electron Beams*, Phys. Rev. Lett., **61**, pp. 1713–1715, 1988.
- [26] Stupakov, G., *High-Frequency Impedance of Small-Angle Collimators*, Presented at IEEE Particle Accelerator Conference (PAC2001), Chicago, Illinois, 18–22 June 2001.
- [27] Piwinski, A., *Wake fields and ohmic losses in flat vacuum chambers*, DESY-HERA-92-04.
- [28] Tenenbaum, P., *Collimator Wakefield Calculations for ILC-TRC Report*, SLAC, LCC-Note LCC-0101, 2002.
- [29] Drozhdin, A. *et al.*, *Comparison of the TESLA, NLC, and CLIC Beam Collimation Systems Performance. Fourth Edition.*, 2002  
[http://www-ap.fnal.gov/~drozhdin/prdriver/pap\\_TESLA\\_NLC\\_comparis4\\_no\\_distributions\\_aug30.ps](http://www-ap.fnal.gov/~drozhdin/prdriver/pap_TESLA_NLC_comparis4_no_distributions_aug30.ps)

- [30] Brinkmann, R., Raimondi, P., and Seryi, A. *Halo reduction by means of nonlinear optical elements in the NLC final focus system*, Presented at IEEE Particle Accelerator Conference (PAC 2001), Chicago, Illinois, 18–22 Jun 2001
- [31] NLC Post-Linac Collimation Task Force, *New Post-Linac Collimation System for the Next Linear Collider*, SLAC, LCC-Note LCC-0052, 2001  
[http://www-project.slac.stanford.edu/lc/ilc/TechNotes/lcc\\_notes\\_index.htm](http://www-project.slac.stanford.edu/lc/ilc/TechNotes/lcc_notes_index.htm)
- [32] Tenenbaum, P. *et al.*, *An apparatus for the direct measurement of collimator transverse wakefields*, Contributed to IEEE Particle Accelerator Conference (PAC 99), New York, NY, 29 Mar-2 Apr 1999.
- [33] Brinkmann, R., Napoly, O., and Schulte, D., *Beam-Beam Instability Driven by Wakefields*, CERN, CLIC-Note 505, 2001.
- [34] Schulte, D., *Luminosity in Future Linear Colliders in the Presence of Static Wakefield Effects in the Main Linac*, CLIC-Note 544 (2002).
- [35] Yokoya, K. and Chen, P., *Multiple Bunch Crossing Instability*, SLAC-PUB-4653.
- [36] Raubenheimer, T. and Ruth, R. D., *A Dispersion free trajectory correction technique for linear colliders*, Nucl. Instrum. Meth., **A302**, pp. 191–208, 1991.
- [37] Bowden, G., Holik, P., Wagner, S.R., Heimlinger, G., and Settles, R., *Precision magnet movers for the final focus test beam*, Nucl. Instrum. Meth., **A368**, pp. 579–592, 1996.
- [38] Adolphsen, C. *et al.*, *Wakefield and beam centering measurements of a damped and detuned X-band accelerator structure*, Presented at IEEE Particle Accelerator Conference (PAC 99), New York, NY, 29 Mar-2 Apr 1999.
- [39] Raubenheimer, T.O. and Schulte, D., *The ballistic alignment method*, CERN/PS-99-024(LP), 1999.
- [40] R. Assmann *et al.*, *The Computer Program LIAR for the Simulation and Modeling of High Performance Linacs*, Proceedings of the 1997 Particle Accelerator Conference, 1997.
- [41] d’Amico, E.T., Guignard, G., Leros, N., Schulte, D., *Simulation Package Based on PLACET*, Proceedings of the 2001 Particle Accelerator Conference, 2001.
- [42] Tenenbaum, P., 2001  
[http://www-project.slac.stanford.edu/lc/local/MAC/OCT2001/PTmacoct2001\[1\].pdf](http://www-project.slac.stanford.edu/lc/local/MAC/OCT2001/PTmacoct2001[1].pdf)
- [43] Tenenbaum, P. and Brinkmann, R. and Tsakanov, V., *Beam-based alignment of the TESLA main linac*, Presented at 8th European Particle Accelerator Conference (EPAC 2002), Paris, France, 3–7 Jun 2002.
- [44] Brinkmann, R. and Tsakanov, V., *Emittance preservation in TESLA* Prepared for APS / DPF / DPB Summer Study on the Future of Particle Physics (Snowmass 2001), Snowmass, Colorado, 30 Jun-21 Jul 2001.

## BIBLIOGRAPHY FOR CHAPTER 7

- [45] Shulte, D. and Walker, N., *TESLA beam-based alignment studies*, in preparation, 2002.
- [46] T. Raubenheimer, "Comments on Linear Collider Beam-Based Alignment," August, 2002.
- [47] Jones, R.M. *et al.*, *Manifold damping of wakefields in high phase advance linacs for the NLC*, 2002.
- [48] Baboi, N. and Brinkmann, R., *Higher Order Mode Effects and Multibunch Orbit Stability in the TESLA Main Linac*, DESY-TESLA-00-28, 2000.
- [49] D. Schulte, *Emittance Growth in the Main Linac of CLIC at 500 GeV*, CLIC-Note 545 (2002).
- [50] Tenenbaum, P., *Spectral Content of the NLC Bunch Train due to Long Range Wakefields*, SLAC, LCC-Note LCC-0015, 1999  
[http://www-project.slac.stanford.edu/lc/ilc/TechNotes/LCCNotes/lcc\\_notes\\_index.htm](http://www-project.slac.stanford.edu/lc/ilc/TechNotes/LCCNotes/lcc_notes_index.htm)
- [51] G. Bowden, personal communication, 2002. In these studies, the SLD door was closed, SLD water was ON, magnetic field was OFF. The data shown in the plot were taken on November 3, 1995 at 2:30am.
- [52] Seryi, A., *Ground Motion Models for ILC-TRC Studies*, in preparation, 2002.
- [53] Montag, C., *Ground motion in the HERA interaction region*, Published in Stanford 2000, Ground motion in future accelerators, pp. 139–146, 2000.
- [54] Assmann, R., Coosemans, W., Guignard, G., Leros, N., Redaelli, S., Schulte, D., Wilson, I., and Zimmermann, F., *Status of the CLIC Study on Magnet Stabilization and Time-Dependent Luminosity*, To be published in *Proceedings, EPAC2002*, 2002.
- [55] Hendrickson, L., 2002  
<http://www.slac.stanford.edu/~ljh/nlcfbck/fbck.htm> and  
<http://www.slac.stanford.edu/~ljh/fdesign.htm>
- [56] Hendrickson L., Algorithms and simulation results for NLC IP and linac feedback systems, Nanobeam 2002, Lausanne, September 2002  
<http://icfa-nanobeam.web.cern.ch/>
- [57] Hendrickson L., et al., Implementation of Dynamic Misalignments and Luminosity Stabilization by Beam-Beam Feedbacks in Simulations of Linear Colliders, submitted to PAC2003.
- [58] Seryi, A., et al., Effects of Dynamic Misalignments and Feedback Performance on Luminosity Stability in Linear Colliders, submitted to PAC2003.
- [59] White, G., *Simulations of TESLA intratrain fast feedback*, 2002  
<http://www-project.slac.stanford.edu/lc/local/AccelPhysics/GroundMotion/mtgs/july102002/>

- [60] Le Pimpec, F. et al., Vibrational Stability of NLC Linac Accelerating Structure, EPAC2002, 2000. See also in the Proceedings of LINAC2002 and ICFA Nanobeam 2002 Workshop.
- [61] Fenn, R., Slaton, T., and Woods, M., *Quadrupole Vibration Measurements for QM1B and QC3 in the Final Focus Test Beam at SLAC*, SLAC, LCC-Note LCC-0036, 2000.
- [62] Assmann, R, and Frisch, J., *Nanobeam 2002*, 2002. Reports about stabilization studies in CLIC and NLC  
<http://icfa-nanobeam.web.cern.ch/>
- [63] R.W. Assmann, et al., Status of the CLIC Study on Magnet Stabilization and Time-Dependent Luminosity, EPAC2002 ,2002.
- [64] Liepe, M., *PAC 2001*, 2001. Dynamic Lorentz Force Compensation with a Fast Piezoelectric Tuner.
- [65] Liepe, M., *Active Control of Lorentz-Detuning and Microphonics*, April, 2001.
- [66] Pagani, C., *Advances in Cryomodule Design and New Approches*, Proceedings of 9th Workshop on RF Superconductivity, Santa Fe, 1999.
- [67] Weise, H., *The TESLA Test Facility (TTF Linac—A Status Report)*, Proceedings of PAC 95, 1995.
- [68] The Next Linear Collider Design Group, T.O. Raubenheimer, editor, *Zeroth Order Design Report for the Next Linear Collider*, Stanford University, **2**, Chapter 11, p. 713, 1996.
- [69] The TESLA Collaboration, R. Brinkmann, editor, *TESLA Technical Design Report*, DESY, **II**, Chapter 7, p. 193, 2001.
- [70] The Next Linear Collider Design Group, T.O. Raubenheimer, editor, *Zeroth Order Design Report for the Next Linear Collider*, Stanford University, **2**, Chapter 11, p. 770, 1996.
- [71] The Next Linear Collider Design Group, T.O. Raubenheimer, editor, *Zeroth Order Design Report for the Next Linear Collider*, Stanford University, **2**, Chapter 11, p. 769, 1996.
- [72] Woodley, M., Tenenbaum, P., Hendrickson, L. and Seryi, A., *Optics simulations for the NLC main linac*, Contributed to IEEE Particle Accelerator Conference (PAC 2001), Chicago, Illinois, 18–22 Jun 2001.
- [73] R. Assmann, personal communication, 2002.
- [74] Smith, S.R., Tenenbaum, P., and Williams, S.H., *Performance of the beam position monitor system of the final focus test beam*, Nucl. Instrum. Meth., **A431**, pp. 9–26, 1999.
- [75] Shiltsev, V., personal communication, 2002.

## BIBLIOGRAPHY FOR CHAPTER 7

- [76] K. Yokoya, *et. al.*, see  
<http://www-acc-theory.kek.jp/members/cain/>
- [77] D. Schulte, CERN-PS/99-014-LP (1999).
- [78] The original comparison, made in O. Napoly, I. Reyzl and N. Tesch, DESY-TESLA-99-20A (1999), does show good agreement on the beamstrahlung flux, but suggests that pair-related computations are not fully consistent. This was eventually traced by D. Schulte and the above authors to (i) a cut, in one of the programs, on the pair energy (which eliminated 20% of the particles), and (ii) the fact that GUINEA-PIG outputs the energy and the number of pairs from both beams, while other programs return the background for one beam only. Once these points are taken into account, the agreement is satisfactory.
- [79] T. Barklow, *et. al.*, SLAC-PUB-8043 (1999).
- [80] D. Schulte, TESLA-97-08 (1996).
- [81] S. P. Baranov, O. Duenger, H. Shooshtari and J. A. Vermaseren, in \*Hamburg 1991, Proceedings, Physics at HERA, vol. 3\* 1478–1482 (see HIGH-ENERGY PHYSICS INDEX 30 (1992) No. 12988).
- [82] G. Wagner, “Neutron Background at TESLA,” presentation at the 9<sup>th</sup> International Workshop on Linear Colliders (LC02), Menlo Park, USA (2002).
- [83] T. Markiewicz, “NLC IR Overview,” presentation at the 9<sup>th</sup> International Workshop on Linear Colliders (LC02), Menlo Park, USA (2002)  
[http://www-conf.slac.stanford.edu/lc02/wg4/WG5\\_Markiewicz\\_NLCIROverview\(rotated\).pdf](http://www-conf.slac.stanford.edu/lc02/wg4/WG5_Markiewicz_NLCIROverview(rotated).pdf)
- [84] ACFA Linear Collider Working Group, “Particle Physics Experiments at JLC,” KEK Report 2001-11 (2001).
- [85] G. A. Schuler and T. Sjöstrand, CERN-TH/96-119 (1996).
- [86] P. Chen and M. E. Peskin, SLAC-PUB-5873 (1992).
- [87] M. Drees and K. Grassie. *Z. Phys. C*, **28** (1985) 451–462.
- [88] M. Glück, E. Reya and A. Vogt, *Phys. Rev. D* **46** (1992) 1973.
- [89] O. Napoly and D. Schulte, “Luminosity Monitor Options For Tesla,” CERN-OPEN-2000-135, contributed to 19th International Linear Accelerator Conference (Linac 98), Chicago, Illinois, 23–28 Aug 1998.
- [90] A. Seryi, “FD Stabilization in NLC,”  
[http://www-conf.slac.stanford.edu/lc02/wg4/wg4\\_seryi\\_0207\\_2\[1\].pdf](http://www-conf.slac.stanford.edu/lc02/wg4/wg4_seryi_0207_2[1].pdf);  
J. Frisch, “IP Stabilization for the NLC,”  
[http://www-conf.slac.stanford.edu/lc02/wg4/WG3-4\\_Frisch.pdf](http://www-conf.slac.stanford.edu/lc02/wg4/WG3-4_Frisch.pdf),  
presentations at the 9<sup>th</sup> International Workshop on Linear Colliders (LC02), Menlo Park, USA (2002).

- [91] P. Tenenbaum, J. Irwin, and T.O. Raubenheimer, to be submitted to PRSTAB.
- [92] D. Schulte and F. Zimmermann, “The Crossing Angle in CLIC,” Proc. 2001 Particle Accelerator Conference (PAC’2001), Chicago, Illinois, USA (2001).
- [93] TESLA Technical Design Report, DESY 2001-011, ECFA 2001-209, March 2001.
- [94] E. Merker *et. al.*, “The TESLA High-Power Extraction Line,” TESLA-01-19 (2001).
- [95] A. Seryi, “Beamstrahlung Photon Load on the TESLA Extraction Septum Blade,” LCC-Note-0104, SLAC, 2002.
- [96] Y. Nosochkov and K. A. Thompson, “Beam Losses in the NLC Extraction Line for High Luminosity Beam Parameters,” LCC - 0049 11//00 (2000). Although the parameters in that study are slightly different from those in the present report (Table 7.22), cases 500-H and 1000-H are actually a little more demanding than the current parameters because the vertical spot size is 10% smaller while the number of bunches is 1% lower.
- [97] G. White, “IP Feedback Simulation,” talk at the ECFA/DESY Workshop, Cracow, Sept.2001:  
<http://fatcat.ifj.edu.pl/ecfadesy-krakow> ;  
<http://www-project.slac.stanford.edu/lc02/>, presentation at the 9<sup>th</sup> International Workshop on Linear Colliders (LC02), Menlo Park, USA (2002).
- [98] S. R. Smith, “Design of an NLC Intrapulse Feedback System’, Linear Collider Note LCC-056 03/01 (2001).
- [99] A. Devred *et al.*, “Conceptual Design for the Final Focus Quadrupole Magnets for TESLA,” TESLA-2001-17 (2001).
- [100] A. Ringwall, “Detector Solenoid Field Effects’, in  
<http://www-sldnt.slac.stanford.edu/nlc/Meetings/beamdelivery/2000-03-13-Ringwall,Nosochkov,Seryi/index.htm>
- [101] T. Raubenheimer & P. Tenenbaum, private communication. An adjustable PM final-doublet concept has been studied (with an earlier version of the FFS optics) using counter-rotating longitudinal slices. In order to obtain 50% strength variation and limit the aberrations, it was necessary to subdivide the quadrupole longitudinally in many 2 cm slices. A potentially more attractive alternative consisted of just two counter-rotating magnets, one inside the other. This was aperture-limited at the downstream end, but could work for roughly half the magnet.
- [102] KEK Report 92-16, “JLC-I,” (Dec 1992), pp 214–215.
- [103] M. Alksa, S. Russenschuck, “Study of Some Options for the CLIC Final Focusing Quadrupole,” CLIC Note 596 (2002).
- [104] A. Drozhdin, *et. al.*, “Comparison of the TESLA, NLC and CLIC Collimation-System Performance,” in preparation.

## BIBLIOGRAPHY FOR CHAPTER 7

- [105] P. Tenenbaum, T.O. Raubenheimer, and M. Woodley, “Sources of Beam Halo in the Next Linear Collider Main Linac,” PAC-2001-FPAH071, SLAC-PUB-8935 (July 2001) (<http://www.slac.stanford.edu/pubs/slacpubs/8000/slac-pub-8935.html>)
- [106] R. Brinkman, N. J. Walker, and G.A. Blair, “The TESLA Post-linac Collimation System,” TESLA 2001-12.
- [107] “A 3 TeV  $e^+e^-$  Linear Collider based on CLIC Technology,” CERN 2000-008 (2000) <http://cern.web.cern.ch/CERN/Divisions/PS/CLIC/General.html>
- [108] P. Raimondi, “NLC Beam Delivery System Developments,” [http://www-project.slac.stanford.edu/lc/local/MAC/MAY2001/Talks/Mac\\_May%20Panta.pdf](http://www-project.slac.stanford.edu/lc/local/MAC/MAY2001/Talks/Mac_May%20Panta.pdf)  
J. Frisch, *et. al.*, “Collimator Design and R&D,” <http://www-project.slac.stanford.edu/lc/local/MAC/MAY2001/Talks/Frisch%20MAC%20May.pdf>  
P. Raimondi, A. Seryi, and P. Tenenbaum, “Tunability Of The NLC Final Focus System,” PAC 2001;  
“2001 Report on the Next Linear Collider,” Report Submitted to Snowmass ’01, FERMILAB-Conf-01/075-E, LBNL-PUB-47935, SLAC-R-571, UCRL-ID-144077;  
P. Raimondi, ”NLC Beam Delivery System & Collimation,” [http://www-conf.slac.stanford.edu/lc02/wg3/WG3\\_Raimondi\\_P.pdf](http://www-conf.slac.stanford.edu/lc02/wg3/WG3_Raimondi_P.pdf)
- [109] G.A. Blair, H. Burkhardt, H.J. Schreiber, “Background Simulation for the CLIC Beam Delivery System with Geant,” CERN-SL-2002-029 (AP), CLIC Note 519 (2002).
- [110] E. Doyle, J. Frisch and K. Skarpaas VIII, “Advanced Collimator Engineering for the NLC,” PAC 2001.
- [111] R. Assmann, *et. al.*, CERN-SL-2000-058-AP, Proc. EPAC 2000, Vienna (2000).
- [112] D. Schulte and F. Zimmerman, “Failure Modes in CLIC,” CERN-SL-2001-034(AP).
- [113] World Studies on Physics and Detectors for a Linear Collider <http://hepwww.physics.yale.edu/lc/>
- [114] J. Brau, C. Damerell, G. Fisk, Y. Fujii, R. Heuer, H. Park, K. Riles, R. Settles and H. Yamamoto, “Linear Collider Detector R&D,” <http://blueox.uoregon.edu/~jimbrau/LC/LCrandd.ps>
- [115] T. Markiewicz, “NLC IR Layout and Background Estimates,” Snowmass 2001 [http://www-sldnt.slac.stanford.edu/nlc/Meetings/2001-06-30\\_Snowmass/T1\\_Talks/2001-07-05%20Snowmass%20-%20NLC%20Backgrounds.ppt](http://www-sldnt.slac.stanford.edu/nlc/Meetings/2001-06-30_Snowmass/T1_Talks/2001-07-05%20Snowmass%20-%20NLC%20Backgrounds.ppt)
- [116] See *e.g.*, Ch. II-7.4.3 and IV-7.1 of Ref. [93]. Table IV-7.1.6 provides a concise overview of the various background sources and of their relative importance.
- [117] T. Tauchi, “JLC IR Overview,” presentation at the 9<sup>th</sup> International Workshop on Linear Colliders (LC02), Menlo Park, USA (2002). <http://www-conf.slac.stanford.edu/lc02/wg4/WG4-Tauchi.pdf>

- [118] D. Schulte, “Update of the Status of Machine Detector Interface Studies for CLIC,” CERN-PS 2001-074(AE).
- [119] F. Zimmermann, “Machine Backgrounds in CLIC,” presentation at the 9<sup>th</sup> International Workshop on Linear Colliders (LC02), Menlo Park, USA (2002).  
[http://www-conf.slac.stanford.edu/lc02/wg4/WG4\\_Zimmermann\\_0205\\_b.pdf](http://www-conf.slac.stanford.edu/lc02/wg4/WG4_Zimmermann_0205_b.pdf)
- [120] See for instance  
[http://www-dapnia.cea.fr/ecfadesy-stmalo/Sessions/MachineDetectorInterface/R\\_Settles.pdf](http://www-dapnia.cea.fr/ecfadesy-stmalo/Sessions/MachineDetectorInterface/R_Settles.pdf)  
 There is, however, a varying degree of conservatism in the quoted “pain thresholds.” JLC sets significantly tighter limits than TESLA on tolerable vertex-detector occupancy and muon flux per train [117]. The BABAR detector, in contrast, was designed with 10% as the occupancy limit in the drift chamber [128].
- [121] In NLC, SR photons are required not to strike masks or detector elements between 13 m upstream of the IP and 6 m downstream. The TESLA requirements are detailed in Ref. [129].
- [122] K. Stefanov *et al.*, “Studies of CCDs for Vertex Detector Applications,” presentation at LCWS2000 at FNAL.
- [123] V. Gharibyan, N. Meyners, K. Schuler, “The TESLA Compton Polarimeter,” LC-DET-2001-047 (Feb. 2001).
- [124] A hybrid FD for NLC was discussed in Ref. [130]. The defocusing magnet next to the IP was a PM magnet fixed in strength. The energy variability was attained with an SC quadrupole just upstream, and a normal electro-magnet upstream of this which acted as the QF. This system seemed to perform quite well over roughly a factor of 3–4 in energy; beyond this, the PM would have to be modified.
- [125] R. Settles, Proceedings of LC93 at SLAC.
- [126] D. Schulte, “Backgrounds at Future Linear Colliders,” CLIC Note 424, CERN/PS 99-069. Also in Proc. of the Workshop on the Development of Future Linear Electron-Positron Colliders for Particle Physics Studies and for Research Using Free Electron Lasers, Lund, Sweden, 23–26 Sep 1999.
- [127] D. Schulte, “Machine-Detector Interface at CLIC,” Proc. 5th International Linear Collider Workshop (LCWS 2000), Fermilab, Batavia, Illinois, 24–28 Oct 2000.
- [128] BABAR Technical Design Report, SLAC-R-95-457 (1995).
- [129] O. Napoly, “Collimation Depth Requirements for the TESLA IR,” DESY TESLA-01-18, 2001.
- [130] Zeroth Order Design Report for the Next Linear Collider, Stanford University, 1996.

